ACKNOWLEDGMENTS

The author is deeply indebted to his supervisor, Prof. William Kozicki, for the advice, guidance, encouragement and personal understanding throughout the course of this work. He also wishes to acknowledge Prof. B. C. Y. Lu for the suggestions in the preparation of this thesis.

The author is grateful to Messrs. C. J. Hsu and A. R. K. Rao for providing the experimental results.

He also wishes to thank National Research Council of Canada for the Studentships awarded to him.

Finally, the author wishes to acknowledge a very special debt to his wife, Esther, for her patience, understanding and skillful typing of the manuscript.

TABLE OF CONTENTS

LIST OF FIGURES

LIST OF TABLES

ABSTRACT

A simple and direct method for prediction of the average velocity and maximum velocity versus potential (pressure) gradient relationships in the isothermal, steady, uniform, laminar flow of any incompressible, time-independent fluid through ducts, closed and open, of arbitrary cross section has been proposed. The method requires only a knowledge of two geometric parameters and a fluid model equation. Geometric parameters have been evaluated for various complicated flow geometries. Comparisons made with available analytical solutions and experimental data for various non-Newtonian fluids and different flow geometries have indicated good agreement.

The general problem of viscous flow of an arbitrary time-independent non-Newtonian fluid through packed beds and porous media is examined. The Blake-Kozeny capillary model, utilizing the general relationships describing flow in straight ducts of arbitrary cross-sectional shape, has yielded a general expression involving the non-Newtonian viscosity and two geometric factors characteristic of the bed. The general relationship has successfully correlated the experimental data by allowing for the existence of an anomalous layer on the solid surfaces attributable to polymer adsorption - gel formation.

The equation for the flow of non-Newtonian fluids through porous media is applied to the filtration of non-Newtonian fluids. The success of the extended filtration theory in the analysis and correlation of the experimental results has been found to be satisfactory.

A generalized friction factor - Reynolds number formulation for the laminar flow of any time-independent fluid in a straight duct of arbitrary cross section, as well as through packed beds and porous media has been presented. The Ryan and Johnson stability parameter criterion has been extended to predict the transition point from laminar to turbulent flow of power law fluids exhibiting anomalous surface effects in circular pipes. A general correlation for the turbulent flow of purely viscous fluids is also given.

The drag reduction effect observed with viscoelastic non-Newtonian fluids in turbulent flow is studied. It is found that the drag reduction phenomenon can be attributed mainly to an increase in the laminar sub-layer thickness. This increase in thickness may be a manifestation of eddy suppression, as a result of the mechanical resistance associated with preferred orientations and alignment of long-chain polymer molecules in the high shear field.

Finally, a generalization of the laminar flow behaviour of non-Newtonian jets applicable to arbitrary cross

section has been presented. An improvement in agreement in the deviatoric normal stress difference determined by the extrusion method with extrapolated rheogoniometer data is achieved by taking into consideration the anomalous behaviour of the fluid.

I - INTRODUCTION

Fluids are generally classified into two main categories as Newtonian and non-Newtonian according to their behaviour at constant temperature under a shearing force. Those fluids for which the rate of deformation under laminar conditions is directly proportional to the shear stress are known as Newtonian fluids. This is the simplest stress - rate of strain relationship, and fortunately, many fluids do behave in this fashion under the usual conditions of interest. However, a significant number of fluids, such as solutions and melts of high polymers, suspensions of solids in liquids, and emulsions do not behave in this simple fashion. It therefore becomes necessary to consider these non-Newtonian fluids because many of them are of commercial importance as well as of theoretical interest.

Industries in which non-Newtonian flow behaviour is encountered include those dealing with rubber, plastics and synthetic fibers, soap and detergents, pharmaceuticals, pulp and paper, and many other light and heavy chemicals. It is evident that an understanding of non-Newtonian flow may enable substantial economic improvement to be made in a wide diversity of processing techniques.

One area of study in the field of non-Newtonian technology is being explored by physical chemists, who

are primarily interested in relating the flow to the physical, chemical and molecular properties of the fluid. Another approach is that of rheologists, who are concerned with the formulation of the rheological equations of state in terms of a mathematical model, but who it seems have rarely attempted to obtain relationships of immediate value to the engineer. This thesis deals with the presentation of quantitative relationships that are more immediately useful in engineering applications and expressed in terms of readily measurable properties of the fluid in question.

It is common knowledge that exact solutions of the Navier-Stokes equations (the equations of motion for Newtonian fluids) are known for only relatively few cases. Once the restriction of Newtonian behaviour is removed, the solution to the equations of motion can become extremely complicated because the non-Newtonian viscosity is no longer constant but is at least a function of shear stress or shear rate. In recent years, considerable effort has been expended in obtaining solutions for different non-Newtonian systems by insertion of a different constitutive equation of state into the equations of motion. The solutions applicable to many non-Newtonian systems in simple flow conditions have been reviewed extensively and presented in a multitude of textbooks (e.g.,2,60). It is not surprising that, despite the progress which has been made, the available

knowledge concerning non-Newtonian fluid mechanics is such as to encourage additional investigation (experimental and theoretical) in this area. Indeed, there are a large number of problems in this area which require further research.

This thesis represents the results of the theoretical and experimental investigations which were conducted in the field of non-Newtonian flow at the Department of Chemical Engineering of the University of Ottawa during the past five years. An attempt has been made to present the analysis in the chronological order of development of the subject matter as well as to show the interrelation of the various topics.

The purpose of this study is to present some design equations, useful in engineering applications, involving the flow of non-Newtonian fluids under various flow conditions, and which may also add to the understanding of the flow behaviour of these fluids. A simple and useful method for prediction of the flow rate - pressure drop relationship in the laminar flow of any time-independent fluid in ducts of arbitrary cross section is presented. The general flow rate - pressure drop relationship is applied to predict the flow of non-Newtonian fluids through packed beds and porous media. The equation describing the flow through porous media is applied to the filtration of non-Newtonian fluids. The generalized friction factor - Reynolds number correlations are also given, together with a criterion

for the prediction of the transition point from laminar to turbulent conditions for the flow of power law fluids exhibiting anomalous surface effects. The anomalous wall effects and associated drag reduction observed with certain polymer solutions in turbulent flow is examined analytically. Finally, the flow characteristics of viscoelastic fluids, exhibiting both viscous and elastic properties, are analyzed by consideration of the expansion and contraction behaviours of the liquid jets.

The subject matters presented in this thesis were investigated analytically. The equations or expressions found in the context of the thesis were derived analytically and some were deduced intuitively without the rigorous mathematical proof. The detailed derivations of some fundamental relationships are shown in the Appendices. The derived relationships have been substantiated either by comparison with available analytical results or by comparison with experimental data given by other investigators or obtained in the laboratory of the Department of Chemical Engineering of the University of Ottawa.

II - LITERATURE SURVEY

The flow of purely viscous non-Newtonian fluids, with or without a yield stress, through channels of commonly occurring geometries such as circular, parallel plates, concentric annuli and rectangular channels, has been reviewed thoroughly by Skelland (60). Recently, non-Newtonian flow through some other geometries has also appeared in the literature. For example, Mizushima et al (43) applied the variational principle to obtain a solution for the flow of power law fluids through elliptical ducts. Mitsuishi et al (42) used the same principle to derive solutions for the flow of power law fluids through rectangular, right-isosceles and equilateral triangular conduits.

Previous studies on the flow of fluids through porous media were restricted mostly to Newtonian fluids (4,55). In recent years, the flow of non-Newtonian fluids through packed beds and porous media has received considerable attention because of its important industrial applications. Sadowski (52) made an extensive study for the flow of Ellis fluids through packed beds. Christopher and Middleman (5) modified the Blake-Kozeny equation for power law fluids. McKinley et al (35) extended Darcy's law to non-Newtonian flow by considering the porous medium

as a capillary with equivalent radius proportional to the square root of the ratio of permeability to porosity of the bed. Recently, Marshall and Metzner (31) suggested a correlation for the flow of viscoelastic fluids through porous media.

Whitaker (66) showed the theoretical development of the continuity equation and the equation of motion for the flow of Newtonian fluids in anisotropic porous media and established the conditions under which Darcy's law is valid. Recently, Slattery (61) derived the same equations for the flow of viscoelastic fluids through porous media. Numerous investigators (e.g.,4,55) have applied Darcy's law with modifications to various facets of the general flow problem involving transient, multi-dimensional, compressible flow through anisotropic, compressible porous media. A most important application of Darcy's law is in industrial filtration. Tiller (62) has derived a one dimensional nonlinear partial differential equation for Newtonian filtration involving a compressible cake taking into account the variation of the superficial velocity through the filter cake. It appears from the literature that the problem of non-Newtonian filtration was yet to be studied.

In the conventional engineering analysis, the flow rate - pressure drop data are usually represented as friction factor and Reynolds number correlations. Metzner and

Reed (37) derived an appropriate Reynolds number for use with non-Newtonian fluids of a power law type. Ryan and Johnson (51) introduced a stability parameter to predict the onset of transition to turbulent flow for purely viscous fluids in circular pipes. Hanks (14) generalized the stability parameter criterion to predict the transition point in geometries other than a circular pipe. For turbulent flow, Dodge and Metzner (6) proposed a correlation equation for purely viscous fluid based on the extension of the von Karman equation.

The drag reduction effect exhibited by certain polymer solutions in turbulent flow has been observed and reported repeatedly in the literature. This effect was first noticed by Toms (64) in 1948 while conducting measurements on solutions of polymethylmethacrylate in monochlorobenzene. Subsequently, numerous papers have been published reporting this effect, obtained through the addition of additives. Dodge and Metzner (6) observed a lowering of the friction coefficient in the turbulent flow of aqueous CMC solutions when compared with other non-Newtonian purely viscous fluids. Shaver and Merrill (56) reported the same phenomenon for solutions of long polymer molecules and suggested a correlation for these fluids. Wells (65), Elata and Tirosh (7), Hoyt and Fabula (21), and Goren and Norbury (13) found separately that Newtonian

fluids with minute concentrations of various additives showed remarkable drag reduction. Meter and Bird (36) also found that friction factors were significantly lower for aqueous natrosol hydroxyethylcellulose solutions.

Many tentative interpretations of the turbulent drag reduction phenomenon have been proposed. Dodge and Metzner (6) made reference to the viscoelastic effect of the fluid in providing an explanation for the turbulence suppression, and numerous investigators (1, 54, 65) have referred to this hypothesis. Recently, Hershey and Zakin (20) proposed another mechanism which postulates that the drag reduction effect is due to the extension of the laminar region to higher Reynolds numbers, in addition to the viscoelastic effect of the fluid. However, this area of investigation still remains highly controversial.

Liquid jets have been the subject of considerable experimental and theoretical investigation of late, prompted by practical problems encountered in processing and manufacturing industries, and by theoretical considerations as to the rheological behaviour exhibited by the fluids when extruded. The investigations of Pearson (47) into the melt-flow instability of extruded polymers serve to exemplify a problem of practical and theoretical interest. Much of the past work relating to jet studies has been reported by Middleman (41), and Metzner, et al (12, 39, 40, 57).

Gaskins and Philippoff (10) suggested measurements of the expansion of a jet of fluid issuing from a capillary as a convenient means of measuring normal stresses at high shear rates. Investigations into this area were also conducted by Gill and Gavis (11), Sakiadis (53), Philippoff and Gaskins (48), and Metzner, et al (39). Subsequently, Harris (17, 18) pointed out that measurement of the jet diameter introduced an unnecessary artifice, since the thrust of the jet is the primary quantity required for determination of the normal stress. Metzner and colleagues (12,39,40,57) developed analyses for use in the evaluation of the normal stress from measurements of either the jet diameter or the thrust of the jet.

III - THEORETICAL FORMULATIONS

1. Non-Newtonian Flow in Channels of Arbitrary Cross Section

This section deals with relationships which are useful for prediction of the flow rate and pressure drop of time-independent non-Newtonian fluids in straight channels of arbitrary cross sectional geometry.

In the following analysis, a generalized design equation relating the average velocity and potential (pressure) drop in the isothermal, steady, uniform, laminar flow of any incompressible, time-independent fluid in a channel, either closed or open, of arbitrary cross section is presented. An analogous expression relating the maximum velocity to the potential drop is also given. Although the development does not consider secondary flow explicitly, it also does not preclude this aspect of flow. The secondary flow may actually arise in the steady flow through non-circular ducts. Expressions are developed for the most general case involving an effective velocity at the wall which arises from anomalous wall effects exhibited by certain non-Newtonian fluids. The physical interpretation of the anomalous behaviour and the effective velocity at the wall will be discussed in the subsequent section.

For steady, uniform, laminar and isothermal flow of fluids through circular tubes and slits (parallel plates), the Rabinowitsch - Mooney equation (44,50), relating the

average velocity to the shear stress at the wall, may be expressed as

$$\left(-\frac{du}{ds}\right)_w = a\,\tau_w \frac{d\left[\frac{2(\langle u\rangle - u_w)}{r_H}\right]}{d\,\tau_w} + b\left[\frac{2(\langle u\rangle - u_w)}{r_H}\right] \qquad (1)$$

An effective velocity at the solid wall, u_w, is assumed for the most general case. The coefficients "a" and "b" are defined as the geometric parameters. For a circular tube, $a = \frac{1}{2}$, $b = 3/4$, and for parallel plates, $a = \frac{1}{2}$, $b = 1$. A detailed derivation of the Rabinowitsch-Mooney equation for the circular and slit conduits is shown in Appendix A.

The velocity gradient at the solid surface is a function of the wall shear stress determined by the actual fluid model:

$$\left(-\frac{du}{ds}\right)_w = f(\tau_w) = \frac{\tau_w}{\eta} \qquad (2)$$

In the above equation, η is the non-Newtonian viscosity defined in accordance with the following relationship for the fluid expressed in the form of a "generalized Newtonian fluid" (2),

$$\tau_{ij} = -\eta(\partial u_j/\partial x_i + \partial u_i/\partial x_j) = -\eta\gamma_{ij} \qquad (3)$$

where τ_{ij} and γ_{ij} are components of the deviatoric stress tensor τ and the rate of deformation tensor γ, respectively. It is presumed that the non-Newtonian viscosity η is a scalar function of either of the second invariants.

$$\tau = +\sqrt{\tfrac{1}{2}(\tau:\tau)} = +\sqrt{\tfrac{1}{2}\sum\sum \tau_{ij}^2} \qquad (4)$$

or

$$\gamma = +\sqrt{\tfrac{1}{2}(\gamma:\gamma)} = +\sqrt{\tfrac{1}{2}\sum\sum \gamma_{ij}^2} \qquad (5)$$

From the similarity of the Rabinowitsch-Mooney equations for circular tubes and parallel plates, a generalization of Eq.(1) applicable to any arbitrary geometry is assumed as follows

$$\frac{1}{c}\oint_c f(\tau_w)dl = a\bar{\tau}_w \frac{\partial\left[\frac{2(\langle u\rangle - \bar{u}_w)}{r_H}\right]}{\partial\bar{\tau}_w} + b\left[\frac{2(\langle u\rangle - \bar{u}_w)}{r_H}\right] \qquad (6)$$

where

$$\bar{u}_w = \frac{1}{c}\oint_c u_w dl \qquad (7)$$

and

$$\bar{\tau}_w = \frac{1}{c}\oint_c \tau_w dl = r_H\left(-\frac{dP}{dx}\right) \qquad (8)$$

The hydraulic radius r_H for an arbitrary cross section is defined as the ratio of the cross sectional area to the wetted perimeter. The geometric parameters "a" and "b" are used to characterize the shape of the flow channel. The effective velocity at the wall, u_w, is presumed to be a function of the local wall shear stress, τ_w, which in general varies with position along the contour of the wall. Equation (6) is justified subsequently by comparison of predicted results with available analytical and experimental data. Equations (7) and (8) define the contour integrated average valuesof u_w and τ_w, respectively. The last equality of Eq.(8) can be shown to follow directly from the equation of motion.

The quantity $\frac{1}{c}\oint_c f(\tau_w)dl$ in Eq.(6) is found to be equal to $f(\bar{\tau}_w)$ in the flow of any time-independent fluid through circular and slit cross sections, as well as in the flow of Newtonian and Bingham fluids through an arbitrary section. Hence, the substitution

$$f(\bar{\tau}_w) = \frac{1}{c}\oint_c f(\tau_w)dl \qquad (9)$$

is conveniently made in Eq.(6) to effect an overall simplification of the problem. This circumvents the difficulty of requiring a knowledge of the shear stress distribution along the contour of the wetted perimeter.

The generalized Rabinowitsch-Mooney equation thus becomes

$$f(\bar{\tau}_w) = a\bar{\tau}_w \frac{\partial\left[\frac{2(\langle u\rangle - \bar{u}_w)}{r_H}\right]}{\partial\bar{\tau}_w} + b\left[\frac{2(\langle u\rangle - \bar{u}_w)}{r_H}\right] \qquad (10)$$

which may be integrated to yield the general result,

$$\frac{2(\langle u\rangle - \bar{u}_w)}{r_H} = \frac{1}{a}\bar{\tau}_w^{-\xi}\int_{\tau_y}^{\bar{\tau}_w} \tau^{\xi-1} f(\tau)\,d\tau \qquad (11)$$

where the aspect factor ξ is equal to b/a. For a fluid without a yield stress, the lower integration limit in the above equation becomes equal to zero.

Equation (11) can also be expressed in the following equivalent alternative forms,

$$\frac{2(\langle u\rangle - \bar{u}_w)}{r_H} = \frac{1}{a}\bar{\tau}_w^{-\xi}\int_{\tau_y}^{\bar{\tau}_w} \frac{\tau^{\xi}}{\eta}\,d\tau \qquad (12)$$

and

$$\frac{2(\langle u\rangle - \bar{u}_w)}{r_H} = \frac{1}{a}\bar{\tau}_w^{-\xi}\int_{\tau_y}^{\bar{\tau}_w} \tau_w^{\xi-1}\left[\frac{8(\langle u\rangle - u_w)}{r_H}\right]\left[\frac{3n' + 1}{4n'}\right]d\tau_w \qquad (13)$$

which utilize the non-Newtonian viscosity η defined by

Eq.(2) and the empirical data evaluated with the circular capillary tube viscometer, respectively. The flow behaviour index n' for a circular capillary is determined experimentally employing the relation

$$n' = \frac{d \ln \tau_w}{d \ln \frac{8(\langle u \rangle - u_w)}{D}} \qquad (14)$$

An analogous expression relating the maximum velocity to the potential drop can also be generalized to any arbitrary cross section in terms of the geometric parameter "a" as follows

$$\frac{2(u_{max} - \bar{u}_w)}{r_H} = \frac{1}{a\bar{\tau}_w} \int_{\tau_y}^{\bar{\tau}_w} f(\tau)\, d\tau \qquad (15)$$

The equations developed above for closed conduit flow are directly applicable to open channel flow provided proper geometric parameters evaluated for the latter are used. This is justified by the fact that the solutions for flow in open channels are the same as for the corresponding closed conduits obtained by reflecting the solid boundary in the free surface. For example, the solutions for the flow down a semi-circular open channel or an inclined plane of infinite width are the same as those

for the circular pipe and parallel plates, respectively. The only difference in the solutions for the open channel flow is that the contour integrated average quantities given by Eqs.(7) to (9) become the integrated average values along the wetted perimeter of the open channel. Also, the following additional assumptions must be imposed in the open channel flow:

(1) There is no shear stress; hence, no velocity gradient at the free surface in contact with the gas
(2) No ripples or waves form on the free surface
(3) The solid surface is smooth

From the generality of Eq.(11), the average velocity of any incompressible fluid without a yield stress in a tube of arbitrary cross section may be represented by the following expression involving the geometric aspect factor:

$$\langle u \rangle = (\xi - 1)\bar{\tau}_w^{1-\xi} \int_0^{\bar{\tau}_w} u\tau^{\xi-2}\, d\tau \qquad (16)$$

The detailed derivation of the above equation is shown in Appendix B.

Equation (16) can also be effectively interpreted as defining an operator which averages a point function of the position, in this case the velocity, over the tube cross section. The significance of this result is demonstrated in a later section, dealing with the expansion and

contraction behaviour of non-Newtonian jets, when it is applied to obtain the area average of the normal stress.

a. Application to Various Fluid Models

For illustrative and practical purposes, the bulk velocity - pressure drop relationships for various fluid models including those of practical interest to chemical engineers are presented in Appendix C. These relationships are obtained by substitution of the appropriate expressions for $f(\tau)$ or η in Eqs.(11) or (12) and performance of the indicated integrations. The analogous expressions for the maximum velocity, determined from Eq.(15), for various fluids are also given in the same section of the appendix.

b. Evaluation of Geometric Parameters

The values of the geometric parameters applicable to the circular tube and the slit in the case of closed conduit flow, as well as to the semi-circular arc and the inclined plane of infinite width for the case of open channel flow follow directly from the development of the Rabinowitsch-Mooney equation. For other more complicated flow geometries, the available analytical solutions or experimental data for Newtonian flow may be used in the evaluation of the geometric parameters "a" and "b",

since the geometric parameters are postulated to be functions of the flow geometry only and to be independent of the fluid model.

For a Newtonian fluid for which $f(\tau) = \tau/\mu$, Eqs.(11) and (15) integrate to yield

$$\frac{2\langle u \rangle}{r_H} = \frac{\bar{\tau}_w}{(a + b)\mu} \tag{17}$$

and

$$\frac{2u_{max}}{r_H} = \frac{\bar{\tau}_w}{2a\mu} \quad . \tag{18}$$

respectively. The effective velocity at the wall, $\bar{u}_w$, for the Newtonian fluid of interest is zero. Hence, a knowledge of the average velocity and maximum velocity relationships for Newtonian fluids enables one to evaluate the geometric parameters "a" and "b", characteristic of a particular flow cross section. The geometric parameters may also be evaluated from flow measurements obtained using simple non-Newtonian fluids such as the Ostwald-de Waele (power law)fluid .

Values and expressions for "a" and "b" determined for various channel shapes have been published in the literature. Kozicki, Chou and Tiu (24) reported geometric

parameters for concentric annuli, elliptic ducts, rectangular ducts, and isosceles triangular ducts. Kozicki and Tiu (15) also evaluated geometric parameters for the rectangular, semi-elliptic, 60° and 90° symmetric triangular open channels. Recently, additional geometric constants for other complicated flow geometries including the polygon with circular centered core, triangular and square arrays of circular tubes, regular polygonal and star-shaped conduits with various number of sides and points, respectively, were obtained by Phung (49). Some of these geometric parameters are tabulated in Appendix D.

2. Non-Newtonian Flow Through Packed Beds and Porous Media

The flow of fluids through porous materials is a subject of great importance in many fields of engineering. It occurs in filtration, in which the filter cake itself is at least a portion of the porous medium. The flow of underground water is another example of considerable importance. However, the petroleum industry has probably shown the most extensive interest in this field in connection with the production of crude oil from the underground reservoirs where it occurs naturally.

In the preceding section, a general equation for the prediction of the average velocity in the flow of non-Newtonian fluids through conduits of arbitrary cross sections was proposed. In this section, the same relationship is utilized in the flow through packed beds and porous media when the anomalous surface effect also becomes noticeable.

a. General Formulation

In the Blake-Kozeny model, the packed bed or porous medium is envisaged as a conduit, or conduits, of complicated cross-sectional geometry. Hence, Eqs.(12) and (15) are also applicable to flow through packed beds or porous media. These equations may be written in the present

instance as:

$$\frac{(\langle u\rangle - \bar{u}_w)}{r_H} = \frac{1+\xi}{k_1 \bar{\tau}_w^{\xi}} \int_{\tau_y T}^{\bar{\tau}_w} \frac{\tau^{\xi}}{\eta} d\tau \qquad (19)$$

and

$$\frac{u_{max} - \bar{u}_w}{r_H} = \frac{1+\xi}{k_1 \bar{\tau}_w} \int_{\tau_y T}^{\bar{\tau}_w} \frac{\tau}{\eta} d\tau \qquad (20)$$

The impermeability factor, $k_1 = 2(a+b)$, and the aspect factor, $\xi = b/a$, are used here to facilitate direct comparisons with previously published relationships. The maximum velocity expression is some extra information provided by the theory which is not utilized hereafter. The lower limit in the integrals has been modified in each of the above equations to account for the tortuosity of the actual capillaries in the bed.

In the flow through packed beds or porous media, the average velocity through the pore, $\langle u\rangle$, is related to the superficial velocity based on the cross-sectional area of the empty bed by

$$\langle u\rangle = \frac{u_s}{\epsilon} \qquad (21)$$

The average effective velocity at the pore wall, $\bar{u}_w$, is similarly related to the superficial effective velocity at the wall by

$$\bar{u}_w = u_{ws}/\epsilon \tag{22}$$

The hydraulic radius for an isotropic bed is defined by

$$r_H = \frac{\text{cross section available to flow}}{\text{wetted perimeter}}$$

$$= \frac{\text{volume available to flow}}{\text{total wetted surface}}$$

$$= \frac{\epsilon}{(1-\epsilon)\, s_o} \tag{23}$$

where the specific surface per unit volume of particles for a bed comprised of uniform spheres is

$$s_o = 6/D_p \tag{24}$$

For a bed of irregular particles, Eq.(24) serves as the defining relation for the particle diameter.

b. Special Cases

The integrated forms of Eq.(19) for the Ellis and

power law fluid models are now examined and compared with similar expressions developed by other investigators.

For an Ellis fluid, the non-Newtonian viscosity η is defined by

$$\frac{1}{\eta} = \frac{1}{\eta_o}\left[1 + \left(\frac{\tau}{\tau_{\frac{1}{2}}}\right)^{\alpha-1}\right] \qquad (25)$$

When this function for η is substituted in Eq.(19), the resulting expression can be integrated to yield:

$$\langle u\rangle - \bar{u}_w = \frac{\bar{\tau}_w r_H}{k_1 \eta_o}\left[1 + \frac{1+\xi}{\alpha+\xi}\left(\frac{\bar{\tau}_w}{\tau_{\frac{1}{2}}}\right)^{\alpha-1}\right] \qquad (26)$$

Equation (26) is found to be in agreement with the representation by Sadowski (52) of the experimental data for an Ellis fluid for $k_1 = 5.0$ and $\xi = 3$. This value of the aspect factor, ξ, is the same as for circular and elliptical conduits.

For a power law fluid, η is given by

$$\frac{1}{\eta} = \frac{1}{\tau}\left(\frac{\tau}{K}\right)^{1/n} \qquad (27)$$

which when substituted into Eq.(19), the resulting integration, after setting $\xi = 3$ as determined for the Ellis fluid, gives

$$\bar{\tau}_w = K\left(\frac{k_1}{2}\right)^n \left(\frac{3n+1}{4n}\right)^n \left[\frac{2(\langle u\rangle - \bar{u}_w)}{r_H}\right]^n \qquad (28)$$

Equation (28) is in agreement with a similar result derived by Bird et al (2) for the flow of a power law fluid through a packed bed if $k_1/2 = 25/12$. Sadowski and Bird (52) found however that their previously reported equation for the power law fluid did not agree with the experimental data. This was attributed to limitations of the power law model in characterization of the fluid behaviour. It was subsequently proposed (5) that the quantity $(25/12)^n$ be replaced simply by 25/12 which improved the agreement slightly. It is evident here that the same value of 2.5 satisfying Eq.(26) for the Ellis fluid should apply as well to $k_1/2$ in Eq.(28) for the power law fluid, corresponding to the specification of a constant bed impermeability factor with the same bed but different fluid models.

Equation (28) may be expressed in terms of the quantity K' determined directly with the capillary tube viscometer as follows:

$$\bar{\tau}_w = K'\left(\frac{k_1}{2}\right)^n \left[\frac{2(\langle u\rangle - \bar{u}_w)}{r_H}\right]^n \qquad (29)$$

where

$$K' = K\left(\frac{3n+1}{4n}\right)^n \qquad (30)$$

If the relationship between $\bar{\tau}_w$ and $2(\langle u \rangle - \bar{u}_w)/r_H$ for a power law fluid flowing through a packed bed is represented by

$$\bar{\tau}_w = K^* \left[\frac{2(\langle u \rangle - \bar{u}_w)}{r_H} \right]^n \tag{31}$$

then K^* is related to K' by

$$K^* = K' \left(\frac{k_1}{2} \right)^n \tag{32}$$

Equation (32) enables one to compute the fluid consistency index K^* for the flow of a power law fluid, with a constant flow behaviour index n, through a packed bed from a knowledge of K' and n, obtained directly with the capillary tube viscometer, and the impermeability factor of the bed. It should be noted that the above result was derived for beds with aspect factor ξ equal to 3.

Carman (4) lists values of the impermeability factor, k_1, for beds of different packing material and variable porosity, which were determined from measurements conducted with Newtonian fluids. Values of k_1 for different packing material and porosity are tabulated in Appendix E. In this connection, the best accepted value of k_1 for a bed of uniform spheres is 4.8, with a usual range of

variation from 4.5 to 5.10.

It has been pointed out earlier that the value of 3 determined for the aspect factor ξ from Sadowski's data (52) and substantiated as well by the present investigation subsequently is the same as for the circular conduit. This fact can be utilized to establish a simple and important relationship between the quantity $2(\langle u\rangle - \bar{u}_w)/r_H$ evaluated separately with the capillary tubes and packed beds.

For a circular tube, Eq.(12) with the appropriate substitution made for the geometric parameters (i.e., $a = \frac{1}{4}$, $\xi = 3$) may be expressed as:

$$\left[\frac{2(\langle u\rangle - \bar{u}_w)}{r_H}\right]_{ct} = 4\bar{\tau}_w^{-3}\int_{\tau_y}^{\bar{\tau}_w} \frac{\tau^3}{\eta}\, d\tau \qquad (33)$$

Comparing the above result with Eq.(19) for a fluid without a yield stress, $\tau_y = 0$, one gets

$$\left[\frac{2(\langle u\rangle - \bar{u}_w)}{r_H}\right]_{pb} = \left(\frac{2}{k_1}\right)_{pb}\left[\frac{2(\langle u\rangle - \bar{u}_w)}{r_H}\right]_{ct} \qquad (34)$$

In other words, $2(\langle u\rangle - \bar{u}_w)/r_H$ for a packed bed is $(2/k_1)_{pb}$ times the value determined with a capillary tube

viscometer at the same shear stress, $\bar{\tau}_w$. Hence, for a packed bed with $\xi = 3$, the flow characteristics relative to any fluid without a yield stress are readily determined from capillary tube viscometer data if the impermeability factor of the bed is known.

c. Anomalous Surface Effects

With certain non-Newtonian fluids the velocity gradient in the vicinity of the tube wall may induce a preferred orientation of polymeric molecules or dispersed floes present in the fluid. In some instances, the dispersed material may move slightly away from the wall region, leaving a thin layer of solvent adjacent to the solid surface. This phenomenon is referred to as the "separation phenomenon". This effect is observed in the flow of an aqueous suspension of paper pulp through a glass tube. A thin layer of clear water can be detected in the immediate proximity of the tube wall. An analogous phenomenon also occurs in the flow of blood (19). Effects of this sort lead to a reduction in the viscosity of the fluid in the vicinity of the wall, with results analogous to those which would be expected if there was actual slip between the bulk fluid and the solid surface. Since true slip is not believed to occur, the phenomenon is also referred to as an effective velocity of slip near the tube wall.

On the other hand, the polymeric molecules may be oriented in such a way that give rise to a more viscous anomalous layer near the wall. This phenomenon is compatible with polymer adsorption-gel formation, observed experimentally by Sadowski (52).

Therefore, whenever an anomalous surface effect is detected, corrections must be applied accordingly to arrive at the appropriate velocity.

(i) Evaluation of the Effective Surface Velocity

The method for obtaining the relationship of the mean effective velocity, $\bar{u}_w$, to the wall shear stress, $\bar{\tau}_w$, was originally proposed by Oldroyd (46) for flow in a circular tube. Substantially, the same procedure is applied here to an arbitrary cross section.

Equation (12) may be rewritten in the following form :

$$\frac{2\langle u\rangle}{r_H} = \frac{2\bar{u}_w}{r_H} + \frac{2(1+\xi)}{k_1}\bar{\tau}_w^{-\xi}\int_{\tau_y}^{\bar{\tau}_w}\frac{\tau^{\xi}}{\eta}\,d\tau \qquad (35)$$

In the presence of a surface effect, plots of $2\langle u\rangle/r_H$ versus $\bar{\tau}_w$ are expected to yield separate curves for different values of the hydraulic radius, r_H. From these

curves, at a selected value of $\bar{\tau}_w$, a plot of $2\langle u\rangle/r_H$ versus $1/r_H$ can be constructed. The curve obtained should be a straight line, whose slope is given by $2\bar{u}_w$. By repeating the procedure at different values of $\bar{\tau}_w$, the effective velocity at the wall can be determined as a function of the contour integrated average shear stress. The same procedure is applicable of course to flow through packed beds and porous media.

It is to be noted that inherent in this procedure is the assumption that $\bar{u}_w$ is independent of r_H, being a function only of $\bar{\tau}_w$. In the most general case, the effective wall velocity may vary with both hydraulic radius and shear stress. Jastrzebski (23) has found experimentally that the slip coefficient ζ, defined as (45,46),

$$\zeta = \frac{\bar{u}_w}{\bar{\tau}_w} \tag{36}$$

is not only a function of the shear stress but varies inversely with the tube radius R or the hydraulic radius r_H. Thus, one can define a corrected slip coefficient ζ_o as

$$\zeta_o = \zeta/r_H \tag{37}$$

which varies only with shear stress, but is independent of

the hydraulic radius.

(ii) Estimation of the Anomalous Layer Thickness

Following Oldroyd (46), the velocity gradient in the anomalous layer within a normal distance δ_1 from the solid boundary may be represented by

$$\frac{du}{dy} = f(\tau) + g(\delta_1, \tau, y) \tag{38}$$

where y is the normal distance measured from the wall, $f(\tau)$ is the velocity gradient characteristically ascribable to the fluid under laminar conditions, and $g(\delta_1, \tau, y)$ is the correction term accounting for the anomalous behaviour in the vicinity of the solid wall. Outside of the anomalous layer, i.e., at $y > \delta_1$, the function $g(\delta_1, \tau, y) = 0$.

The velocity u just outside the region of anomalous layer is thus given by

$$u - u_w = f(\tau_w) y \tag{39}$$

where

$$u_w = \int_0^{\delta_1} g(\delta_1, \tau_w, y)\, dy \tag{40}$$

Equation (40) is the defining equation for the effective

velocity at the wall in laminar flow. The effective velocity u_w is the value ascribed to u at y equals to zero.

Two possible cases of anomalous behaviour are illustrated in Figs. (1a) and (1b). When $g(\delta_1, \tau, y)$ is positive, the anomalous layer is less viscous than the fluid in the main stream giving rise to an effective velocity of slip (positive) as shown in Fig. (1a). On the other hand, when $g(\delta_1, \tau, y)$ is negative, the presence of the wall gives rise to a more viscous anomalous layer and a negative effective velocity at the wall, as depicted in Fig. (1b).

An estimate of the thickness of the anomalous layer is relatively simple to perform. If there is an effective slip velocity (positive), and the layer adjacent to the tube wall is pure solvent, then the velocity gradient in the anomalous layer is simply $du/dy = \tau_w/\mu_s$ and Eq.(39) yields the following simple relation:

$$u_w = \delta_1 \left[\frac{\tau_w}{\mu_s} - f(\tau_w) \right] \qquad (41)$$

Thus, the anomalous layer thickness δ_1 can be solved by means of Eq.(41) with a knowledge of the effective slip velocity.

When the effective velocity at the wall is negative, the velocity gradient in the anomalous layer is very small

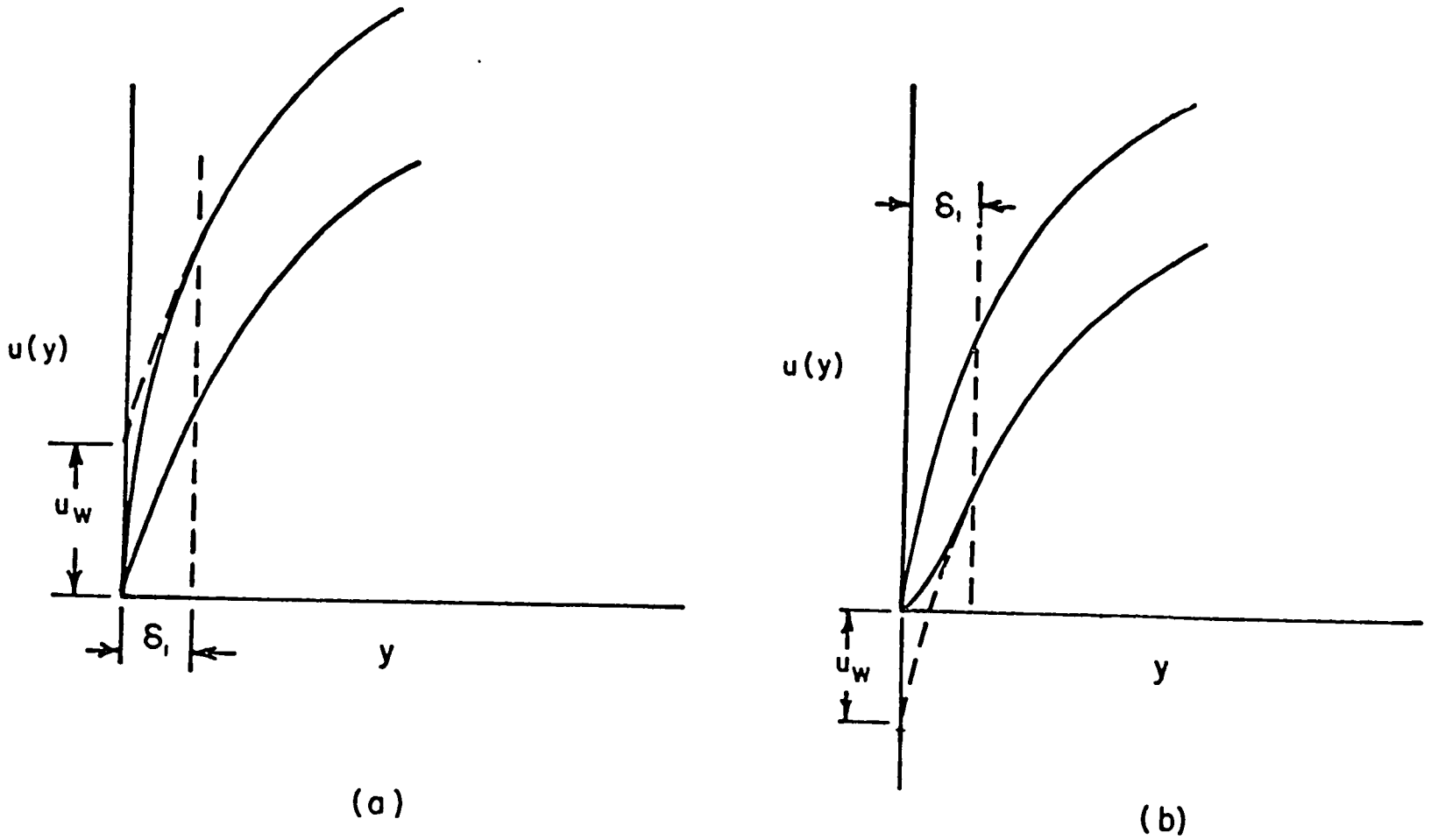

Fig. 1 Velocity Profiles Adjacent to a Solid Boundary in Laminar Flow; (a) Positive Effetive Slip Velocity, (b) Negative Effective Velocity at the all

and can be assumed equal to zero, i.e., $du/dy \approx 0$. The anomalous layer thickness is then found from Eq.(39) to be

$$u_w = -\delta_1 f(\tau_w) \tag{42}$$

For conduits of arbitrary cross section, the corresponding relations are analogous to those presented above with the exception that τ_w and u_w are replaced by the contour integrated average quantities $\bar{\tau}_w$ and $\bar{u}_w$ respectively.

d. Flow Through Porous Media

The relationships applicable to the flow of Newtonian fluids through porous media will be developed first. The corresponding expressions for non-Newtonian fluids in terms of the apparent viscosity are presented subsequently.

For a Newtonian fluid, $\eta = \mu$, Eq.(19) expressed in terms of the superficial velocity, using Eq.(21), becomes

$$u_s = \epsilon \bar{u}_w + \frac{\epsilon r_H \bar{\tau}_w}{k_1 \mu} \tag{43}$$

Introducing the surface resistance coefficient n defined as

$$n = 1/\zeta = \bar{\tau}_w / \bar{u}_w \tag{44}$$

in Eq.(43), and expressing the shear stress in terms of the pressure gradient using Eq.(8), one obtains

$$u_s = \left(\frac{\epsilon r_H}{m} + \frac{\epsilon r_H^2}{k_1 \mu} \right) \left(- \frac{dP'}{dx} \right) \tag{45}$$

Equation (45) may be expressed in vector notation as follows

$$\bar{u}_s = \left(\frac{k_m}{m} + \frac{k}{\mu} \right) (- \nabla P') \tag{46}$$

where k_m and k are the permeabilities to slip and viscous flow, defined respectively by

$$k_m = \epsilon r_H = \frac{\epsilon^2 D_p}{6(1-\epsilon)} \tag{47}$$

and

$$k = \frac{\epsilon r_H^2}{k_1} = \frac{\epsilon^3 D_p^2}{36 k_1 (1-\epsilon)^2} \tag{48}$$

The last equalities in Eqs.(47) and (48) are obtained using the definitions of r_H and S_o given by Eqs.(23) and (24).

For Newtonian fluids, there is no effective velocity at the wall, hence, $m = \infty$, and Eq.(46) reduces simply to the well-known Darcy's law:

$$\vec{u}_s = \frac{k}{\mu}(-\nabla p') \tag{49}$$

For non-Newtonian fluids, one can write the following equation analogous to Eq.(43),

$$u_s = \epsilon \bar{u}_w + \frac{\epsilon r_H \bar{\tau}_w}{k_1 \eta_{ap}} \tag{50}$$

where the apparent viscosity is defined by

$$\bar{\tau}_w = k_1 \eta_{ap} \left[\frac{(\langle u \rangle - \bar{u}_w)}{r_H} \right] \tag{51}$$

Using the general relationship given by Eq.(19), η_{ap} is found to be given by

$$\eta_{ap} = \frac{\bar{\tau}_w^{1+\xi}}{(1+\xi) \int_{\tau_y}^{\bar{\tau}_w} \frac{\tau^\xi}{\eta} d\tau} \tag{52}$$

It should be noted that in Eq.(52) the apparent viscosity for a non-Newtonian fluid without a yield stress flowing through a packed bed or porous medium is the same as determined with the capillary tube viscometer if the aspect factor ξ of the bed is equal to 3.

Using the same procedure as above for Newtonian flow, the vector equation describing the flow of non-Newtonian fluids through porous media can be written as :

$$\vec{u}_s = (k_m/m + k/\eta_{ap})(-\nabla p') \qquad (53)$$

Equation (53) reduces to a result in agreement with an analytical result presented by McKinley et al (35) for a non-Newtonian fluid not exhibiting the anomalous surface effect.

For a power law fluid without the anomalous wall effect, $m = \infty$, Eq.(53) becomes

$$\vec{u}_s^{\,n} = \frac{k}{\eta_{eff}}(-\nabla p') \qquad (54)$$

where

$$\eta_{eff} = \kappa\left(\frac{3n + 1}{4n}\right)^n \left[\frac{\epsilon r_H}{k_1}\right]^{1-n} \qquad (55)$$

Equation (54) agrees with the result presented by Bird et al (2) for a porous bed with an impermeability factor k_1 equal to 25/6.

3. Filtration of Non-Newtonian Fluids

In the preceding section, equations describing the flow of non-Newtonian fluids through porous media have been derived. These equations are now applied to the problem of non-Newtonian filtration which is of great industrial interest. The equation of continuity and the equation of motion for flow through porous media are also given in this section.

The equation of continuity is developed by consideration of a finite volume. This volume element is small compared to the gross dimensions of the porous media, but large compared to the characteristic volume of the voids so that the irregularities of the flow inside the void space are effectively averaged.

From the statement of the conservation of mass, that is,

$$\text{input} - \text{output} = \text{accumulation} \tag{56}$$

with no sources or sinks, the continuity equation for the flow of a fluid through a porous medium is found to be (27,63):

$$\nabla\cdot(\rho\tilde{u}_s) + \frac{\partial}{\partial\theta}(\epsilon\rho) = 0 \tag{57}$$

For an incompressible fluid, the mass density ρ is constant, and Eq.(57) becomes:

$$\nabla \cdot \vec{u}_s + \partial \epsilon / \partial \theta = 0 \qquad (58)$$

Introducing the modified Darcy's equation for non-Newtonian fluids, Eq.(53) in Eq.(58), and after considerable but straight forward manipulation (27,63), one obtains the following equation of motion for the flow of non-Newtonian fluids through compressible isotropic porous media:

$$A_1(\nabla \epsilon \cdot \nabla p') + A_2(\nabla \frac{1}{\eta_{ap}} \cdot \nabla p') + A_3(\nabla^2 p') + A_4(\nabla m \cdot \nabla p') = \frac{\partial \epsilon}{\partial \theta} \qquad (59)$$

where

$$A_1 = \frac{\epsilon(2-\epsilon)}{S_o(1-\epsilon)^2 m} + \frac{\epsilon^2(3-\epsilon)}{S_o^2 k_1 (1-\epsilon)^3 \eta_{ap}} \qquad (60)$$

$$A_2 = \frac{\epsilon^3}{S_o^2 k_1 (1-\epsilon)^2} \qquad (61)$$

$$A_3 = \frac{\epsilon^2}{S_o(1-\epsilon)m} + \frac{\epsilon^3}{S_o^2 k_1 (1-\epsilon)^2 \eta_{ap}} \qquad (62)$$

and

$$A_4 = -\frac{\epsilon^2}{S_o(1-\epsilon)m^2} \qquad (63)$$

In some cases, it may be permissible to assume that the surface resistance coefficient m is constant. That is to say, the average effective velocity at the particle surface is a linear function of the average surface shear stress. This assumption has been verified experimentally for non-Newtonian flow through packed beds (refer to Fig. 9). Thus, Eq.(59) may be written as:

$$A_1(\nabla\epsilon \cdot \nabla P') + A_2(\nabla \frac{1}{\eta_{ap}} \cdot \nabla P') + A_3(\nabla^2 P') = \frac{\partial \epsilon}{\partial \theta} \qquad (64)$$

For Newtonian fluids, $\eta_{ap} = \eta = \mu$, and Eq.(64) reduces to the following relatively simple expression:

$$\nabla^2 P' + \frac{3 - G}{\epsilon(1 - \epsilon)}(\nabla P' \cdot \nabla \epsilon) = \frac{S_o^2 k_1 \mu (1 - \epsilon)^2}{\epsilon^3}(\frac{\partial \epsilon}{\partial \theta}) \qquad (65)$$

It will now be shown that Eq.(65) reduces to the one-dimensional equation derived by Tiller and Cooper (62) for constant-pressure filtration. In the classical filtration theory, it is convenient to lump those parameters which are functions only of the pressure drop across the filter bed into a single quantity α_x, called the local specific cake resistance. Mathematically, α_x is defined by (33):

$$\alpha_x = \frac{S_o^2 K_1 (1 - \epsilon)}{\epsilon^3 \rho_s} \qquad (66)$$

With the aid of Eq.(66), Eq.(65) in one-dimensional form may be written as:

$$\frac{\partial^2 P'}{\partial x^2} - \left(\frac{\partial P'}{\partial x}\right)\frac{\partial}{\partial x} \ln \alpha_x (1 - \epsilon) = \mu \rho_s \alpha_x (1 - \epsilon) \frac{\partial \epsilon}{\partial \theta} \qquad (67)$$

Inside the filter cake, the solid compressive pressure is related to the fluid pressure by

$$P_s = P_a - P' \qquad (68)$$

where P_a is the fluid pressure at the upstream face of the cake. When the filtration is conducted under constant pressure, the differential change in pressure is simply:

$$dP_s = - dP' \qquad (69)$$

For a compressible cake, the specific cake resistance α_x and the porosity ϵ are usually assumed to be functions of solid compressive pressure P_s alone (33). Thus, Eq.(67) can be expressed as

$$\frac{\partial^2 P_s}{\partial x^2} - \left(\frac{\partial P_s}{\partial x}\right)^2 \frac{d}{dP_s} \ln \alpha_x (1 - \epsilon) = - \mu \rho_s \alpha_x (1 - \epsilon) \left(\frac{d\epsilon}{dP_s}\right)\left(\frac{\partial P_s}{\partial \theta}\right) \qquad (70)$$

which is the nonlinear partial differential equation derived by Tiller and Cooper (62) for a constant-pressure filtration involving a slurry of a Newtonian fluid and a compressible filter cake.

a. Filtration Equations for Power Law Fluids

It is evident that exact solutions of the equations of motion for flow through porous media are extremely difficult, if not impossible, to obtain even for the simpler Newtonian systems. Assumptions usually are made to simplify the problem sufficiently so as to render it tractable. In this section, workable filtration equations are derived for the power law fluid utilizing the traditional assumptions made in filtration theory supplemented by additional assumptions to simplify the problem.

The extended one-dimensional Darcy's equation for non-Newtonian fluids, Eq.(50), when expressed in terms of pressure drop, may be written as:

$$u_s = u_{ws} + \frac{\epsilon r_H^2}{k_1 \eta_{ap}} \left(\frac{dP}{dx}\right) \qquad (71)$$

The minus sign usually appearing in the pressure gradient term has been dropped in the present instance since the position variable x is measured from the filter medium, that is, in the direction opposite to the direction of

fluid flow, as seen in Fig. 2.

When Eq.(71) is expressed in terms of the mass of solids dm_x in the filter cake of thickness dx according to

$$dm_x = \rho_s(1 - \epsilon)Adx \tag{72}$$

one gets, after the introduction of the specific cake resistance α_x defined by Eq.(66),

$$\frac{dP'}{dx} = \frac{\eta_{ap}(u_s - u_{ws})}{A} dm_x \tag{73}$$

Substitution of the corresponding apparent viscosity expression for the power law fluid in the above equation, and integrating from $P_a - P' = 0$ when $m_x = 0$ to $P_a - P' = P_a - P^*$ when $m_x = m_0$, yields

$$\int_0^{P_a - P^*} \frac{d(P_a - P')}{\gamma_x} = \left(1 - \frac{u_{ws}}{u_s}\right)^n (u_s)^n \frac{Km_0}{A} \tag{74}$$

where the generalized cake resistance γ_x defined by

$$\gamma_x = \alpha_x \left(\frac{k_1}{\epsilon r_a}\right)^{n-1} \left[\frac{1 + n\xi}{n(1 + \xi)}\right]^n \tag{75}$$

is assumed to be a function of $P_a - P'$. In performing the

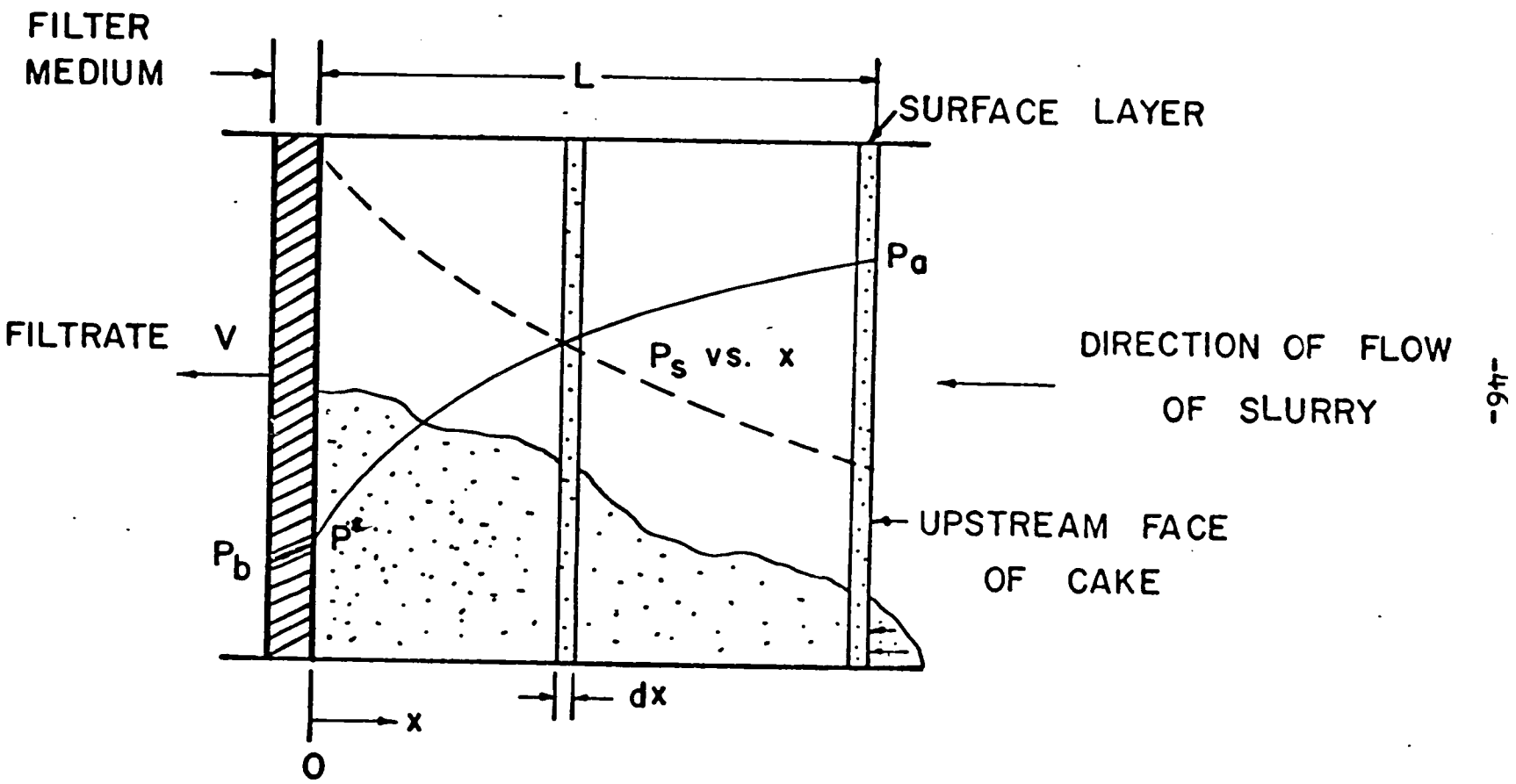

Fig. 2 Schematic Diagram of a Filter Bed Showing the Pressure Distribution

above integration, the slip velocity ratio u_{ws}/u_s is also presumed constant throughout the filter cake.

Following the traditional method of formulation of the filtration problem, an average generalized cake resistance γ' is defined as

$$\int_0^{P_s - P^*} \frac{d(P_s - P')}{\gamma' x} = \frac{P_s - P^*}{\gamma'} = \frac{\Delta P_c'}{\gamma'} \qquad (76)$$

which is a function of pressure drop across the cake $\Delta P_c'$ and of the flow behaviour index n of the fluid. Thus, Eq. (74) may now be expressed as:

$$\frac{\Delta P_c'}{\gamma'} = \left(1 - \frac{u_{ws}}{u_s}\right)^n (u_s)^n \frac{K m_c}{A} \qquad (77)$$

A generalized filter medium resistance R_m is defined analogously by the equation:

$$\frac{P^* - P_b}{R_m} = \frac{\Delta P_m'}{R_m} = K(u_s - u_{ws})^n \qquad (78)$$

Combining Eqs.(77) and (78), one obtains

$$\Delta P' = \Delta P_c' + \Delta P_m' = K\left(1 - \frac{u_{ws}}{u_s}\right)^n (u_s)^n \left(\frac{m_c \gamma'}{A} + R_m\right) \qquad (79)$$

In filtration, the superficial velocity u_s and the mass of solids m_c are traditionally expressed in terms of filtrate volume V by

$$u_s = \frac{d(V/A)}{d\theta} \tag{80}$$

and

$$m_c = VC \tag{81}$$

respectively, where C is the mass of the particles deposited in the filter per unit volume of filtrate.

Substitution of Eqs.(80) and (81) in Eq.(79) gives finally the important relationship:

$$d\theta = \left(\frac{KC\gamma}{\Delta P'}\right)^{1/n}\left(1 - \frac{u_{ws}}{u_s}\right)\left(\frac{V}{A} + \frac{R_m}{C\gamma}\right)^{1/n} d\left(\frac{V}{A}\right) \tag{82}$$

b. <u>Constant-Pressure Filtration</u>

When $\Delta P'$ is constant, the only variables in Eq.(82) are V/A and θ. The equation may then be integrated to yield

$$\theta\left(\frac{n+1}{n}\right)\left(\frac{\Delta P'}{KC}\right)^{1/n} = \chi\left[\left(\frac{V}{A} + \frac{R_m}{C\gamma}\right)^{1+1/n} - \left(\frac{R_m}{C\gamma}\right)^{1+1/n}\right] \tag{83}$$

where

$$\chi = \gamma^{1/n} \left(1 - \frac{u_{mg}}{u_g} \right) \tag{84}$$

It has been found experimentally that R_m/Cf is negligible for Newtonian fluids. If this quantity is also assumed negligible for power law fluids, then Eq.(83) becomes:

$$\theta = \frac{n}{n+1} \left(\frac{KC}{\Delta P'} \right)^{1/n} \chi \left(\frac{V}{A} \right)^{1+1/n} \tag{85}$$

It is seen from Eq.(85) that the availability of experimental constant-pressure filtration data enables one to determine the relationship between $\Delta P'$ and χ, characteristic of the filter bed and the flow behaviour index n. The empirical relationship between $\Delta P'$ and χ may be used in the prediction of the constant-rate filtration, with the assumption that $\Delta P_m' \ll \Delta P'$.

c. Constant-Rate Filtration

In the case of constant-rate filtration, the superficial velocity, $u_g = V/A\theta$, is constant, and Eq.(77) finally becomes

$$\Delta P_c' = KC\chi^n \left(\frac{V}{A\theta} \right)^{1+n} \theta \tag{86}$$

Therefore, if χ is a known function of $\Delta P_c'$, and if

$\Delta P_m'$ can be estimated, then Eq.(86) may be used directly to relate the overall pressure drop to time when the flow rate of the filtrate is constant. On the other hand, χ can be evaluated directly from the constant-rate data using Eq.(86). Hence, the prediction of the pertinent variables for constant-pressure filtration is also feasible from data obtained in constant-rate filtration.

If the relationship between $\Delta P_c'$ and χ can be reasonably approximated by

$$\chi = \chi_o(\Delta P_c')^q = \chi_o(\Delta P' - \Delta P_m')^q \qquad (87)$$

then Eq.(86) becomes

$$(\Delta P_c')^{1-nq} = (\Delta P' - \Delta P_m')^{1-nq} = K_r\theta \qquad (88)$$

where

$$K_r = KC\chi_o^n\left(\frac{V}{A\theta}\right)^{1+n} \qquad (89)$$

Taking the logarithms of both sides of Eq.(88) gives

$$\log\theta = (1 - nq)\log(\Delta P' - \Delta P_m') - \log K_r \qquad (90)$$

It is seen that a straight line should be obtained whose slope is $(1 - nq)$ in a log-log plot of $(\Delta P' - \Delta P_m')$

versus θ.

The method for the estimation of $\Delta P_m'$, the pressure drop across the filter medium, in non-Newtonian filtration is the same as for the Newtonian filtration. The procedure has been discussed thoroughtly in the literature (33,27).

4. Generalized Friction Factor - Reynolds Number Correlations

In this section, the generalized friction factor - Reynolds number relationship for the laminar flow of any time-independent fluid in a straight duct of arbitrary cross section, as well as through packed beds and porous media is presented. The Ryan and Johnson stability parameter criterion (51) is extended to predict the transition point from laminar to turbulent flow of power law fluids exhibiting anomalous surface effects in circular pipes. A tentative method of correlation for the turbulent flow of purely viscous non-Newtonian fluids through channels of arbitrary cross section is proposed, though this aspect of the flow is not explicitly studied in the course of the present investigation.

a. Friction Factor - Reynolds Number Relationship for Laminar Flow

In laminar flow, the Fanning friction factor and Reynolds number are related according to the following relationship:

$$f = \frac{2\bar{\tau}_w}{\rho(\langle u \rangle - \bar{u}_w)^2} = \frac{16}{Re} \qquad (91)$$

The Reynolds number, expressed in terms of the apparent viscosity, is given by:

$$Re = \frac{4r_H(\langle u\rangle - \bar{u}_w)\rho}{(a+b)\eta_{ap}} = \frac{8r_H(\langle u\rangle - \bar{u}_w)\rho}{k_1\eta_{ap}} \qquad (92)$$

Employing indices analogous to those originally defined for the circular tube by Metzner and Reed (37), the Reynolds number can also be expressed alternatively by

$$Re = \frac{\rho(\langle u\rangle - \bar{u}_w)^{2-n^*} r_H^{n^*}}{2^{n^*-3} K^*} \qquad (93)$$

where n^* and K^* are defined respectively by

$$n^* = \frac{\partial \ln \bar{\tau}_w}{\partial \ln \frac{2(\langle u\rangle - \bar{u}_w)}{r_H}} \qquad (94)$$

and

$$K^* = \bar{\tau}_w \left[\frac{2(\langle u\rangle - \bar{u}_w)}{r_H}\right]^{-n^*} \qquad (95)$$

The partial differentiation in Eq.(94) is performed at constant values of geometric parameters, corresponding to a fixed flow geometry.

The general flow equation, Eq.(12), developed earlier may be utilized to express η_{ap}, n^* and K^* in terms of the non-Newtonian viscosity, η, of the fluid and the geometric parameters, ξ and k_1, of the flow channel as follows:

$$\eta_{ap} = \frac{\bar{\tau}_w^{1+\xi}}{(1+\xi)\int_{\tau_y}^{\bar{\tau}_w} \frac{\tau^\xi}{\eta}\, d\tau} \tag{96}$$

$$n^* = \frac{\eta_w \int_{\tau_y}^{\bar{\tau}_w} \frac{\tau^\xi}{\eta}\, d\tau}{\bar{\tau}_w^{1+\xi} - \xi\eta_w \int_{\tau_y}^{\bar{\tau}_w} \frac{\tau^\xi}{\eta}\, d\tau} \tag{97}$$

and

$$K^* = \bar{\tau}_w^{1+\xi n^*} \left[\frac{k_1}{2(1+\xi)}\right]^{n^*} \left[\int_{\tau_y}^{\bar{\tau}_w} \frac{\tau^\xi}{\eta}\, d\tau\right]^{-n^*} \tag{98}$$

where η_w is the value of η evaluated at $\bar{\tau}_w$. It should be noted that Eq.(96) is similar to Eq.(52), the expression of η_{ap} for flow in porous media, except that the lower integration limit τ_y in the former equation is replaced by $\tau_y\Gamma$ to account for the tortuosity of the actual capillary inside the porous medium, consistent with the Blake-Kozeny concept. Analogously, Eqs.(97) and (98) are directly

applicable to flow through packed beds or porous media with the proper modification of the lower integration limits for a fluid with a yield stress (e.g., Bingham plastic).

Therefore, the friction factor and Reynolds number relationships presented in this section are applicable to any time-independent fluid, characterized by the non-Newtonian viscosity η, and to any shape of flow channel, characterized by the geometric parameters ξ and k_1 (or "a" and "b").

b. **Application to Power Law Fluids**

In order that the power law fluid relationship shall be of engineering value, it is necessary for n and K values to remain constant over considerable ranges of shear rate. Furthermore, the actual values used are those evaluated for the shear stress at the wall. If the flow behaviour index n*, defined by Eq.(94), is constant, then Eq.(93) reduces to the following Reynolds number defined by Metzner and Reed (37) for the flow of power law fluids and without anomalous surface effects in a circular pipe:

$$Re = \frac{D^n \langle u \rangle^{2-n} \rho}{8^{n-1} K'} \qquad (99)$$

where

$$n^* = n' = n \tag{100}$$

and

$$K^* = K' = K\left(\frac{3n+1}{4n}\right)^n \tag{101}$$

One can easily verify that Eq.(99) reduces to the conventional Reynolds number for Newtonian flow in a circular pipe by setting $n = 1$ and $K' = \mu$.

In the most general case, power law fluids may be represented by

$$\tau = K(-du/ds)^n = K\, f(\tau)^n \tag{102}$$

where n and K may vary continuously with shear rate.

A logarithmic form of the power law model is

$$\log \tau = \log K + n \log f(\tau) \tag{103}$$

If n and K are assumed to be constant over at least a differential range of shear rate, then Eq.(103) may be differentiated as follows, within this range:

$$n = \frac{d \log \tau}{d \log f(\tau)} \tag{104}$$

The shear rate at the wall, $(-du/ds)_w$, or more generally $f(\bar{\tau}_w)$, can be shown to be related to the average

velocity and the geometric parameters by the general flow equation, Eq.(11), as follows:

$$f(\bar{\tau}_w) = \frac{2(\langle u \rangle - \bar{u}_w)}{r_H} \left(\frac{a + bn^*}{n^*}\right) \qquad (105)$$

Converting Eq.(105) to logarithmic form,

$$\log f(\bar{\tau}_w) = \log \frac{2(\langle u \rangle - \bar{u}_w)}{r_H} + \log \left(\frac{a + bn^*}{n^*}\right) \qquad (106)$$

and differentiating this result with respect to $\log \bar{\tau}_w$ at constant values of geometric parameters, one obtains:

$$\frac{\partial \log f(\bar{\tau}_w)}{\partial \log \bar{\tau}_w} = \frac{\partial \log \frac{2(\langle u \rangle - \bar{u}_w)}{r_H}}{\partial \log \bar{\tau}_w} + \frac{\partial \log \left(\frac{a + bn^*}{n^*}\right)}{\partial \log \bar{\tau}_w} \qquad (107)$$

Substituting the definitions of n and n^*, given by Eqs.(104) and (94) respectively, in the above equation, one gets:

$$\frac{1}{n} = \frac{1}{n^*} + \frac{\partial \log \left(\frac{a + bn^*}{n^*}\right)}{\partial \log \bar{\tau}_w} \qquad (108)$$

The subscript w may be omitted from Eq.(108) because

n and n* are understood to refer to a particular value of shear stress, regardless of whether this occurs at a tube wall or elsewhere.

Rearranging Eq.(108), one may obtain the expression for n in the following:

$$n = \frac{1}{\frac{1}{n^*} + \frac{\partial \log(a+bn^*)/n^*}{\partial \log \tau}}$$

$$= \frac{n^*}{1 - \frac{a}{a + bn^*} \frac{\partial n^*}{\partial \log \tau}} \qquad (109)$$

or, in terms of the aspect factor ξ, n is equal to

$$n = \frac{n^*}{1 - \frac{1}{1 + \xi n^*} \frac{\partial n^*}{\partial \log \tau}} \qquad (110)$$

Equation (110) provides the relationship between n and n* for a power law fluid at any particular shear stress when the plot of $2(\langle u \rangle - \bar{u}_w)/r_h$ versus $\bar{\tau}_w$ is not linear.

c. Prediction of the Laminar - Turbulent Transition Point

The point of transition from laminar to turbulent flow of a fluid exhibiting anomalous behaviour in laminar flow can be expected to be different from one which exhibits no anomalous effects. Ryan and Johnson (51) have introduced a stability parameter Z for flow in pipes, defined as

$$Z = \frac{R \rho u}{\tau_w} \left(- \frac{du}{dr} \right) \qquad (111)$$

which is zero at both centerline and the wall, and reaches a maximum at some intermediate radial position. The critical value of Z_{max}, above which turbulent flow is to be expected, is 808 which is found from the flow of Newtonian fluids in circular pipes. This criterion is used to predict the transition point for non-Newtonian fluids as well, at least those of the purely viscous type. Subsequently, Hanks (14) has generalized the criterion to the form

$$\bar{Z} = \frac{1}{8} \rho \frac{|\vec{u} \cdot \nabla \vec{u}|}{|f - \nabla p|} \qquad (112)$$

which can be applied to channels of arbitrary cross section, with $\bar{Z}_c = 404$.

The maximum value of Z occurs at the critical radial position $\lambda_c = (r/R)_c$, which is obtained by setting the derivative of Z with respect to r to zero, using the known

laminar velocity distribution.

For a power law fluid exhibiting anomalous wall effects, the velocity distribution is obtained by integrating the velocity gradient as follows

$$\int_{u_w}^{u} du = -\int_{R}^{r} (-du/dr)dr = \int_{r}^{R} f(\tau)dr \quad (113)$$

which after some manipulation gives

$$u - u_w = \frac{3n+1}{n+1}(\langle u\rangle - u_w)(1 - \lambda^{(n+1)/n}) \quad (114)$$

Using Eq.(114), it is found that τ_{max} occurs at λ_c, with

$$\lambda_c = \left(\frac{1}{n+2}\right)^{n/(n+1)} \left[1 + \frac{n+1}{3n+1}\frac{u_w}{(\langle u\rangle - u_w)}\right]^{n/(n+1)} \quad (115)$$

and that

$$z_{max} = 808 = \frac{\rho(\langle u\rangle - u_w)^2}{\tau_w}\left[\frac{3n+1}{n+1}(1 - \lambda_c^{(n+1)/n}) + \frac{u_w}{(\langle u\rangle - u_w)}\right](\frac{3n+1}{n})(\lambda_c)^{1/n} \quad (116)$$

The critical friction factor f_c for power law fluids exhibiting anomalous wall effects may be obtained from the above equation as

$$f_c = \left[\frac{2\tau_w}{\rho(\langle u\rangle - u_w)^2}\right]_c$$

$$= \frac{1}{404}\left[\frac{3n+1}{n+1}(1-\lambda_c^{(n+1)/n}) + \frac{u_w}{(\langle u\rangle - u_w)}\right]\left(\frac{3n+1}{n}\right)(\lambda_c)^{1/n} \qquad (117)$$

The corresponding critical Reynolds number Re_c is then

$$Re_c = \frac{D^{n'}(\langle u\rangle - u_w)_c^{2-n'}\rho}{8^{n'-1}K'} = \frac{16}{f_c} \qquad (118)$$

It can be easily verified that Eqs.(115), (116) and (117) reduce to the corresponding expressions given by Ryan and Johnson (51) for power law fluids without the anomalous effect by setting $u_w = 0$. The critical Reynolds numbers for power law fluids with no effective velocity at the wall have been tabulated by Longwell (30) as a function of the flow behaviour index n.

d. Turbulent Flow of Non-Newtonian Fluids

Turbulent flow in arbitrary channels is not considered explicitly in this investigation because of the lack of data for flow geometries of other than circular and slit cross sections. The available information (9,32)

appears to suggest however that negligible error results when turbulent flow data for circular tubes are applied directly to other cross-sectional channels. The revised form of the Dodge-Metzner equation (6) for turbulent flow compatible with this hypothesis is:

$$\frac{1}{\sqrt{f}} = \frac{4.0}{n^{*0.75}} \log\left[Re(f)^{1-\frac{n^*}{2}}\right] - \frac{0.40}{n^{*1.2}} + 4.0\, n^{*0.25} \log\left[\frac{4(a + bn^*)}{1 + 3n^*}\right] \qquad (119)$$

It must be mentioned that the above relationship is applicable only to the purely viscous non-Newtonian fluids. In the case of polymers or polymer solutions which exhibit viscoelastic properties, Meter's correlation (36) can be utilized to predict the flow in the turbulent regime. It will be shown in the next section that if the viscoelastic fluid is treated as a purely viscous fluid by taking into consideration a turbulent effective velocity at the wall due to the anomalous behaviour in the vicinity of the solid boundary, then Eq.(119) is also applicable for the turbulent flow of a viscoelastic fluid in circular pipes.

5. Anomalous Wall Effects and Associated Drag Reduction in Turbulent Flow

The anomalous behaviour of certain polymer solutions in turbulent flow has been observed and reported repeatedly in the literature. The most striking phenomenon is the reduction in the pressure drop required to maintain the average velocity of a liquid under turbulent flow conditions achieved by the addition of a small quantity of foreign materials, such as the high molecular weight additives.

In this section, the analysis of drag reduction in turbulent flow of viscoelastic polymer solutions utilizes only the purely viscous properties of the fluids, consideration also being given to the anomalous behaviour in the vicinity of the conduit wall. The anomalous behaviour is attributed to two phenomena: (1) the anomalous behaviour observed under laminar flow conditions as described in Section 2 (i.e., the separation phenomenon or the polymer adsorption - gel formation phenomenon), and (2) a laminar sub-layer thickness greater than that ascribable to the purely viscous non-Newtonian fluids.

The velocity distribution for the turbulent flow of a viscoelastic non-Newtonian fluid in a pipe is obtained by integration of the velocity gradient,

$$u = \int_0^y (du/dy)dy \qquad (120)^*$$

where y is the normal distance measured from the wall.

In the present case, the velocity gradient in the vicinity of the wall is represented by

$$du/dy = h(\tau,y) + q(\tau,y) \qquad (121)$$

where $h(\tau,y)$ denotes the velocity gradient characteristically ascribable to a purely viscous non-Newtonian fluid, and $q(\tau,y)$ is a correction term necessitated by the anomalous behaviour in the wall region. The function $q(\tau,y)$ is stipulated to be identically zero outside the viscous sub-layer, i.e., at $y \gtrsim \delta_2$.

When Eq.(121) is substituted in Eq.(120), and an integration is carried out to y greater than δ_2, one obtains

$$u = \int_0^y h(\tau,y)dy + \int_0^{\delta_2} q(\tau,y)dy$$

$$= u_t + \int_0^{\delta_2} q(\tau,y)dy \qquad (122)$$

where u_t represents the velocity distribution ascribable

---

* For simplicity, the over-bar commonly used to denote time-smooth quantity has been omitted here, since the time-smooth quantities are quite obvious in the context of this section.

to the fluid in the absence of anomalous effects, i.e., $q(\tau, y) = 0$ at all y.

At $y = 0$, $u_t = 0$ and Eq.(122) becomes

$$u = u_{wt} = \int_0^{\delta_2} q(\tau, y)dy \qquad (123)$$

where u_{wt}, defined by Eq.(123), is the effective velocity at the wall in turbulent flow.

The composition of the function $q(\tau, y)$ in the laminar sub-layer $y \leq \delta_2$, shown in Fig. 3, is postulated as follows:

$$\begin{aligned} q &= g(\delta_1, \tau, y) && 0 \leq y \leq \delta_1 \\ q &= 0 && \delta_1 < y < \epsilon \\ q &= f(\tau) - h(\tau, y) && \epsilon \leq y \leq \delta_2 \end{aligned} \qquad (124)$$

The function $g(\delta_1, \tau, y)$ is the same function used in laminar flow as a correction to the velocity gradient necessitated by the anomalous behaviour under laminar flow conditions. This function has been defined earlier by Eq.(38).

The boundary points used to denote the regions specified in Eq.(124) designate the following: δ_1 is the outer edge of the laminar anomalous layer located within the viscous sub-layer; ϵ represents the boundary of the laminar sub-layer traditionally ascribed to purely viscous

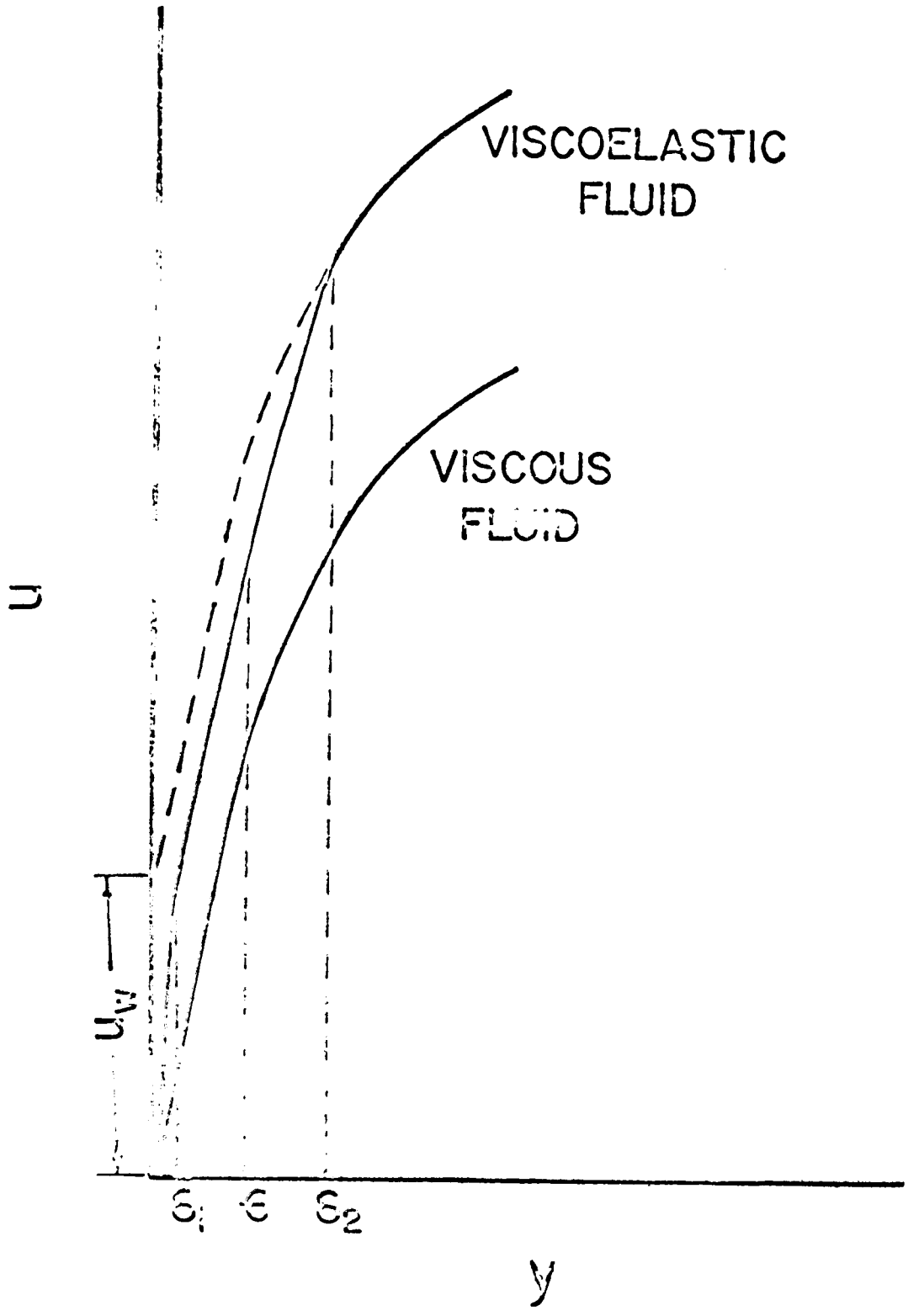

Fig. 3 Velocity Profiles Adjacent to the Tube Wall of Purely Viscous and Viscoelastic Fluids in Turbulent Flow

fluids; and finally, δ_2 is the actual laminar sub-layer thickness in the present case involving the flow of viscoelastic fluids, which is postulated to be greater than ϵ. These regions are also illustrated in Fig. 3.

In view of Eq.(124), the integral in Eq.(123) can be separated into

$$u_{wt} = \int_0^{\delta_1} g(\delta_1, \tau, y)dy + \int_\epsilon^{\delta_2} \left[f(\tau) - h(\tau, y)\right] dy \qquad (125)$$

The first integral on the right-hand side of the above equation is recognized as the effective slip velocity in laminar flow. Turning to the second integral, the lower limit may be replaced by zero since $f(\tau) = h(\tau, y)$ at $y < \epsilon$. Hence, Eq.(125) may be written as,

$$u_{wt} = u_1(\delta_2) - u_t(\delta_2) \qquad (126)$$

where

$$u_1(\delta_2) = u_w + \int_0^{\delta_2} f(\tau)dy \qquad (127)$$

and

$$u_t(\delta_2) = \int_0^{\delta_2} h(\tau, y)dy \qquad (128)$$

In other words, $u_1(\delta_2)$ represents the velocity at $y = \delta_2$ if the laminar sub-layer were to extend this distance from the wall, and $u_t(\delta_2)$ is the velocity at $y = \delta_2$ traditionally ascribed to the purely viscous non-Newtonian

fluid in turbulent flow.

For a power law fluid, in which $f(\tau) = (\tau/K)^{1/n}$, the integral in Eq.(127) becomes

$$\int_0^{\delta_2} f(\tau)dy = \frac{nR}{1+n}\left(\frac{\tau_w}{K}\right)^{1/n}\left[1 - \left(1 - \frac{\delta_2}{R}\right)^{1+1/n}\right]$$

$$= \delta_2\left(\frac{\tau_w}{K}\right)^{1/n}\left[1 - \frac{1}{2n}\left(\frac{\delta_2}{R}\right) + \frac{1-n}{6n^2}\left(\frac{\delta_2}{R}\right)^2 - \ldots\right] \tag{129}$$

Introducing the dimensionless variables u^+ and y^+, defined by

$$u^+ = u/u_* \tag{130}$$

$$y^+ = yu_*\rho/\eta_w \tag{131}$$

where the friction velocity u_* is given by

$$u_* = \sqrt{\tau_w/\rho} \quad , \tag{132}$$

in Eq.(126), and utilizing the result of Eq.(129), one obtains for the power law fluid,

$$u^+_{wt} - u^+_w = \left[\delta_2^+ - (2)^{(8-5n)/2n}\,\phi\,\delta_2^{+2} + \cdots\right] - u_t^+(\delta_2^+) \tag{133}$$

where

$$\phi = \frac{2^{\frac{8-n}{2n}}}{(1+3n)\left[Re(f)^{1-n/2}\right]^{1/n}} \qquad (134)$$

The logarithmic velocity profile developed for the power law fluid by Bogue and Metzner (3) for the turbulent core is given by :

$$u_t^+ = 2.42 \ln y^+ + I(n, Re) + e(y/R, f) \qquad y^+ > y_c^+ \qquad (135)$$

The boundary y_c^+ is the viscous sub-layer thickness including the buffer zone, which is defined by:

$$0.6\, y_c^+ = 2.42 \ln y_c^+ + I(n, Re) - 1.09 \qquad (136)$$

The function I(n,Re) and e(y/R, f) are given by

$$I(n, Re) = -5.57 \log y^+ + 0.984\sqrt{2/f} + 3.63 \qquad (137)$$

and

$$e(y/R, f) = 0.05\sqrt{2/f}\, \exp\left[\frac{-(y/R - 0.8)^2}{0.15}\right] \qquad (138)$$

respectively. Values of these two functions have been

tabulated by the original authors (3).

In the region near the wall, Krantz and Wasan (29) derived the following velocity profile for the power law fluid,

$$u_t^+ = \left[1 - \frac{\phi}{2} y^+ + \frac{1-n}{6} \phi^2 y^{+2}\right] y^+ + u_4^+ y^{+4} + u_5^+ y^{+5}$$

$$0 \leq y^+ \leq y_c^+ \qquad (139)$$

where

$$u_4^+ = \frac{3.03}{(y_c^+)^4} - \frac{1}{(y_c^+)^3} \qquad (140)$$

and

$$u_5^+ = \frac{3y_c^+ - 9.68}{5(y_c^+)^5} \qquad (141)$$

Thus, if effective slip velocity data for both laminar and turbulent flow are available, Eq.(133) in conjunction with Eqs.(135) and (139) enables one to determine, by trial and error procedure, the actual viscous sub-layer thickness δ_2^+ in the turbulent flow of a viscoelastic fluid. The method used for calculation of the anomalous layer thickness in the laminar flow has been discussed in Section 2c.

a. Evaluation of the Effective Velocity at the Wall in Turbulent Flow

Equations (122) and (123) indicate that deviations of the velocity profile for viscoelastic fluids from that proposed by Bogue and Metzner (3) for purely viscous fluids may be expected by virtue of an effective velocity at the wall, u_{wt}. Thus, the slope of the velocity profile for the viscoelastic fluid in the turbulent core will be the same as predicted by Eq.(135) except that it will be shifted linearly upward in a plot of u^+ versus y^+ (for a particular n and Re value) by an amount u_{wt}^+. Therefore, if the shift in the velocity profile from that predicted by Eq.(135) is designated by ΔB, then the effective velocity at the wall is simply

$$u_{wt} = u_* \Delta B \qquad (142)$$

Friction factor-Reynolds number correlations are also amenable to evaluation of the effective velocity at the wall in turbulent flow. The Dodge and Metzner expression, Eq.(119), relating the friction factor and Reynolds number for the turbulent flow of purely viscous pseudoplastic fluids in circular pipes is

$$\frac{1}{\sqrt{f}} = \frac{4.0}{n'^{0.75}} \log\left[Re\,(f)^{1-n'/2}\right] - \frac{0.40}{n'^{1.2}} \qquad (143)$$

The same expression is used for viscoelastic fluids exhibiting effective slip effects with the consequence that the relevant friction factor and Reynolds number expressions are now given by

$$f = \frac{2\tau_w}{\rho(\langle u\rangle - u_{wt})^2} = \frac{2u_*^2}{(\langle u\rangle - u_{wt})^2} \qquad (144)$$

and

$$Re = \frac{D^{n'}(\langle u\rangle - u_{wt})^{2-n'}\rho}{8^{n'-1}K'} \qquad (145)$$

The physical parameters n' and K' for a circular tube are determined from laminar flow measurements using Eqs.(94) and (95).

Equation (143) may be expanded, utilizing Eq.(144), and rewritten in the following form to give the effective velocity at the wall in turbulent flow.

$$u_{wt}^{+} = \frac{u_{wt}}{u_*} = \sqrt{2}\left\{\frac{1}{\sqrt{f'}} - \frac{4.0}{n'^{0.75}} \log\left[Re'(f')^{1-n'/2}\right] + \frac{0.40}{n'^{1.2}}\right\} \qquad (146)$$

where f' and Re' are the conventional friction factor and Reynolds number respectively without the effective velocity u_{wt}.

Hence, the effective velocity at the wall in turbulent flow can be readily evaluated from the deviation between the measured friction factor f' and the corresponding value yielded by the unmodified Dodge-Metzner correlation.

6. Expansion-Contraction Behaviour of Non-Newtonian Jets

The measurement of the expansion of a jet of fluid issuing from a capillary is a convenient means of measuring normal stresses of viscoelastic fluids at high shear rates. The purpose of this investigation is to extend the applicability of the previous analyses of Metzner and colleagues, restricted to circular and slit shaped jets (67), to jets of arbitrary cross section. The anomalous behaviour at the solid-fluid interface is also taken into consideration.

The following assumptions concerning the physical problem, involved in the previous developments of Metzner and colleagues (39,40,58), are also made in the present analysis:

(1) Flow is steady, laminar and isothermal

(2) The L/r_H ratio of the tube is sufficiently great so that the velocity profile at the exit section of the tube is characteristic of the steady state shear stress-shear rate relationship of the fluid ($L/r_H > 800$)

(3) Fluid is incompressible

(4) Gravitational effects and drag of air on jet are insignificant, valid at sufficiently high jet velocities ($Re > 150$)

(5) Interfacial and surface tension effects at tube exit and in jet are negligible, also valid at high jet

velocities

The relationship obtained when the net thrust of the fluid issuing from a tube is equated to the difference between the total momentum of the fluid leaving the tube and the tensile force, exerted on the fluid at the exit section of the tube is

$$T = \iint \rho u^2 \, dA - \iint \pi_{11} \, dA \tag{147}$$

Here, π_{11} denotes the normal component of the total stress tensor in the axial direction. The total stress, π, is related to the isotropic pressure and to the deviatoric tensor by the equation

$$\pi = - pI + \tau \tag{148}$$

where I is the unit tensor, τ is the deviatoric tensor and p is the isotropic pressure given by

$$p = - \frac{1}{3} \operatorname{tr} \pi = - \frac{1}{3} (\pi_{11} + \pi_{22} + \pi_{33}) \tag{149}$$

The thrust of the jet T can be determined by direct measurement (18,57) or established from measurements of the relation size of the jet. The relationship is obtained beginning with the expression for the thrust of the jet,

$$T = A_j \rho u_j^2 \tag{150}$$

which, when combined with the equation of continuity,

$$A_j \rho u_j = A \rho \langle u \rangle \tag{151}$$

becomes

$$T = A_j \rho \left(\frac{A}{A_j}\right)^2 \langle u \rangle^2 \tag{152}$$

The specific thrust is thus readily determined from a knowledge of the relative size of the jet by the simple relationship:

$$\frac{T}{A} = \rho \left(\frac{A}{A_j}\right) \langle u \rangle^2 \tag{153}$$

Hence, a single analysis of the extrusion problem, in terms of T/A as suggested by Harris (17,18), suffices also for the description of the situation relating to the relative jet size.

Equation (147) may be rewritten in terms of average quantities as follows:

$$T/A = \rho \langle u^2 \rangle - \langle \pi_{11} \rangle \tag{154}$$

The contour integrated average effective velocity at the tube wall, $\bar{u}_w$, characterizing the anomalous behaviour along the circumference of the wall, is introduced by the expansion of the first term in the right-hand side of Eq.(154) according to :

$$\rho\langle u^2\rangle = \rho\left[\langle(u - \bar{u}_w)^2\rangle - 2\bar{u}_w(\langle u\rangle - \bar{u}_w) + \bar{u}_w^2\right] \qquad (155)$$

Thus, Eq.(154) yields, after some rearrangements,

$$\tau_w = \rho\langle(u - \bar{u}_w)^2\rangle - \langle\pi_{11}\rangle \qquad (156)$$

where T_w is defined as

$$T_w = \frac{T}{A} - 2\rho\bar{u}_w(\langle u\rangle - \bar{u}_w) - \rho\bar{u}_w^2 \qquad (157)$$

The application of the area averaging operation, defined by the operator given by Eq.(16), to the right-hand side of Eq.(156) leads to

$$\frac{\bar{\tau}_w^{\xi-1}\,T_w}{(\xi-1)} = \rho\int_0^{\bar{\tau}_w}(u - \bar{u}_w)^2\tau^{\xi-2}\,d\tau - \int_0^{\bar{\tau}_w}\pi_{11}\tau^{\xi-2}\,d\tau \qquad (158)$$

Equation (158) is of the same form and directly

reducible to the individual results of Metzner et al (39) for the circular and slit-shaped dies, by substitution of the appropriate values for the geometric aspect factors in the equation (viz., $\xi = 3$ and $\xi = 2$, respectively) and setting $\bar{u}_w$ equal to zero.

Equation (158) is of the form $\Gamma_w = f(\bar{\tau}_w, r_H, \xi)$. Taking the partial derivative of Eq.(158) with respect to $\bar{\tau}_w$, at constant values of the aspect factor and the hydraulic radius, gives the following:

$$(\bar{\pi}_{11})_w = \frac{\rho}{\bar{\tau}_w^{\xi-2}} \frac{\partial I'}{\partial \bar{\tau}_w} - \Gamma_w \left[1 + \frac{1}{\xi - 1} \frac{\partial \ln \Gamma_w}{\partial \ln \bar{\tau}_w} \right] \qquad (159)$$

where I' has been used to denote the integral

$$I' = \int_0^{\bar{\tau}_w} (u - \bar{u}_w)^2 \tau^{\xi-2} \, d\tau \qquad (160)$$

In accordance with the generalization procedure, π_{11} evaluated at $\bar{\tau}_w$ has been designated as $(\bar{\pi}_{11})_w$, although it is not essential to the present analysis to associate a physical significance to this quantity.

Introduction of the physical parameter n^*, given by Eq.(94), in Eq.(159) yields

$$(\bar{\pi}_{11})_w = \frac{\rho}{\bar{\tau}_w^{\xi-2}} \frac{\partial I'}{\partial \bar{\tau}_w} - \Gamma_w \left[1 + \frac{1}{(\xi - 1)n^*} \frac{\partial \ln \Gamma_w}{\partial \ln 2(\langle u \rangle - \bar{u}_w)/r_H} \right] \qquad (161)$$

The quantity $\partial I'/\partial \bar{\tau}_w$ in the above equation is determined by taking the partial derivative of Eq.(160) with respect to $\bar{\tau}_w$ using Leibnitz formula as follows:

$$\partial I'/\partial \bar{\tau}_w = 2\int_0^{\bar{\tau}_w} \tau^{\xi-2}(u - \bar{u}_w)\frac{\partial(u - \bar{u}_w)}{\partial \bar{\tau}_w}\, d\tau \qquad (162)$$

The partial derivative inside the integral of Eq.(162) can be evaluated with the help of Eq.(B-6) in Appendix B as follows:

$$\frac{\partial(u - \bar{u}_w)}{\partial \bar{\tau}_w} = \frac{r_H}{2a}\frac{\partial}{\partial \bar{\tau}_w}\left[\frac{1}{\bar{\tau}_w}\int_\tau^{\bar{\tau}_w} f(\tau)d\tau\right]$$

$$= \frac{1}{\bar{\tau}_w}\left[\frac{r_H f(\bar{\tau}_w)}{2a} - (u - \bar{u}_w)\right] \qquad (163)$$

Substitution of the above result in Eq.(162) gives

$$\partial I'/\partial \bar{\tau}_w = \frac{r_H \bar{\tau}_w^{\xi-2}}{a(\xi - 1)}(\langle u\rangle - \bar{u}_w)f(\bar{\tau}_w) - \frac{2}{\bar{\tau}_w}\int_0^{\bar{\tau}_w}(u - \bar{u}_w)^2\tau^{\xi-2}d\tau \qquad (164)$$

Replacing the function $f(\bar{\tau}_w)$ by Eq.(105) in the above equation finally yields

$$\partial I'/\partial \bar{\tau}_w = \frac{\bar{\tau}_w^{\xi-2} r_H^2}{2(\xi - 1)}\left[\frac{(\xi n^* + 1)}{n^*}\right]\left[\frac{2(\langle u\rangle - \bar{u}_w)}{r_H}\right]^2 - \frac{2}{\bar{\tau}_w}\int_0^{\bar{\tau}_w}(u-\bar{u}_w)^2\tau^{\xi-2}d\tau \qquad (165)$$

By combining Eq.(165) with Eq.(161), one obtains the desired expression for $(\bar{\pi}_{11})_w$:

$$(\bar{\pi}_{11})_w = \rho(\langle u\rangle - \bar{u}_w)^2 \left[\frac{2(\xi n^* + 1)}{n^*(\xi - 1)} - 2\int_0^1 \left[\frac{u - \bar{u}_w}{\langle u\rangle - \bar{u}_w}\right]^2 \left(\frac{\tau}{\bar{\tau}_w}\right)^{\xi - 2} d\left(\frac{\tau}{\bar{\tau}_w}\right)\right]$$

$$- \Gamma_w \left[1 + \frac{1}{n^*(\xi - 1)} \frac{\partial \ln \Gamma_w}{\partial \ln \frac{2(\langle u\rangle - \bar{u}_w)}{r_H}}\right] \qquad (166)$$

If one defines a function A_r' by

$$A_r' = \frac{\langle (u - \bar{u}_w)^2\rangle}{(\langle u\rangle - \bar{u}_w)^2} \qquad (167)$$

and uses the averaging operator defined by Eq.(16), then Eq.(166) becomes

$$(\bar{\pi}_{11})_w = \frac{2\rho(\langle u\rangle - \bar{u}_w)^2}{(\xi - 1)}\left[(\xi + \frac{1}{n^*}) - A_r'\right] - \Gamma_w \left[1 + \frac{1}{\xi - 1}\frac{\partial \ln \Gamma_w}{\partial \ln \bar{\tau}_w}\right]$$

(168)

The normal stress $(\bar{\pi}_{11})_w$ can be shown to be equal to the deviatoric normal stress difference $(\bar{\pi}_{11} - \bar{\pi}_{22})_w$ as follows:

For the flow of a viscoelastic fluid in a circular pipe, the radial component of the equation of motion in cylindrical coordinates becomes

$$\frac{\partial \pi_{22}}{\partial r} + \frac{\pi_{22} - \pi_{33}}{r} = 0 \qquad (169)$$

or, in terms of the isotropic pressure and the deviatoric stresses,

$$-\frac{\partial p}{\partial r} + \frac{\partial \tau_{22}}{\partial r} + \frac{\tau_{22} - \tau_{33}}{r} = 0 \qquad (170)$$

Integrating the above equation from the centerline to the tube wall at the tube end, one gets

$$p(R,L) = p(0,L) + (\tau_{22})_w + \int_0^R (\tau_{22} - \tau_{33}) d \ln r \qquad (171)$$

where the radial normal stress at the centerline, $(\tau_{22})_o$, is assumed zero; p(R,L) is the hydrostatic pressure at the wall, and p(0,L) is the centerline gage pressure at the tube end.

From the definition of the stress tensor, Eq.(148), one finds

$$(\pi_{11})_w = -p(R,L) + (\tau_{11})_w \qquad (172)$$

which, when combined with Eq.(171) gives

$$(\pi_{11})_w = (\tau_{11} - \tau_{22})_w - \left[p(0,L) + \int_0^R (\tau_{22} - \tau_{33}) d \ln r\right] \qquad (173)$$

If the Weissenberg hypothesis is invoked, that is, $\tau_{22} = \tau_{33}$, and the centerline gage pressure p(0,L) is assumed zero, then Eq.(173) becomes simply

$$(\pi_{11})_w = (\tau_{11} - \tau_{22})_w \tag{174}$$

Therefore, for flow of viscoelastic fluids in circular pipes, Eq.(173), after substituting $\xi = 3$ and $n^* = n'$, becomes,

$$(\tau_{11} - \tau_{22})_w = \rho(\langle u \rangle - \bar{u}_w)^2 \left[\frac{3n'+1}{n'} - A_r'\right] - \Gamma_w \left[1 + \tfrac{1}{3} \frac{\partial \ln \Gamma_w}{\partial \ln \bar{\tau}_w}\right] \tag{175}$$

The quantity $(\xi + 1/n^*)$ in Eq.(168), which for a power law fluid with constant flow behaviour index n becomes simply $(\xi + 1/n)$, is found with the aid of Eq. (97) to be given by the following expression in the general case,

$$(\xi + 1/n^*) = \frac{\bar{\tau}_w^{\xi} \, f(\bar{\tau}_w)}{\int_{\tau_y}^{\bar{\tau}_w} \frac{\tau^{\xi}}{\eta} \, d\tau} \tag{176}$$

For an Ellis fluid, one finds

$$(\xi + 1/n^*)_{Ellis} = \frac{1 + (\bar{\tau}_w/\tau_{\frac{1}{2}})^{\alpha-1}}{\frac{1}{1+\xi} + \frac{1}{\alpha+\xi}\left(\frac{\bar{\tau}_w}{\tau_{\frac{1}{2}}}\right)^{\alpha-1}} \tag{177}$$

a. Determination of the Tube to Jet Area Ratio

Equations (153) and (154) are combined to obtain the ratio of the cross-sectional area of the tube to that of the issuing jet.

$$A_r = \frac{A}{A_j} = \frac{\langle u^2 \rangle}{\langle u \rangle^2} - \frac{\langle \pi_{11} \rangle}{\rho \langle u \rangle^2} \qquad (178)$$

The area ratio A_r can be expanded to yield

$$A_r = A_r'(1 - s')^2 + 2s' - s'^2 - \frac{\langle \pi_{11} \rangle}{\rho \langle u \rangle^2} \qquad (179)$$

where $s' = \bar{u}_w/\langle u \rangle$, and A_r' is defined by Eq.(167). In arriving at the above equation, $\langle u^2 \rangle$ in the first term of the right-hand side of Eq.(178) has been expanded according to Eq.(155), and $\langle u \rangle^2$ in the denominator of the same term replaced by

$$\langle u \rangle^2 = \frac{(\langle u \rangle - \bar{u}_w)^2}{(1 - s')^2} \qquad (180)$$

The quantity A_r' is the value of A_r for a fluid not exhibiting anomalous behaviour along the solid boundary and without normal stresses, as seen in Eq.(179)

The quantity $\langle \pi_{11} \rangle$ can be determined with the help of the area averaging operator defined by Eq.(16), provided $(\bar{\pi}_{11})_w$ versus $\bar{\tau}_w$ data determined specifically

for the geometry in question is known. In the absence of such data, it appears that a reasonable approximation would be to use π_{11} versus τ data established from circular capillary measurements.

The quantity A_r' is readily found with the help of Eqs.(11), (16) and (B-6) to be given by

$$A_r' = \frac{(\xi - 1)\bar{\tau}_w^{\xi-1} \int_0^{\bar{\tau}_w} \tau^{\xi-2} d\tau \left[\int_\tau^{\bar{\tau}_w} f(\tau) d\tau \right]^2}{\left[\int_0^{\bar{\tau}_w} \tau^{\xi-1} f(\tau) d\tau \right]^2} \qquad (181)$$

In Appendix F, A_r' can be shown, by successive interchanges in the order of integration, to be given by the following more convenient equation:

$$A_r' = \frac{2\,\bar{\tau}_w^{\xi-1} \int_0^{\bar{\tau}_w} f(\tau) d\tau \int_0^{\tau} \tau^{\xi-1} f(\tau) d\tau}{\left[\int_0^{\bar{\tau}_w} \tau^{\xi-1} f(\tau) d\tau \right]^2} \qquad (182)$$

For an Ostwald-de Waele (power law) fluid, in which $f(\tau) = (\tau/K)^{1/n}$, one finds that A_r' is given by

$$(A_r')_{\substack{\text{power} \\ \text{law}}} = \frac{2(1 + n\xi)}{2 + n(1 + \xi)} \qquad (183)$$

It is interesting to note that the extremum values of the function given by Eq.(183) are $A_r' = 2$ at $n = -1$, and $A_r' = 1$ at $n = 0$ and at $\xi = 1$. Of course, the value of minus one for the flow behaviour index (hence, the value of 2 for A_r') is inadmissible. The lowest known possible value of ξ is two for the parallel plate geometry. Hence, the minimum value of A_r' is unity, corresponding to the case of infinite pseudo-plasticity at n equal to zero which denotes a flat velocity profile or plug flow. This result is in agreement with the result expected intuitively.

At the infinite dilatancy ($n = \infty$) condition, depicting the triangular velocity profile, A_r' becomes $2/(1 + 1/\xi)$, with the unattainable asymptotic value of two (independent of n) as the limiting value for large values of the aspect factor ξ.

For an Ellis fluid, $f(\tau) = \tau/\eta_o \left[1 + (\tau/\tau_{\frac{1}{2}})^{\alpha-1}\right]$, A_r' is found to be

$$(A_r')_{Ellis} = \frac{2\left[\frac{\alpha+\xi}{2\alpha+\xi+1}\left(\frac{\bar{\tau}_w}{\tau_{\frac{1}{2}}}\right)^{2(\alpha-1)} + \frac{(\alpha+\xi)(\alpha+2\xi+1)}{(1+\xi)(\alpha+\xi+2)}\left(\frac{\bar{\tau}_w}{\tau_{\frac{1}{2}}}\right)^{\alpha-1} + \frac{(\alpha+\xi)^2}{(1+\xi)(3+\xi)}\right]}{\left[\left(\frac{\bar{\tau}_w}{\tau_{\frac{1}{2}}}\right)^{\alpha-1} + \frac{\alpha+\xi}{1+\xi}\right]^2} \qquad (184)$$

The result obtained for a Newtonian fluid by setting α equal to unity in Eq.(184) is

$$(A_{r'})_{Newt.} = \frac{2(1+\xi)}{3+\xi} \tag{185}$$

which is seen to be in agreement with the result obtained by setting n = 1 in Eq.(183), as expected.

IV - RESULTS AND DISCUSSION

The method proposed for prediction of non-Newtonian flow in arbitrary flow geometries was tested by comparing the results with the available analytical solutions and experimental data for various fluid models and flow geometries. The results of the comparisons made with the solutions for the flow of power law, Bingham plastic and Rabinowitsch fluids through concentric annuli, rectangular and elliptical ducts have been published elsewhere (24).

The disagreement was generally found to be less than 5% for almost all geometries and fluid models. A greater discrepancy was found in the annular flow region with the aspect ratio k = 0.01 with most of the non-Newtonian fluids. The error in this region could be partly attributed to an unavoidable magnification of errors inherent in calculations associated with this region and to the approximation involved in taking the contour integrated average quantities. Fortunately, from the practical standpoint, one does not usually encounter annuli with this peculiarly small aspect ratio.

A few additional comparisons are made with the recently published solutions on non-Newtonian flow in concentric annuli and triangular ducts which give additional support to the reliability of the present method.

Figure 4 shows a comparison between the results predicted by the present method and the recently published analytical solution of McEachern (34) plotted as the dimensionless flow rate versus dimensionless pressure drop for the flow of an Ellis fluid ($\alpha = 2$) in concentric annuli, with the aspect ratio k as the parameter. Figure 5 is a similar plot with α as the parameter at $k = 0.5$. It is found that the greatest discrepancy occurs at lower k and higher α values. The same result was also found (24) with other non-Newtonian fluid models. For example, at $k = 0.01$ and $\alpha = 2$, the average deviation between the present method and that of McEachern is about 8%; however, at the same value of α but at $k = 0.5$, the agreement is almost perfect.

Figures 6 and 7 compare predictions by the present method with the solutions and experimental data of Mitsuishi et al (42) for the flow of power law fluids (CMC solutions) through equilateral and right isosceles triangular ducts, respectively. The disagreement between the present method has been found to be always less than 10% over the entire range of shear rate. Although the experimental data are not explicitly shown on the figures, it has been found that some of the experimental points actually lie closer to the lines depicting the present analysis, indicating better agreement with the actual experimental data.

Fig. 4 Dimensionless flow rate versus dimensionless pressure drop for the flow of an Ellis fluid (α=2) in concentric annuli, with the aspect ratio k as the parameter

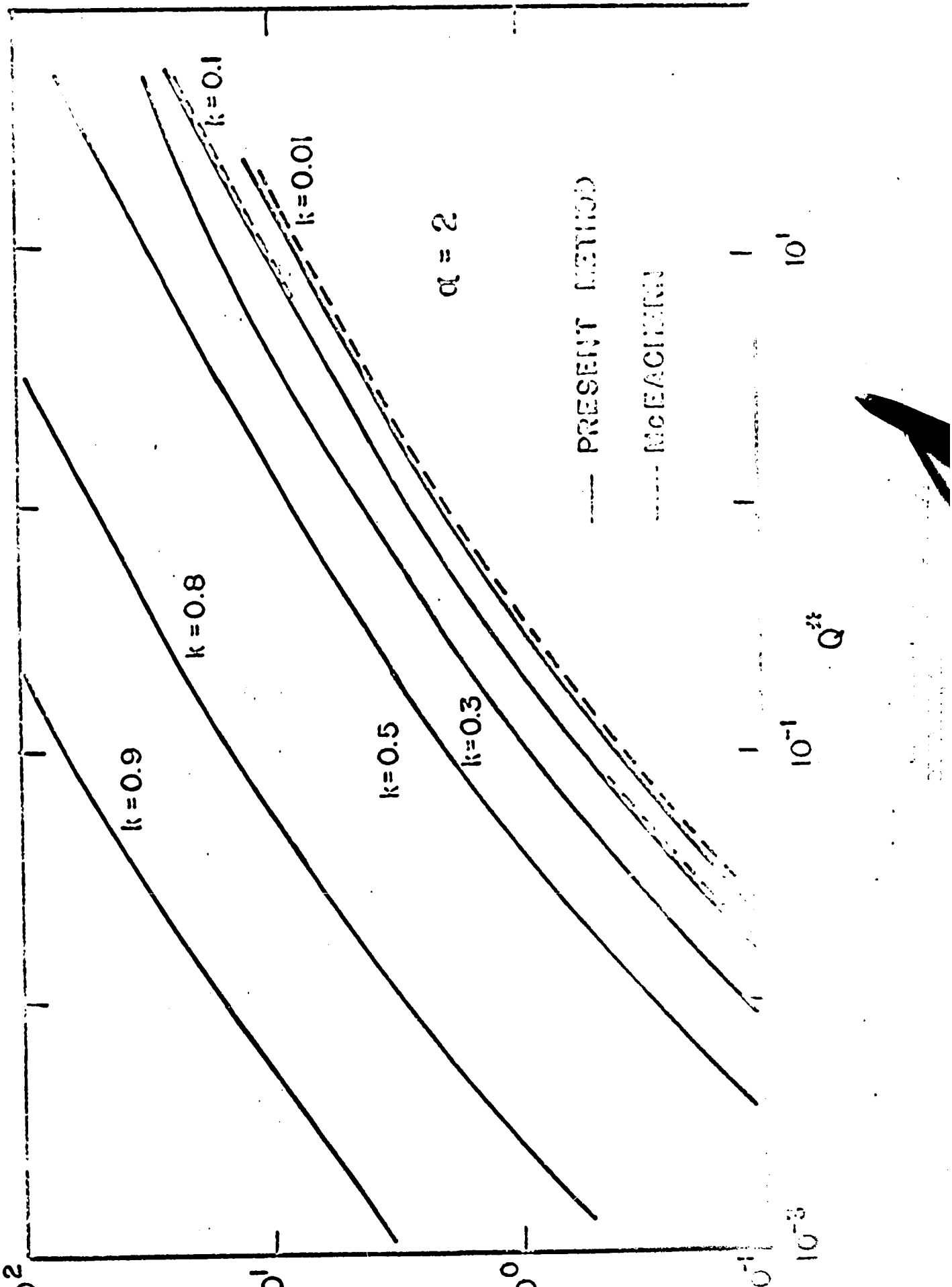

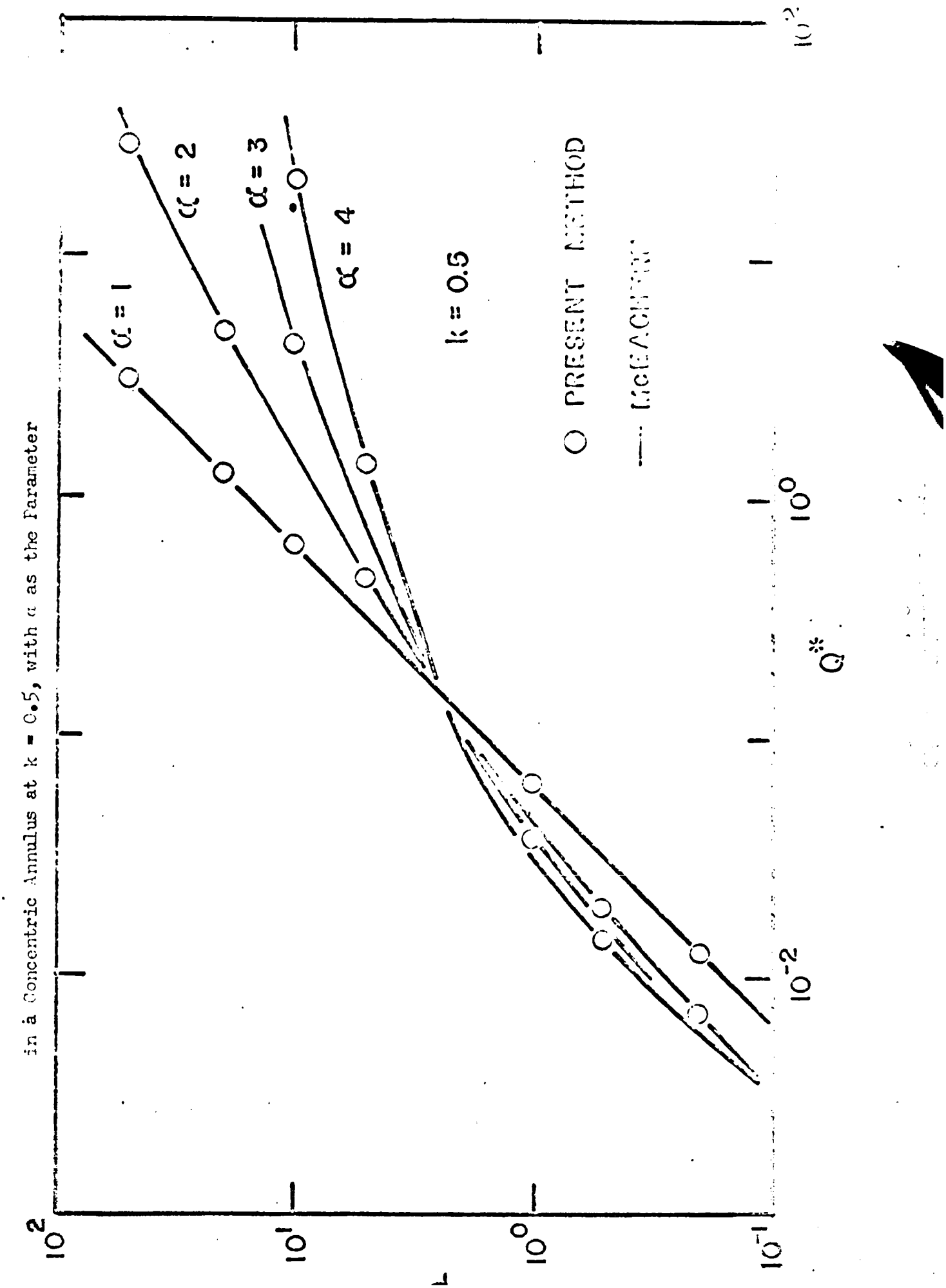

Fig. 5 Dimensionless Flow Rate Versus Dimensionless Pressure Top for the Flow of This Fluids in a Concentric Annulus at k = 0.5, with α as the Parameter

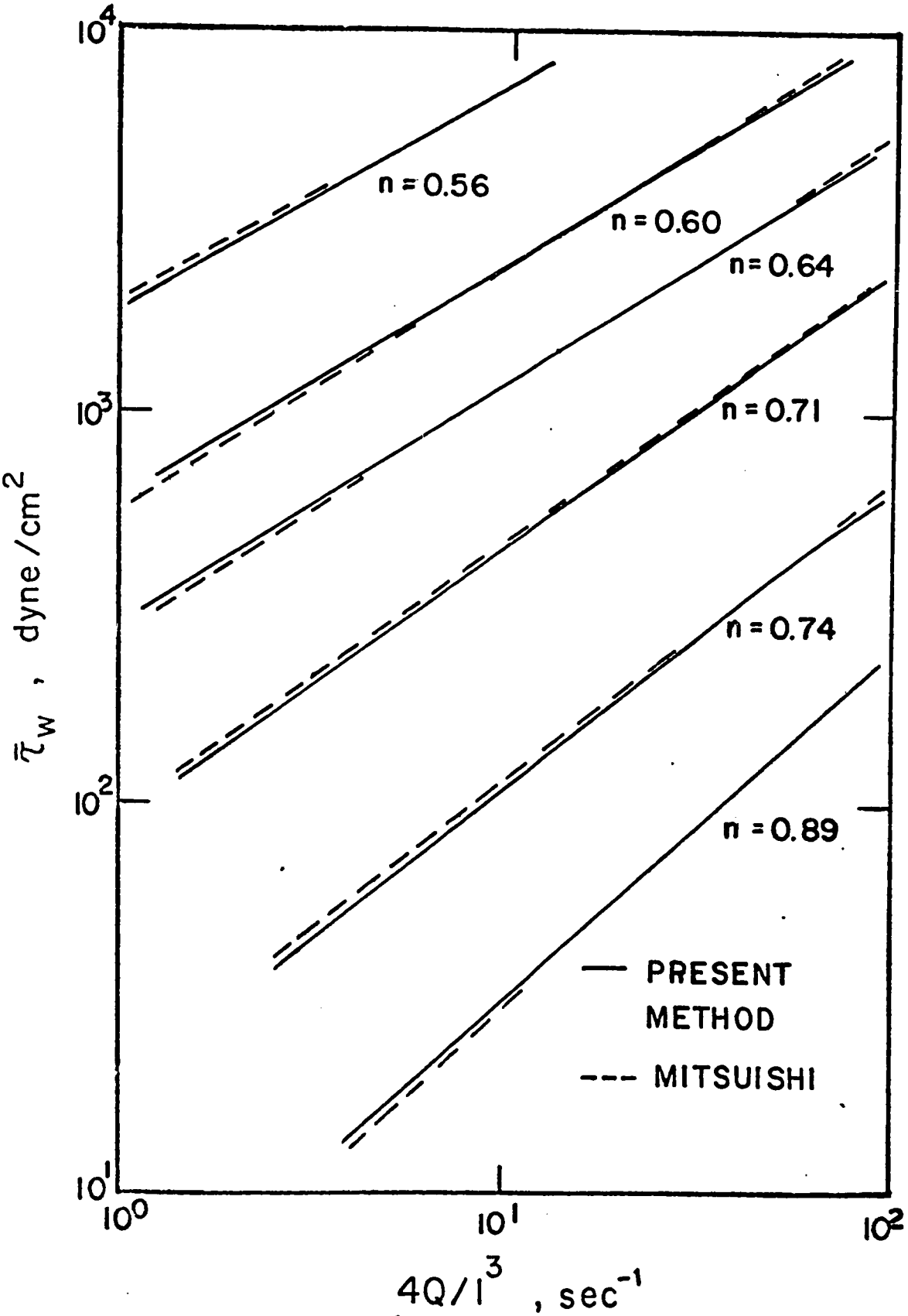

Fig. 6 Plot of $4Q/l^3$ versus $\bar{\tau}_w$ for the Flow of Power Law Fluids Through Equilateral Triangular Duct

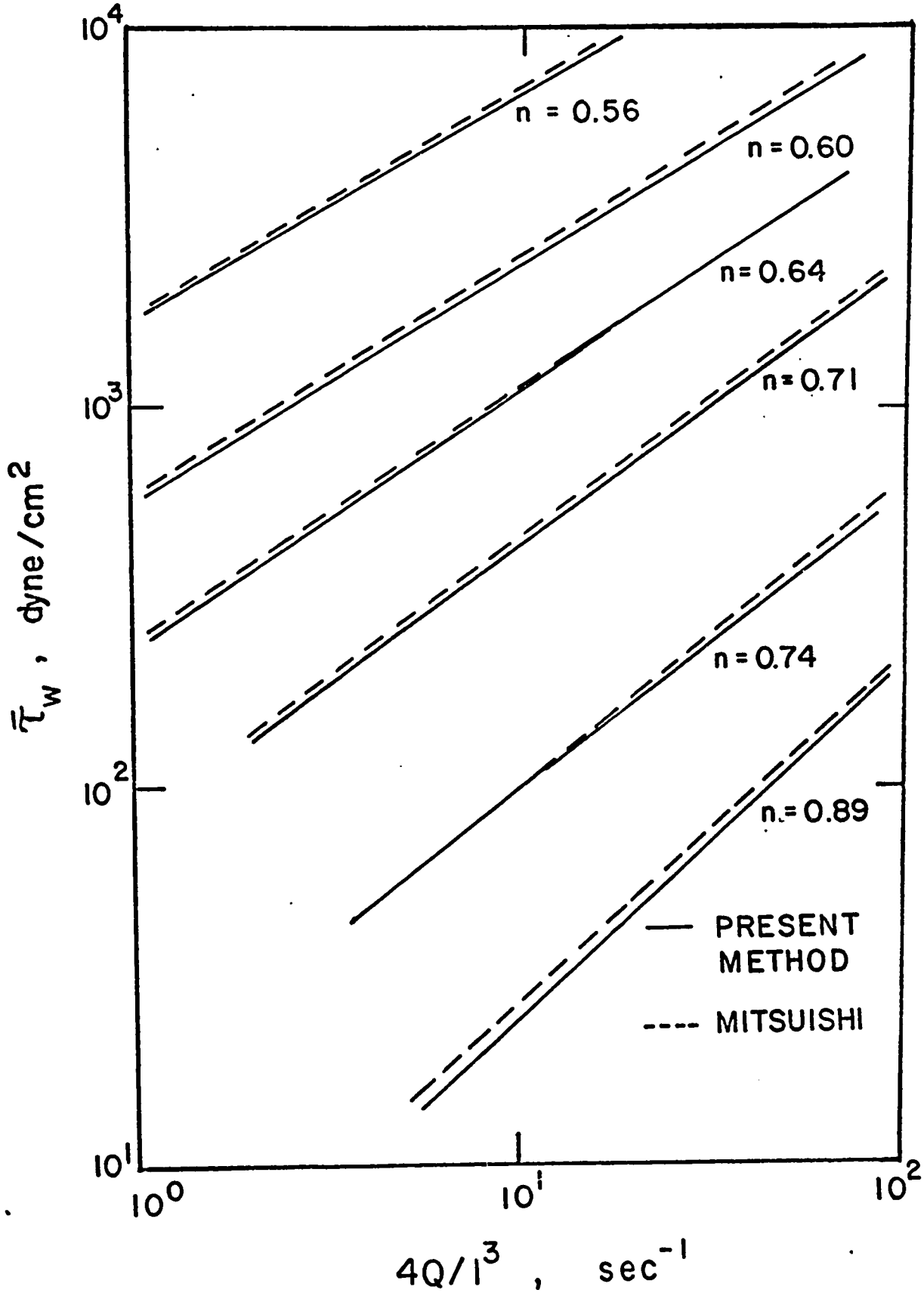

Fig. 7 Plot of $4Q/l^3$ versus $\bar{\tau}_w$ for the Flow of Power Law Fluids Through a Right Isosceles Triangular Duct

There is no available data on the flow of non-Newtonian fluids in open channels to make comparisons. However, in view of the accuracy of the proposed method in predicting the closed conduit flow, and in view of the fact that the analytical solutions for open channel flow are derived directly from the closed conduit flow solutions; it is believed that the proposed method should predict the open channel flow to the same degree of accuracy.

Therefore, the method proposed for prediction of flow rate and maximum velocity in the laminar flow of fluids through arbitrary cross sections, either closed or open, may reasonably be expected to give reliable results, well within the engineering accuracy.

The theory for the flow of fluids through packed beds and porous media has been substantiated by the experimental measurements conducted by Mr. C. J. Hsu, and the data reported by Sadowski (52). A detailed description of the experimental apparatus has been presented in a published article (26). The experimental data for various non-Newtonian fluids flowing through packed beds and capillary tubes are tabulated in Appendix C.

Four fluids were investigated in the experimental work conducted by Hsu, namely, two aqueous solutions of different concentration of each of CMC and of carbopol.

Only one set of data is discussed here, since the others were treated identically. Figure 8 shows the results of experimental measurements conducted with a 2.85% CMC solution. The uppermost curve represents the flow rate and pressure drop data for a packed bed with 0.3175 cm diameter stainless steel spheres, plotted as $2\langle u\rangle/r_H$ versus $\bar{\tau}_w$. The second curve is a similar plot of the data for the bed with 0.3967 cm diameter spheres. Since two distinct curves are obtained, an anomalous surface effect is suggested. The third curve represents the same data obtained with both packed beds plotted as $2(\langle u\rangle - \bar{u}_w)/r_H$ versus $\bar{\tau}_w$ in which the effective velocity on the surface of the particles is taken into consideration. It is seen that the two sets of data are now superimposed on a single curve as expected. The next four relatively closely spaced curves show the capillary tube viscometer data, obtained with four different diameter tubes, plotted as $2\langle u\rangle/r_H$ versus $\bar{\tau}_w$. Again, an anomalous surface effect is suggested from the data. Finally, the lowest curve shows the data for all four tubes plotted as $2(\langle u\rangle - \bar{u}_w)/r_H$ against $\bar{\tau}_w$, which are now satisfactorily described as a single curve.

From the linearity of the $2(\langle u\rangle - \bar{u}_w)/r_H$ versus $\bar{\tau}_w$ plots of the packed bed and viscometer data in Fig. 8, one sees that the fluid is successfully represented by the Ostwald-de Waele (power law) fluid model. Values of the

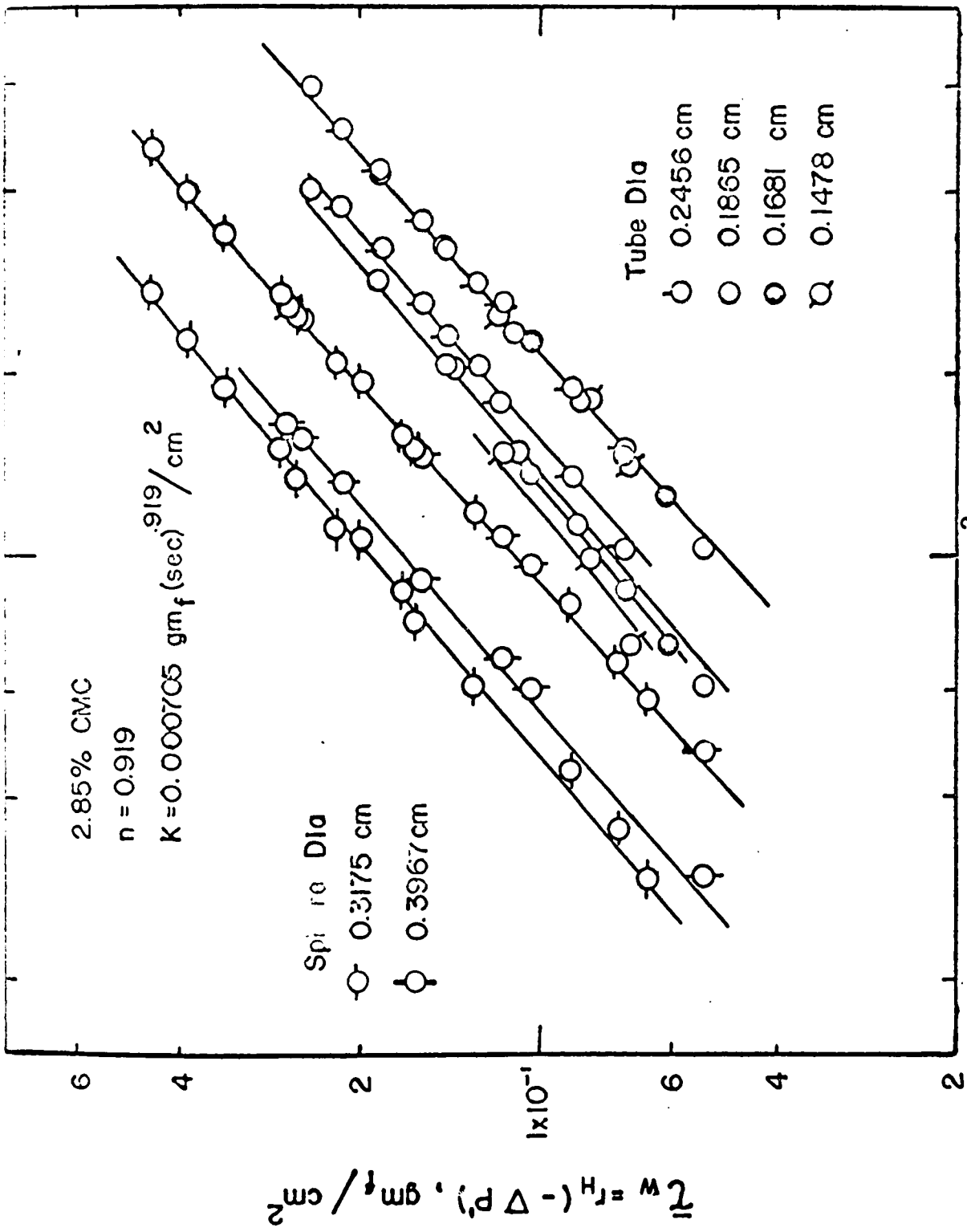

Fig. 8 Experimental Data Determined with the Flow of 2.85% CMC Solution Through Packed Beds and Capillary Tubes

fluid consistency and flow behaviour indices are indicated on the figure.

One knows from the analysis that the impermeability and aspect factors of the packed beds can be evaluated from a knowledge of the individual relationship of $2(\langle u \rangle - \bar{u}_w)/r_H$ versus $\bar{\tau}_w$ determined using the beds and capillary tubes, such as provided by Fig. 8. The data obtained with all four fluids are in concordance with the values of $k_1 = 4.8$ and $\xi = 3$. In actual fact, due to the limited amount of experimental data collected and due to inherent uncertainties in the data collected associated with experimental error, it was more expedient in this instance, particularly since reliable information provided by the work of previous investigators was also known, to assume the above values suggested by previous work and to compare the predictions with the experimental data.

Figure 9 shows the effective velocity at the solid surface as a function of $\bar{\tau}_w$ computed utilizing the data in Fig. 8 for 2.85% CMC solution. Since the effective velocity at the surface is found to be negative, the anomalous layer near the wall is more viscous, attributable to polymer adsorption and gel formation on the solid surfaces. Sadowski (52) also observed the same phenomenon experimentally although he did not attempt to treat the

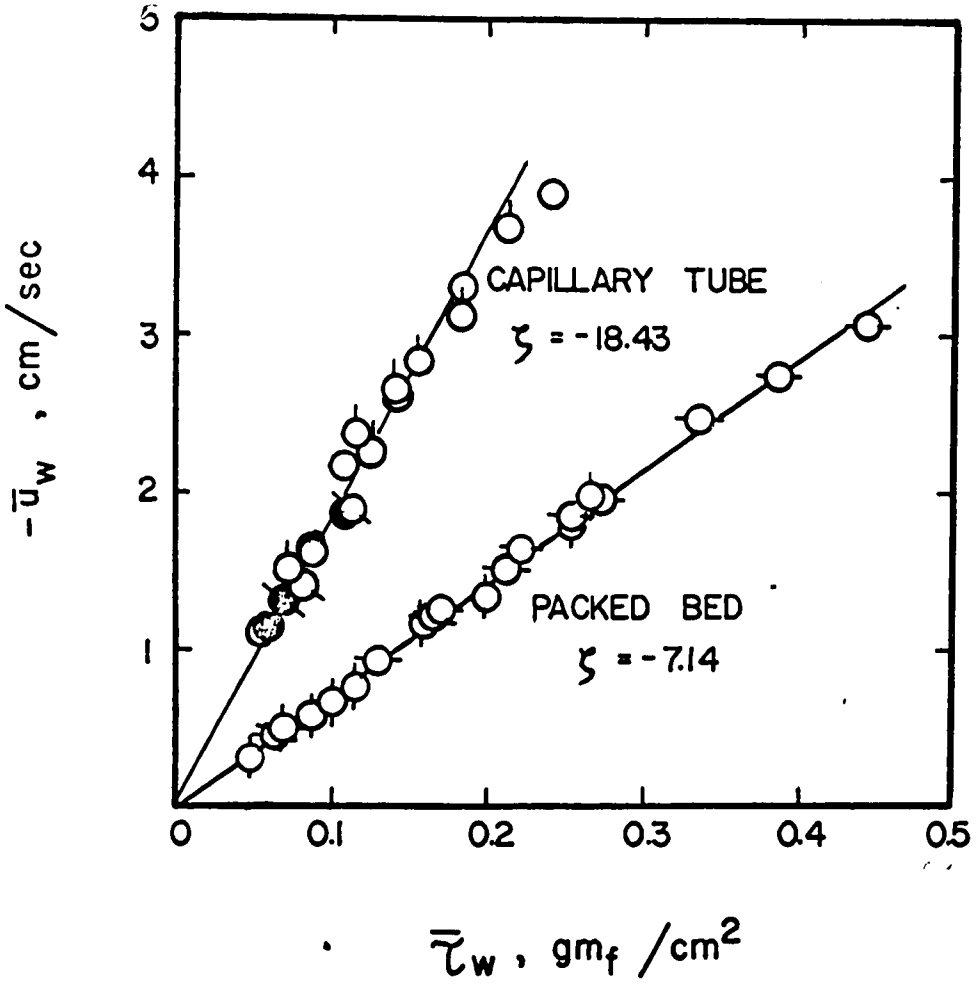

Fig. 9 Effective Velocity at the Solid Boundary as a Function of the Wall Shear Stress for 2.85% CMC Solution

problem quantitatively. Referring to Fig.9, the curves representing the $\bar{u}_w$ versus $\bar{\tau}_w$ relationships for the packed beds and the capillary tubes are linear, corresponding to constant effective slip coefficients for these cases. Values of the effective slip coefficient are tabulated in Table 1 together with the corresponding anomalous layer thickness.

Figure 10 shows all the measurements made with the capillary tubes and packed beds plotted in two separate curves as friction factor versus Reynolds number. It can be seen that all of the experimental points fall on a single line represented by $f = 16/Re$. This also illustrates the generality of Eq.(91) which as stated applies to flow channels of arbitrary cross section.

The original data of Sadowski (52) was recalculated utilizing the power law fluid model to characterize the fluid behaviour, and plotted as f versus Re as shown in Fig.11. It was found necessary to assign different values of k_1 for different packed beds used with the fluids, i.e., 4.96, 4.78 and 4.60 for the beds used with Elvanol, Carbowax, and Natrosol-2500 solutions, respectively. Although a single value of $k_1 = 5.0$ used by Sadowski in conjunction with the Ellis fluid model is also plausible in the case of the power law model, by slight adjustments of the fluid consistency and flow behaviour indices, it is felt that the fluids

Table 1 Computed Effective Slip Coefficients and Anomalous Layer Thicknesses

Solution concn. (nominal)	Capillary tubes Min. dia.=0.1478 cm		Packed beds Min. D_e=0.1297 cm	
	$-\zeta$ cm^3/gm_f-sec	δ_1 cm x 10^{-3}	$-\zeta$ cm^3/gm_f-sec	δ_1 cm x 10^{-3}
2% CMC	11.8	3.9	6.5	2.1
2.85% CMC	18.4	6.8	7.14	2.6
0.35% Carbopol*	47.4	4.22-5.8	25.0	2.0-3.3
0.3% Carbopol	22.3	4.0 - 5.9	14.0	2.0-3.4

* From the amount of residue remaining, it was suspected that the concentration of dissolved carbopol in the actual fluid was somewhat less, perhaps even less than in the nominal 0.3% carbopol solution. The physical property determinations appear to bear this out.

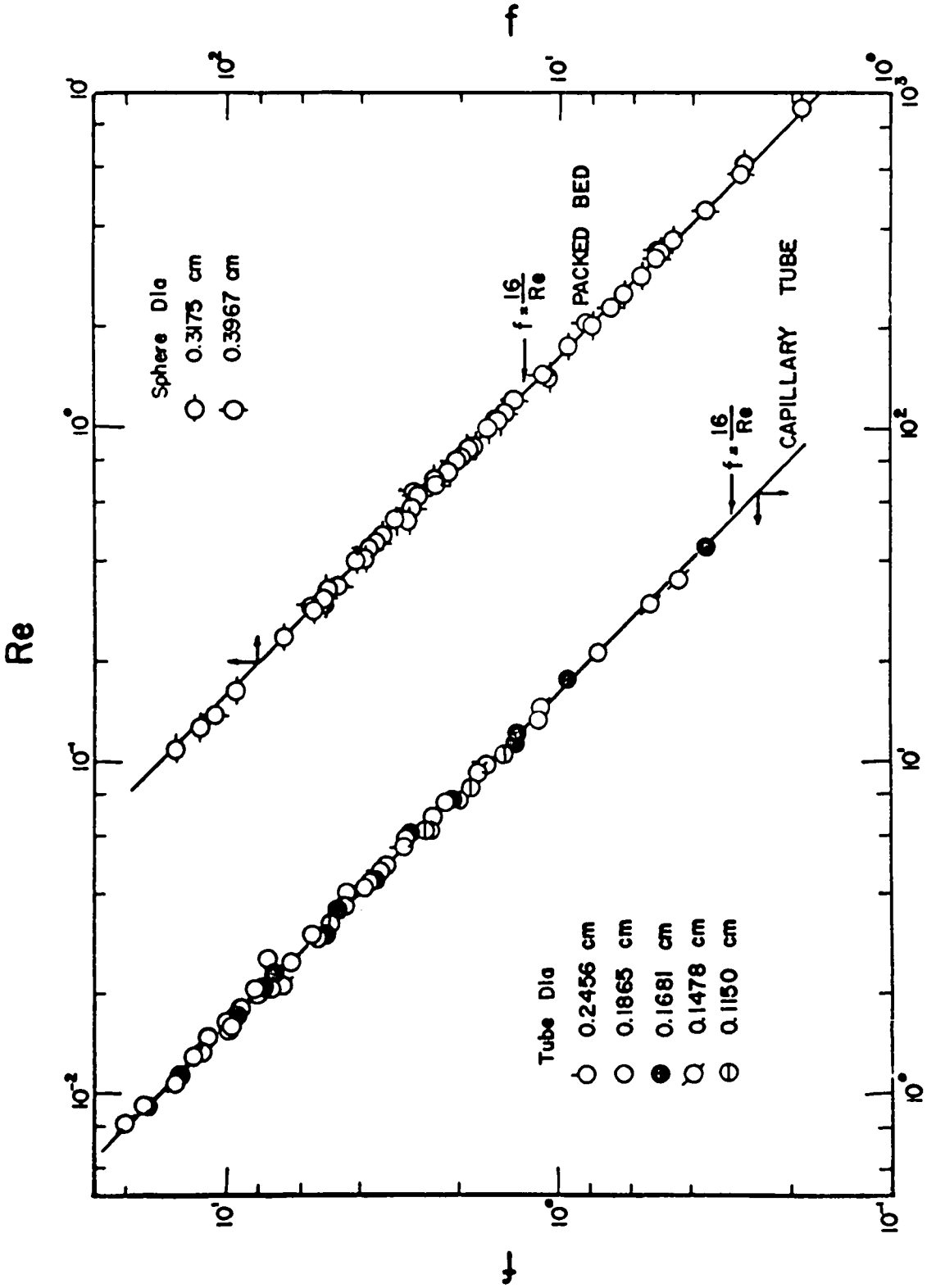

Fig. 10 Friction Factor-Reynolds Number Plot of Experimental Data Determined with CMC and Carbopol Solutions

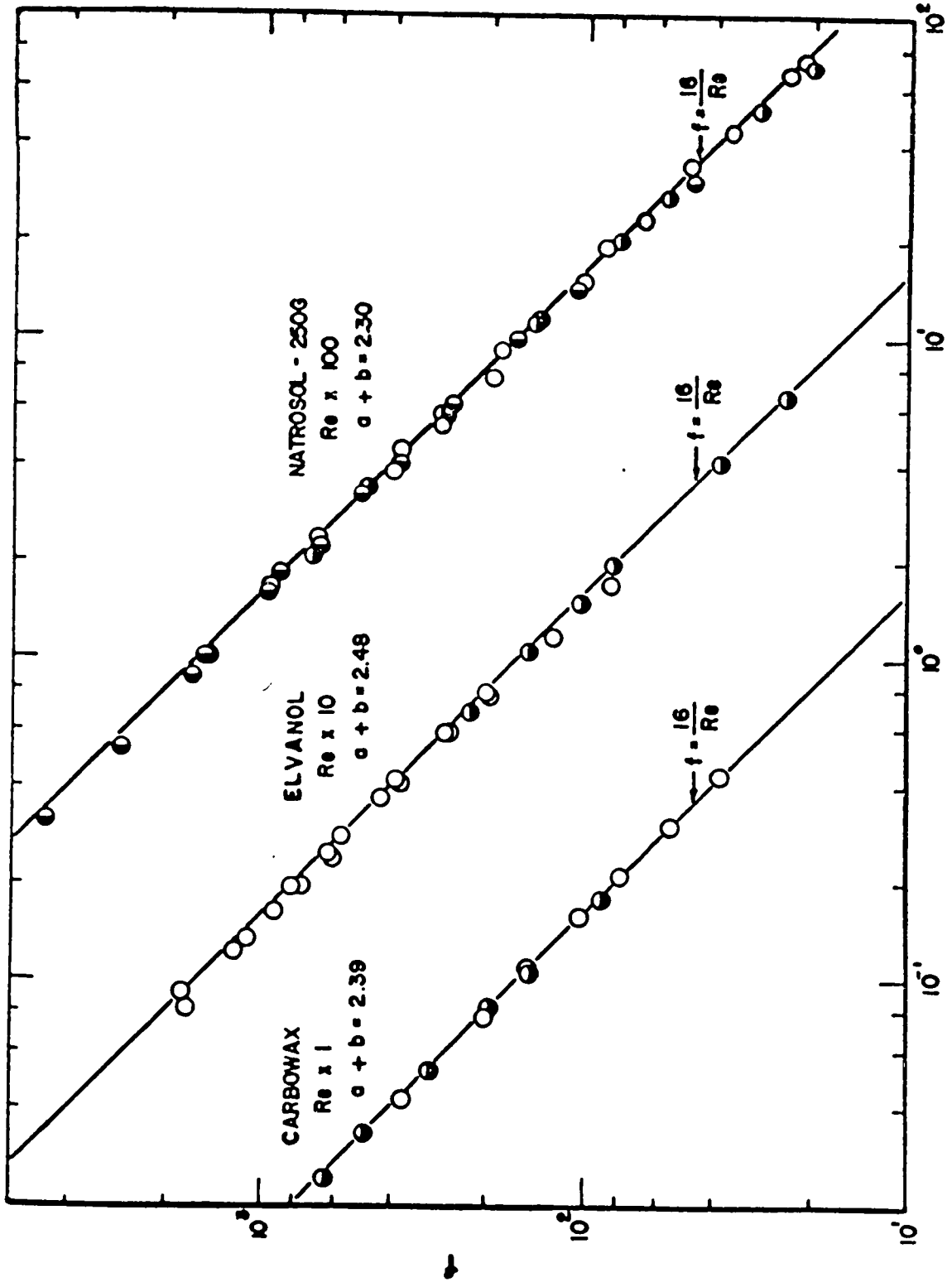

Fig. 11 Plot of Sadowski's Data Utilizing Power Law Model for Representation of the Fluids

are best represented without modification of these parameters, particularly since the variations in k_1 values are within the range usually observed with Newtonian fluids. It is also conceivable that the differences in the k_1 values reflect in some measure small surface effects due to polymer adsorption-gel formation, particularly in the case of the Natrosol-250G solution.

Figure 12 shows a friction factor - Reynolds number plot of Sadowski's data with the high molecular weight Natrosol-250H solutions. The value of k_1 equal to 5.0 and the physical parameters determined by Sadowski (52) for the Ellis fluid model were used in the calculation. However, whereas Sadowski introduced a viscoelastic number, containing a characteristic time parameter of the fluid to correlate the data, Fig. 12 was calculated by the present method allowing for the existence of an anomalous layer. Negative effective velocities on the solid surfaces were also obtained using Sadowski's data, compatible with polymer adsorption-gel formation, observed experimentally by the original author (52).

The theory of non-Newtonian filtration has been subjected to preliminary tests by the experimental work conducted by Mr. A. R. K. Rao. The detailed description of the experimental procedure and results has been presented in a published paper (27). The actual experimental data will be tabulated in Rao's thesis.

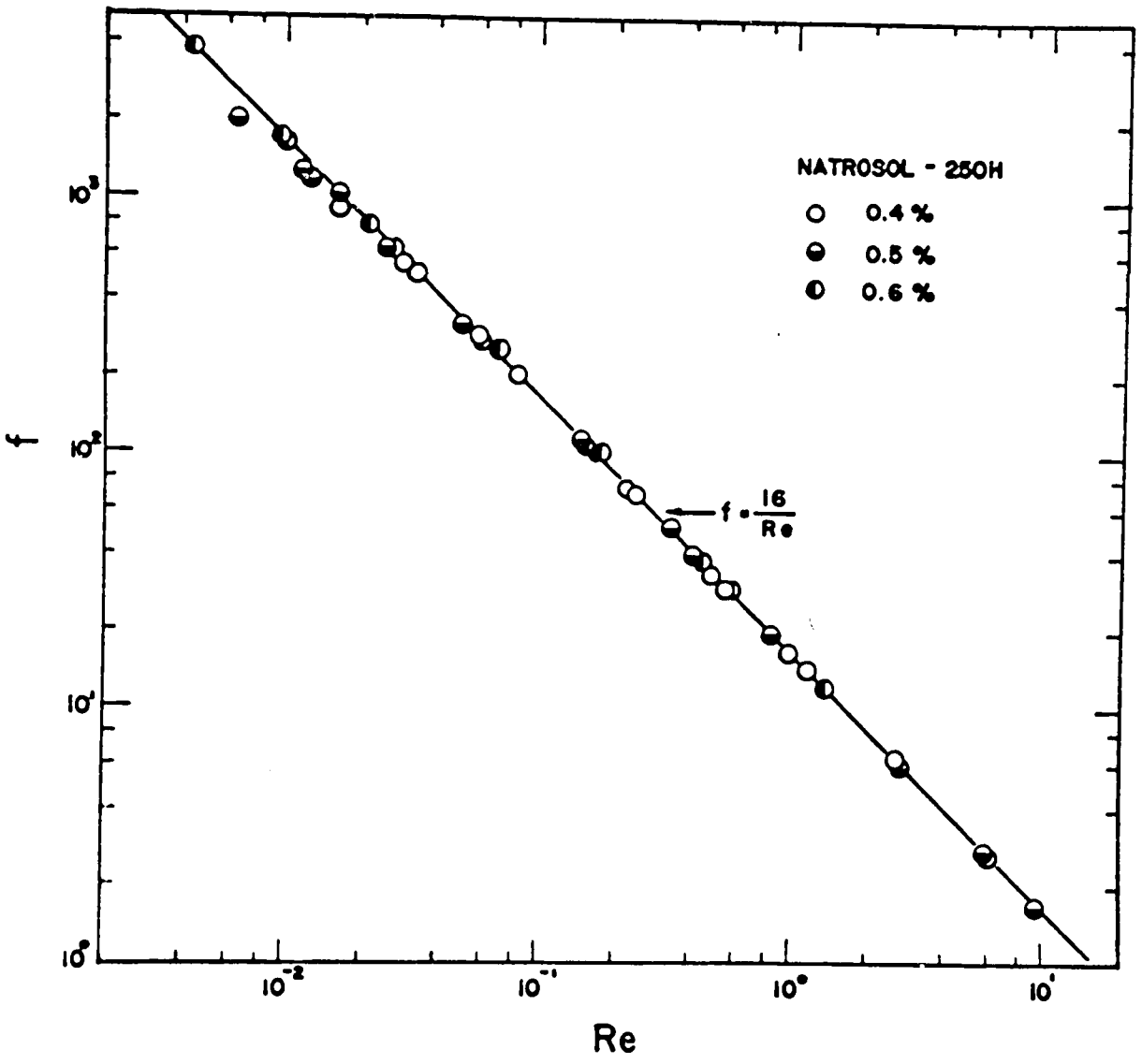

Fig. 12 Friction Factor-Reynolds Number Plot of Natrosol-250H Solution of Sadowski

Figure 13 shows the constant-pressure filtration data obtained with 2.5% $CaCO_3$ in water and in various CMC solutions at 77°F plotted as $\theta(\frac{n+1}{n})(\frac{\Delta P'}{KC})^{1/n}$ versus $(V/A)^{1+1/n}$. The linear relationship obtained using the experimental data indicates the success of the equation, Eq.(85), developed for the constant-pressure filtration, in characterizing the filtration process.

The resistance terms γ and R_m were evaluated from the experimental results obtained with the Newtonian slurries ($CaCO_3$ in water). The term $R_m/C\gamma$ was found to be negligible compared with V/A in Eq.(83). It is recalled that the term $R_m/C\gamma$ has been assumed negligible also for slurries of power law fluids.

It is seen in Fig.13 that some of the straight lines drawn through the experimental points when extended do not pass through the origin in accordance with Eq.(85). This discrepancy, which is not unexpected, is attributable to the unsteady behaviour in the initial stages of the filtration, as well as to the omission of the resistance term $R_m/C\gamma$ in Eq.(83).

It is also noted that the slopes, χ, of the lines in Fig.13 vary with the CMC concentration and pressure drop. This may be interpreted as indicating that the cake resistance as well as the slip velocity ratio u_{ws}/u_s are functions of both CMC concentration and pressure drop, which is anticipated from the analysis presented. As in the case of Newtonian slurries where the cake resistance

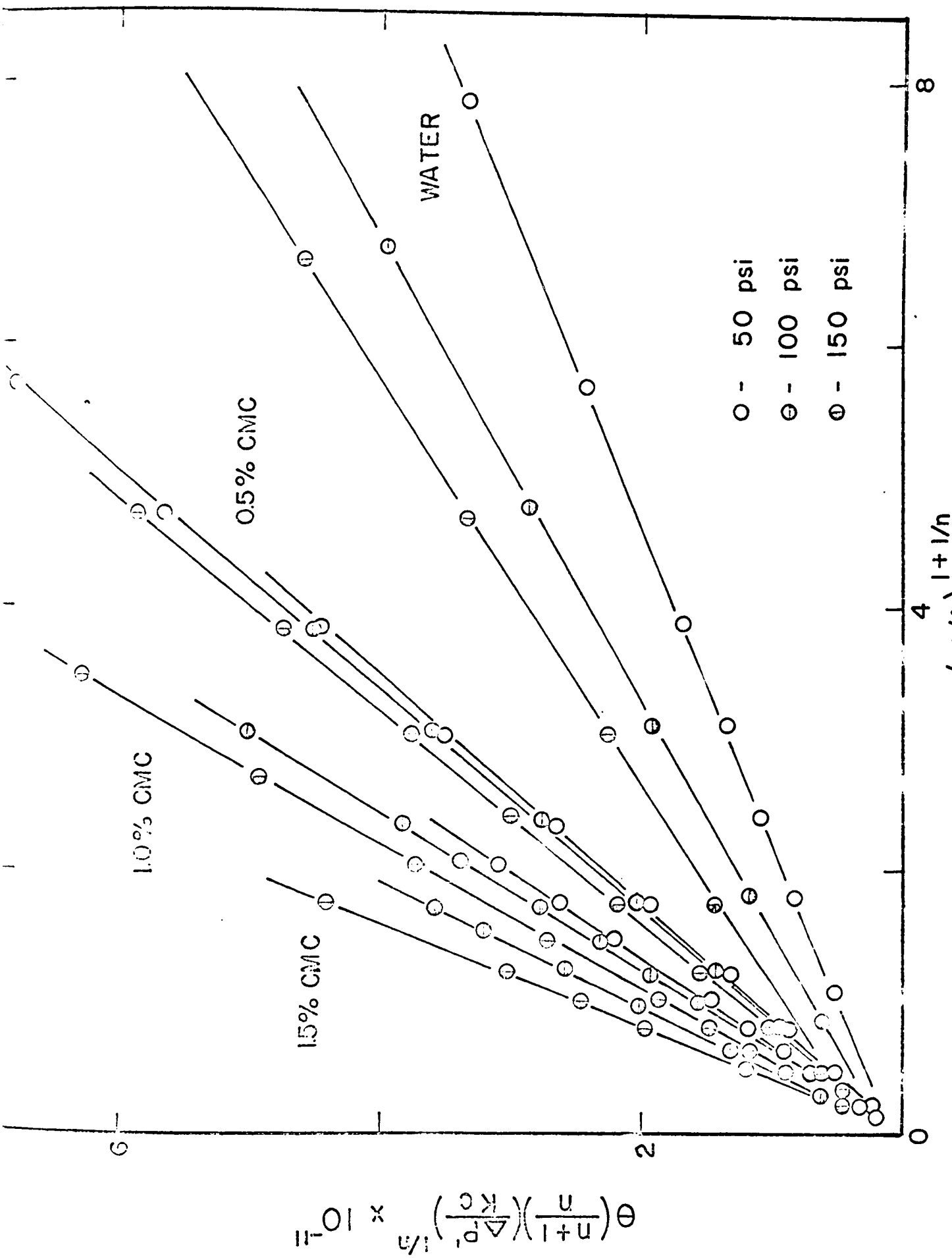

Fig. 13 Constant-Pressure Filtration Data for Various CMC Solutions

can be represented by a power function of the pressure drop across the cake for a moderately compressible sludge, the quantity χ can be successfully correlated by Eq.(87).

Figure 14 shows constant-rate filtration data plotted as time versus pressure drop for various slurries at different flow rate. From the linearity of the curves drawn through the experimental points on a logarithmic plot, one sees that the constant-rate filtration of a power law fluid is well represented by Eqs.(86) or (90). It was also found for this case that the quantity χ could be satisfactorily correlated by a power function of $\Delta P_0'$ according to Eq.(87).

It has been pointed out earlier that the laminar flow data are represented by the equation $f = 16/Re$ regardless of the flow geometry. It is worthwhile to investigate the extent to which or whether the critical Reynolds number, which marks the onset of transition from laminar flow to turbulent flow, is constant for all geometries. Figure 15 gives the critical Reynolds number for the flow of Newtonian fluids in rectangular ducts, based on the prediction of Hanks and Ruo (16), plotted as a function of the aspect ratio E. It is seen that the critical values evaluated in terms of the generalized Reynolds number defined by Eq.(92) are relatively unaffected by the variation in the flow geometry when compared with the corresponding values based on the conventional Reynolds number for Newtonian fluids which takes no consideration of flow geometry as depicted

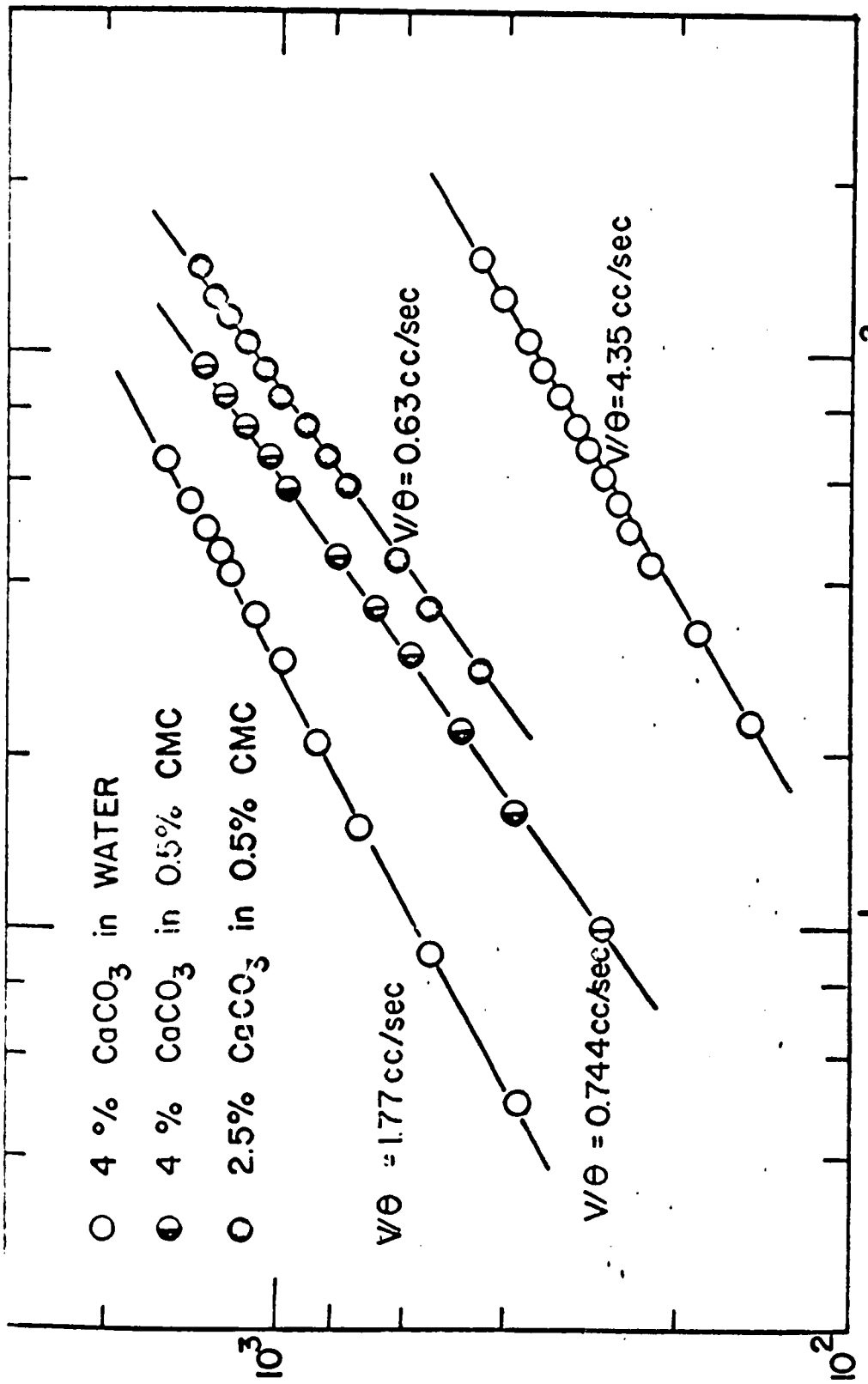

Fig. 14 Constant-Rate Filtration Data for Different Slurry Concentration in Water and CMC Solutions

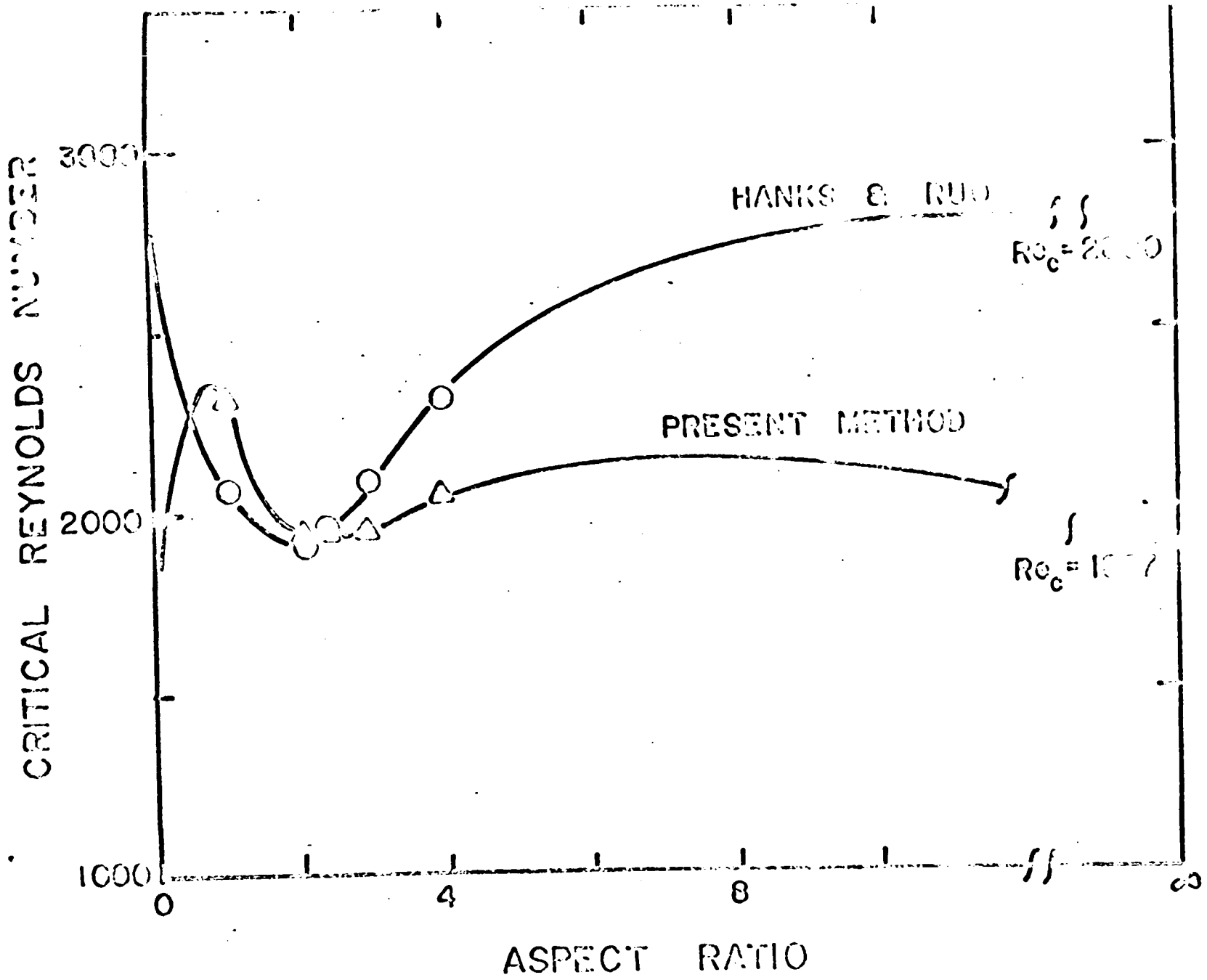

Fig. 15 Plot of Critical Reynolds Number Versus Aspect Ratio for the Flow of Newtonian Fluids in Rectangular Ducts

by Hanks and Ruo (16). The critical value of the generalized Reynolds number is seen to fall around 2,000. The same general result was also found previously (24) in the case of Newtonian flow in concentric annuli with variable aspect ratio, which was also based on the prediction of Hanks (15).

The mechanism describing the drag reduction effect observed with polymer solutions in turbulent flow has been applied to a wide variety of experimental data (28). Ernst (8) conducted velocity measurements close to the wall in the turbulent flow of a 0.05% aqueous CMC solution, whose physical properties are not substantially different from water, in two different diameter pipes and at various Reynolds numbers. It is seen in Fig. 16 that the velocity profiles for the CMC solutions are shifted upward from the velocity profile ascribed to Newtonian fluids. The computed laminar sub-layer thicknesses, the points at the extreme left on the figure, are seen to be situated on the extrapolated laminar sub-layer curve. This figure serves to give an indication of the reasonableness of the computed laminar sub-layer thickness when compared with the experimental data. Thus, the interpretation of the lowering of frictional losses due to an increased laminar sub-layer thickness attributable to the presence of long-chain polymer molecules in the

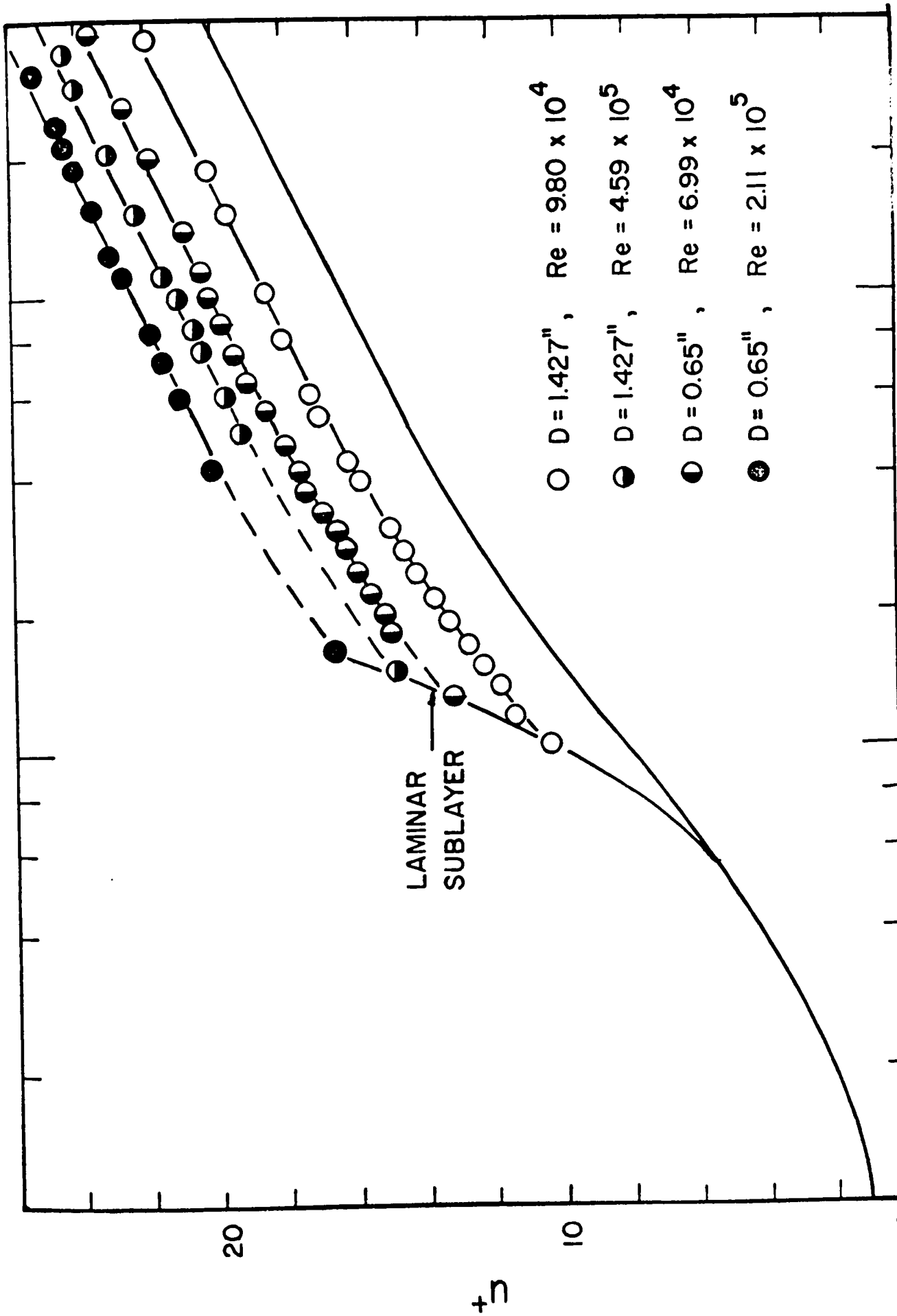

Fig. 16 Plot of Ernst's Experimental Velocity Profile Data Showing the Extended Laminar Sub-layer

high shear field is consistent with the experimental measurements of Ernst.

Figure 17 shows a plot of the laminar sub-layer thickness versus the wall shear stress, computed from the average velocity - pressure drop data obtained by Metzner and Park (38) for the turbulent flow of 0.3% J-100 solution in three different diameter pipes. The smooth curves drawn through the experimental points are extrapolated to intersect the critical radial position versus shear stress curves. The latter curves denote the locii of points on the laminar - turbulent transition curves characteristic of a fluid exhibiting anomalous behaviour in laminar flow. The point of intersection of the laminar sub-layer curve for turbulent flow with the critical radial position curve based on laminar flow considerations indicates the point of transition from laminar to turbulent flow at the given conditions. The lowest curve in the figure which has been included for comparison purposes gives the approximate location of the laminar sub-layer ascribable to the purely viscous fluids, given by $y^+ = \epsilon^+ \approx 5.0$.

Figure 18 shows the effective velocity of slip in turbulent flow computed from the data of Metzner and Park (38). The effective slip velocity attributable to the anomalous surface effect (the separation phenomenon) under laminar flow conditions is also shown. It is seen

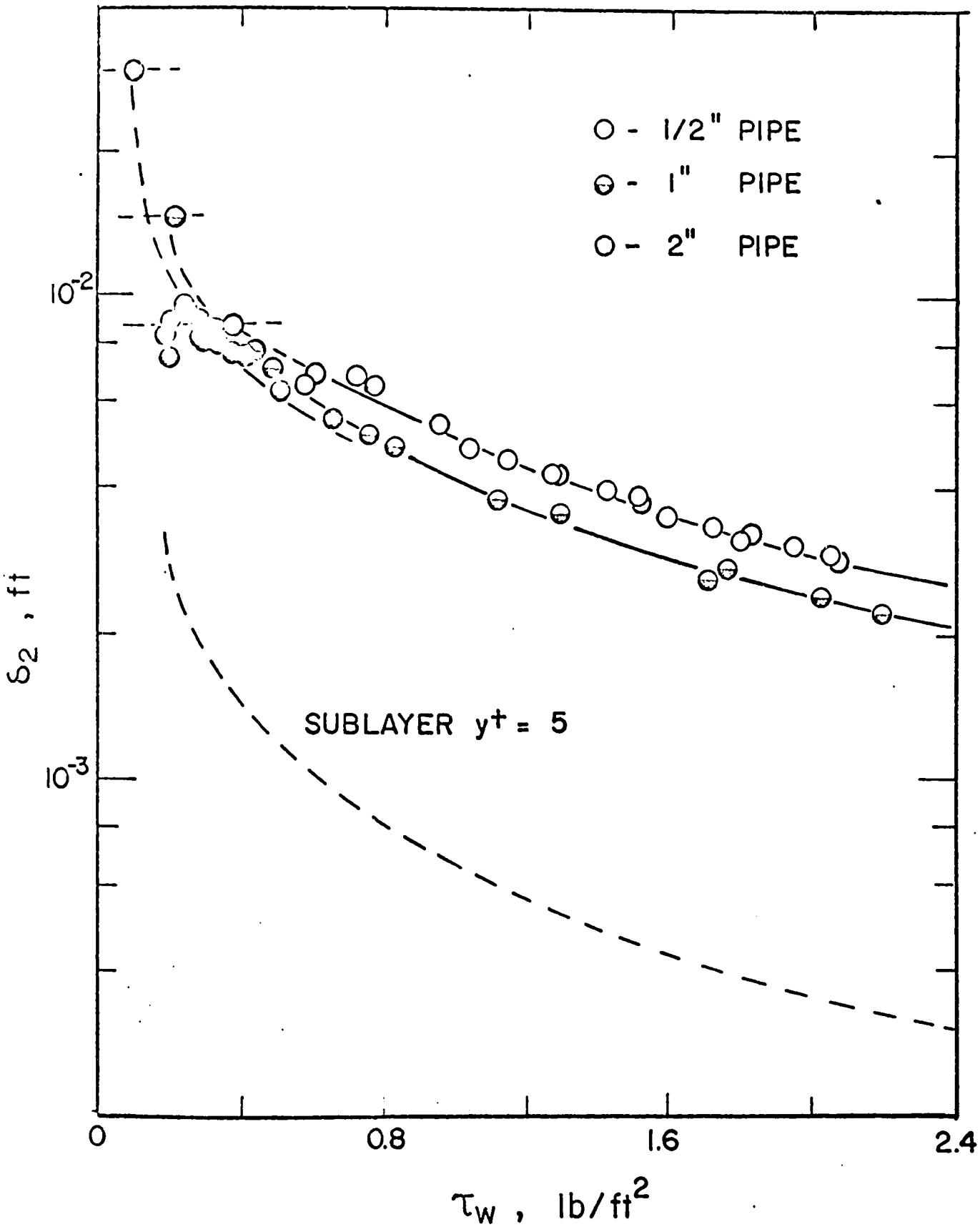

Fig. 17 Laminar Sub-layer Thickness Versus Wall Shear Stress Computed from Data of Metzner and Park

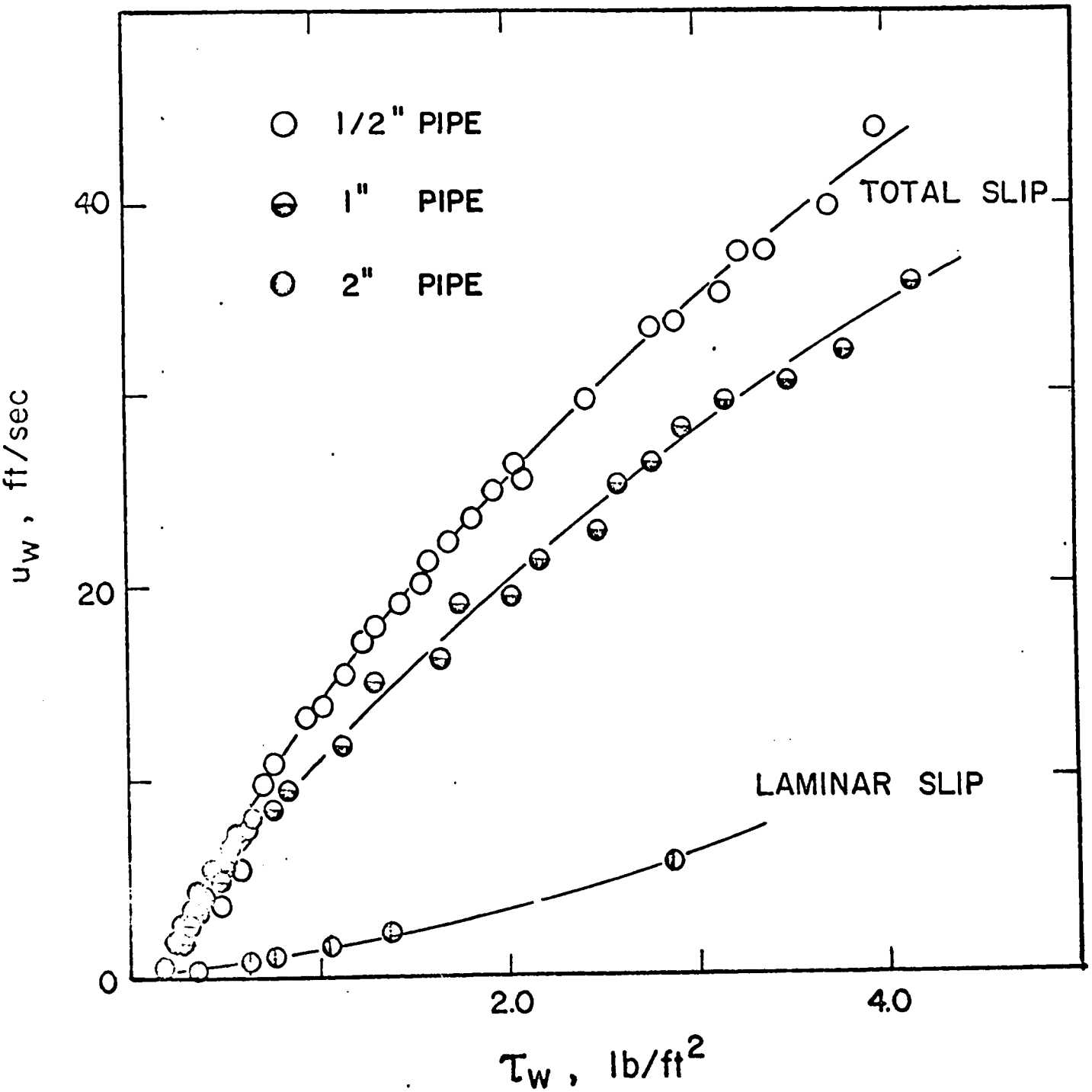

Fig. 18 Effective Velocity at the Wall in Turbulent Flow Including Laminar Slip Evaluated from Data of Metzner and Park

that the separation phenomenon occurring near the wall can account for only a small fraction of the total effective velocity at the wall. Most of the effective velocity of slip in turbulent flow and the associated drag reduction is attributable to the increased thickness of the laminar sub-layer.

Figure 19 presents a δ_2 versus τ_w plot of the experimental measurements conducted by Shaver and Merrill (56) for some CMC solutions. The location of the axis of the tube is shown on the figure in order to gain a proper perspective of the physical situation. The uppermost point on each curve represents the computed critical radial position and the corresponding critical shear stress. It is seen that the computed laminar - turbulent transition points are consistent with the extrapolated curves of the laminar sub-layer thickness. It is worthy to note here that in the case of some systems, the actual transition is not as abrupt as with simple Newtonian systems but more gradual resulting in velocity profiles and calculated friction factors not substantially different from those applicable to laminar flow over a considerable range of τ_w; hence, the reference to turbulent suppression.

Figure 20 shows the variation of the dimensionless laminar sub-layer thickness with concentration, expressed as parts per million by weight, for some natural products in distilled water calculated from the data reported by

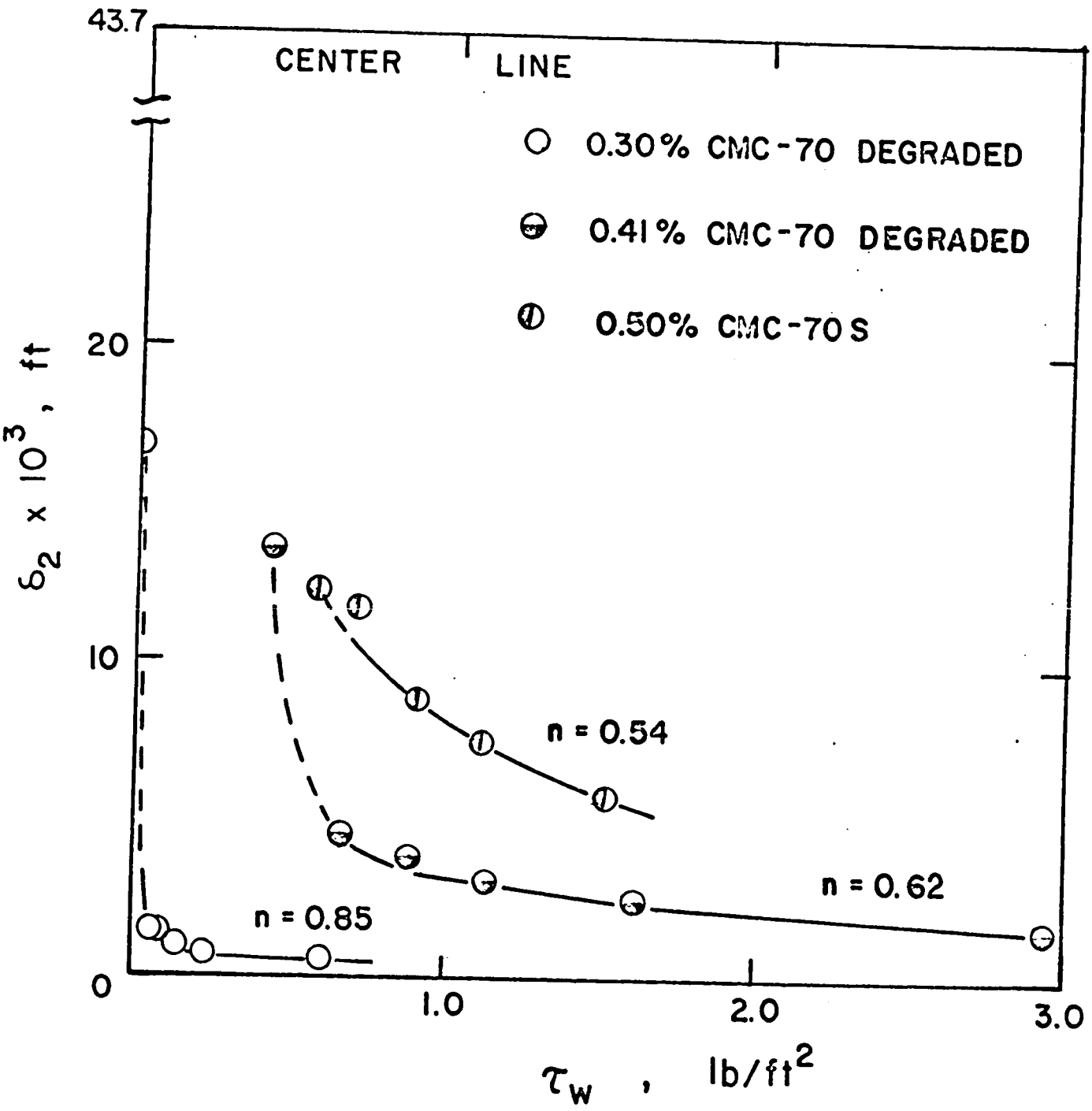

Fig. 19 Laminar Sub-layer Thickness versus Shear Stress Computed from Data of Shaver and Merrill

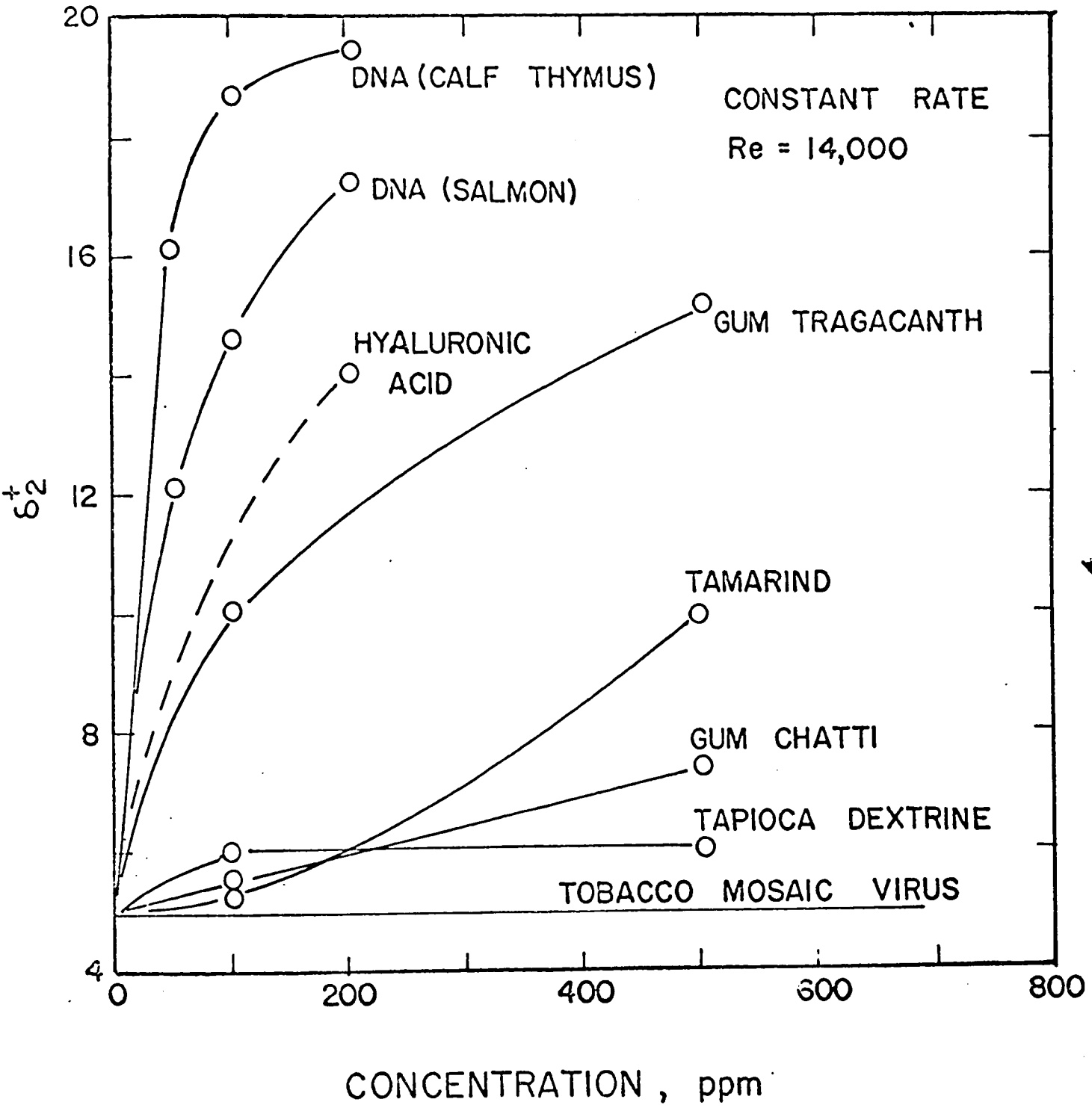

Fig. 20. Dimensionless Sub-layer Thickness as a Function of Concentration for Various Natural Product Solutions Used by Hoyt

Hoyt (22). In most cases, the dimensionless thickness is observed to increase with the concentration of the additive; however, a maximum thickness may be attained at some concentration beyond which the thickness becomes substantially independent of the concentration. This is probably the effect of a balance of an increase in pressure loss, due to an increase in solution viscosity, and an increase in turbulent suppression, due to the higher concentration of the solution.

Finally, the experimental measurements conducted by Shertzer (59) are used to substantiate the theory on the expansion-contraction behaviour of non-Newtonian jets. Figures21 and 22 present the flow data plotted in the standard manner as τ_w versus $8\langle u\rangle/D$ and $8(\langle u\rangle - u_w)/D$ for 0.5% J-100 in water and 3% PIB in decalin, respectively. In the τ_w versus $8\langle u\rangle/D$ plots separate curves can be drawn through the points representing different capillary tube diameters, suggesting anomalous behaviour at the solid boundary. The same data plotted as $8(\langle u\rangle - u_w)/D$ versus τ_w, with the effective velocity at the wall, u_w, established from the separation of the former individual curves, merge so as to be presented by single curves (uppermost curve in each figure with solid points), as expected. The latter curves are used in the evaluation of the shear stress - shear rate relationship characterizing the viscous flow behaviour of the fluids. Because of the curvature in

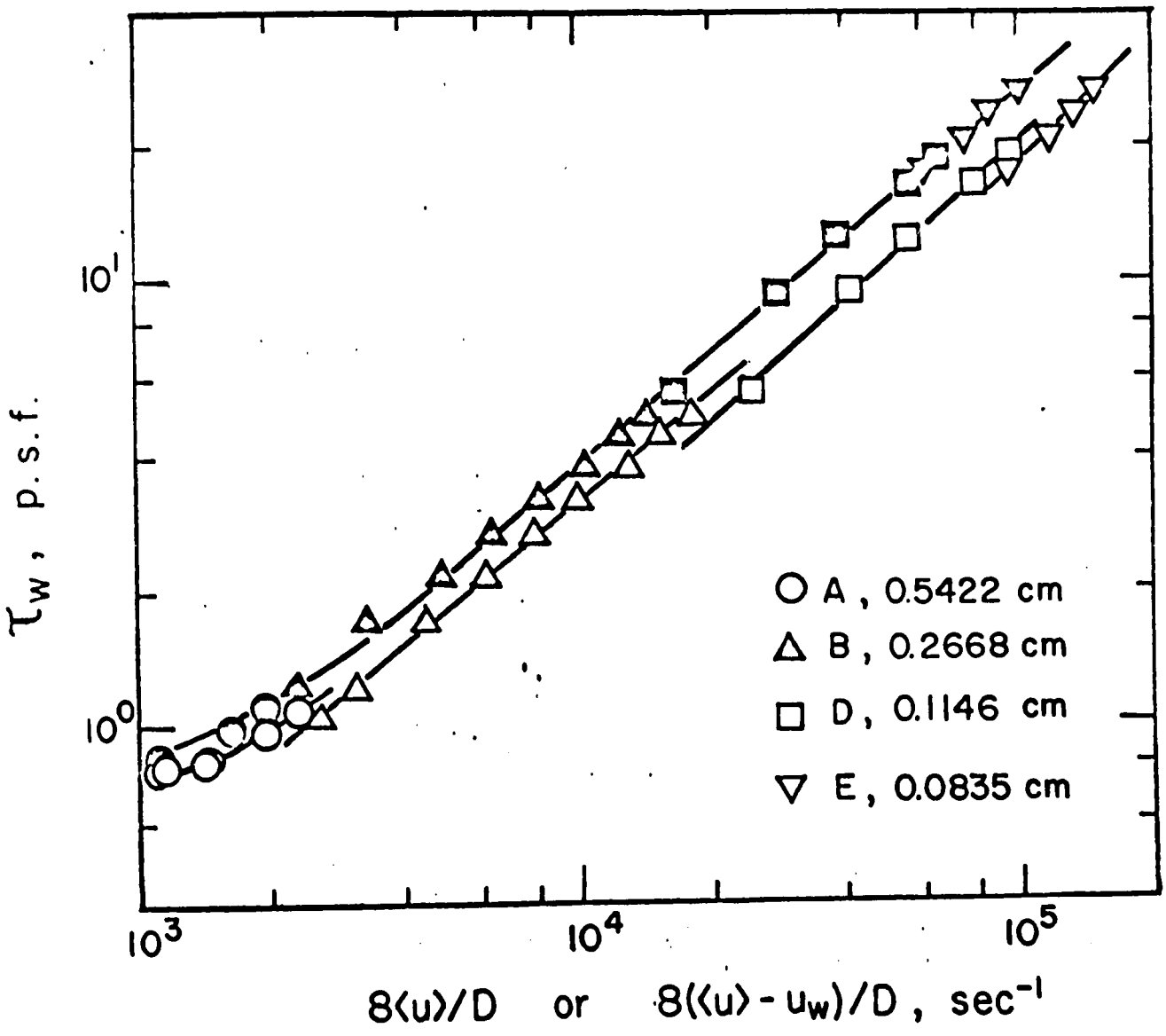

Fig. 21 Flow Curves Determined from Shertzer's Data for 0.5% J-100 in Water Solution

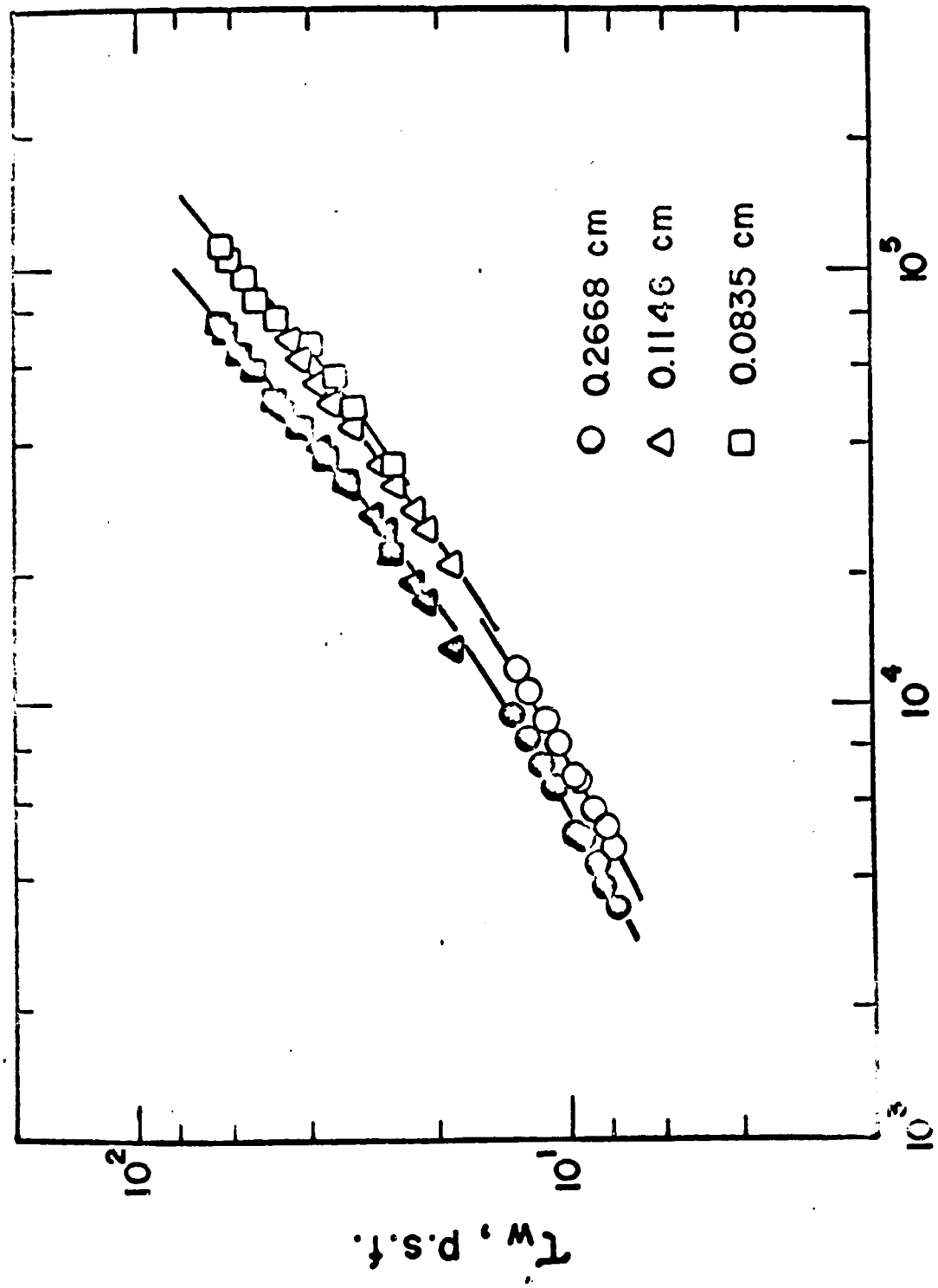

Fig. 22 Flow Curves Determined from Shertzer's Data for 3% PIB in Decalin Solution

the curves, the flow behaviour index n', determined as the slope of the tangent to the curve at a point, is not constant but varies with the wall shear stress from 0.39 to 0.856 for the J-100 solution and from 0.43 to 0.84 for the PIB solution.

Figure 23 shows a plot of the effective velocity at the wall u_w versus wall shear stress τ_w for both J-100 and PIB solutions computed from the capillary tube data obtained by Shertzer (59). Positive effective slip velocities are obtained in both cases suggesting separation of the solute molecules from the solvent and migration in the direction away from the wall, the so-called "separation phenomenon" as a probable mechanism at the solid-fluid interface. The effective velocity of slip is satisfactorily represented by a linear function of the wall shear stress. The slip coefficient ζ computed are 0.694 and 0.187 ft^3/lb_f-sec for the J-100 and PIB solutions, respectively.

Figures 24 and 25 are plots of the deviatoric normal stress difference $(\tau_{11} - \tau_{22})_w$ versus shear rate γ for 0.5% J-100 in water and 3% PIB in decalin solutions, respectively, computed from the thrust measurements of Shertzer on these fluids by the present analysis taking into consideration the effect of the anomalous behaviour. The broken lines in each figure represent the previous correlations and extrapolations. The shaded area and the

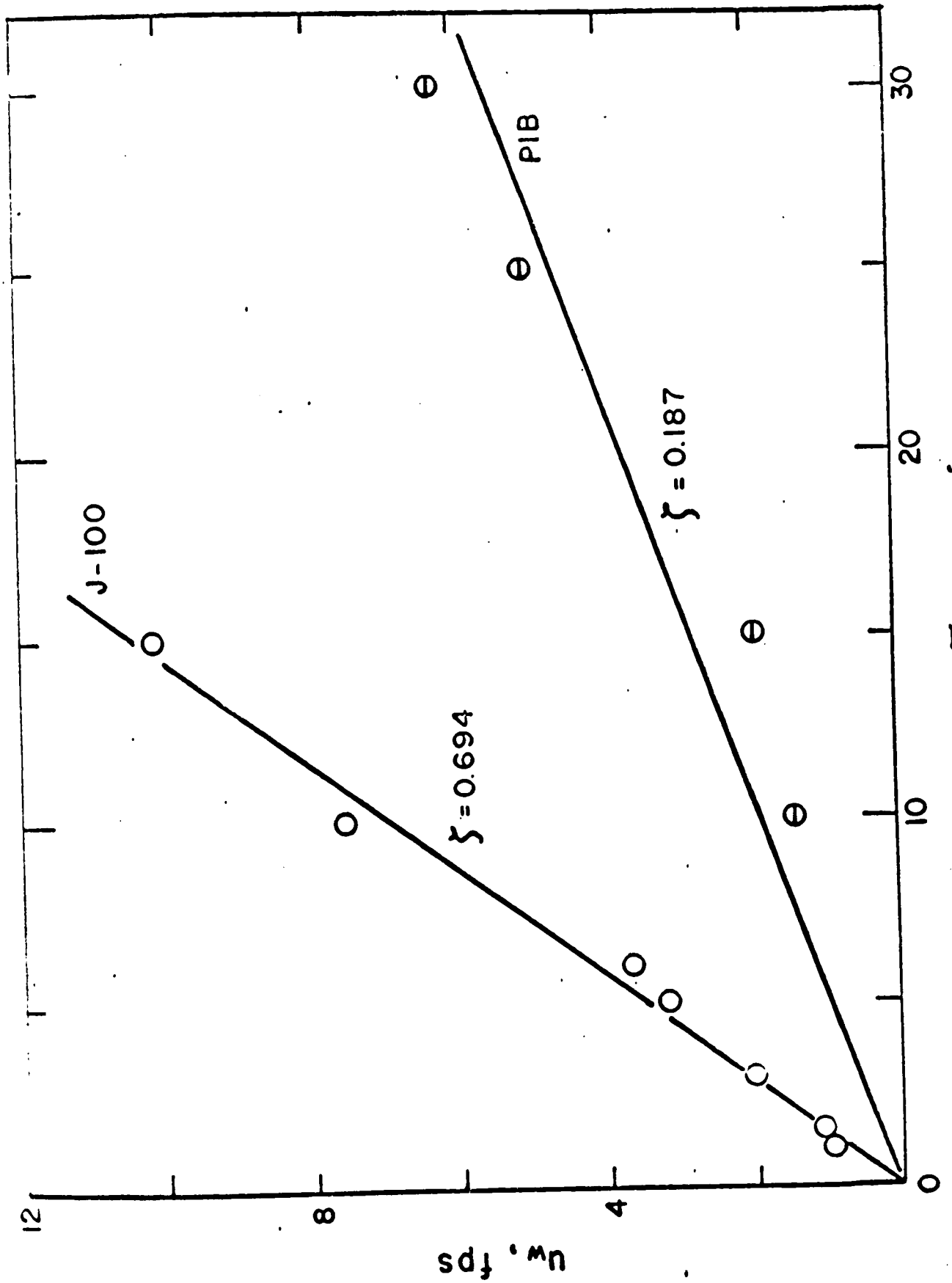

Fig. 23 Effective Velocity of Slip Versus Wall Shear Stress for J-100 and PIB Solutions

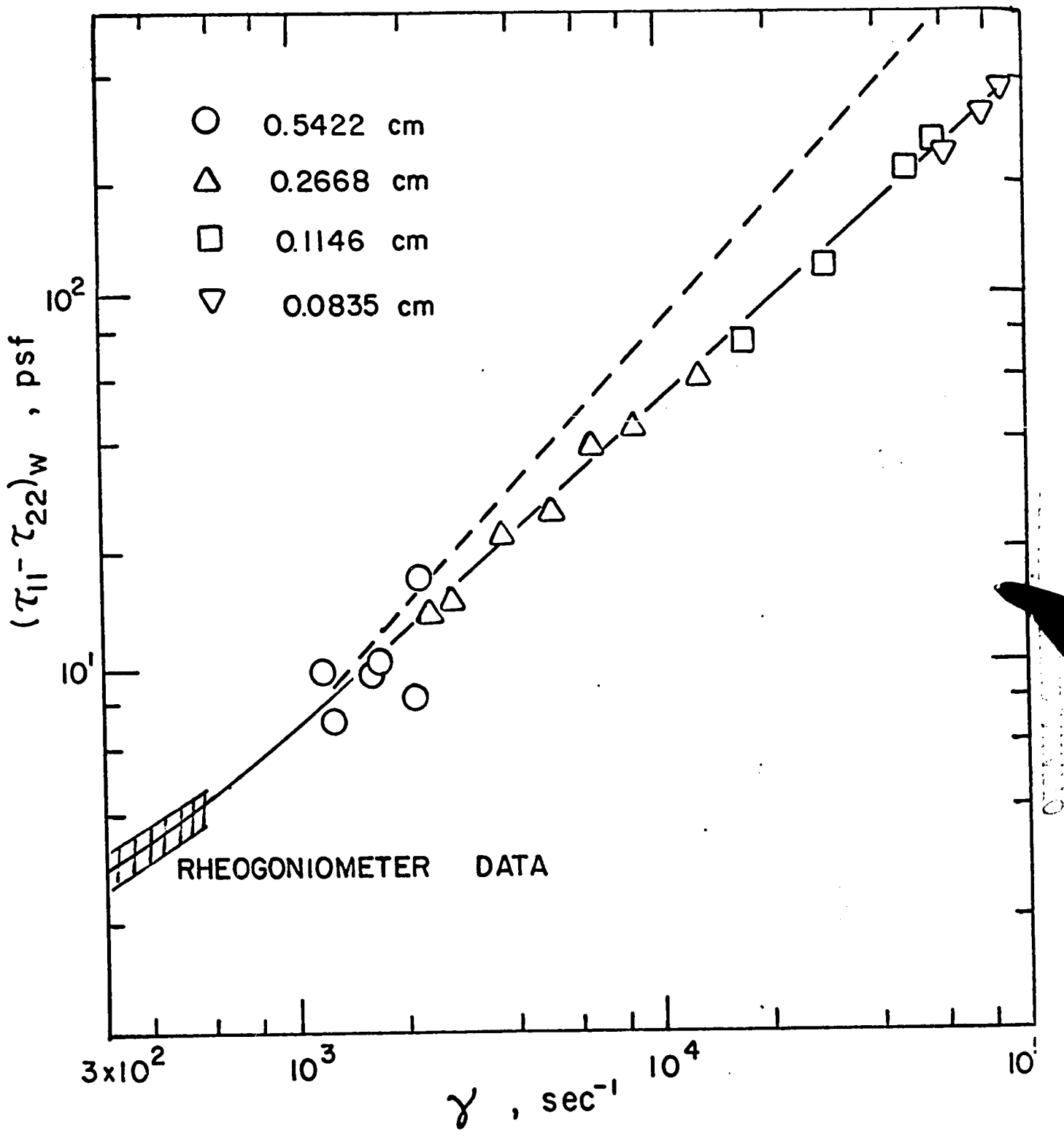

Fig. 24 Deviatoric Normal Stress Difference versus Shear Rate from Ghertzer's Thrust Measurements on 0.5% J-100 Solution

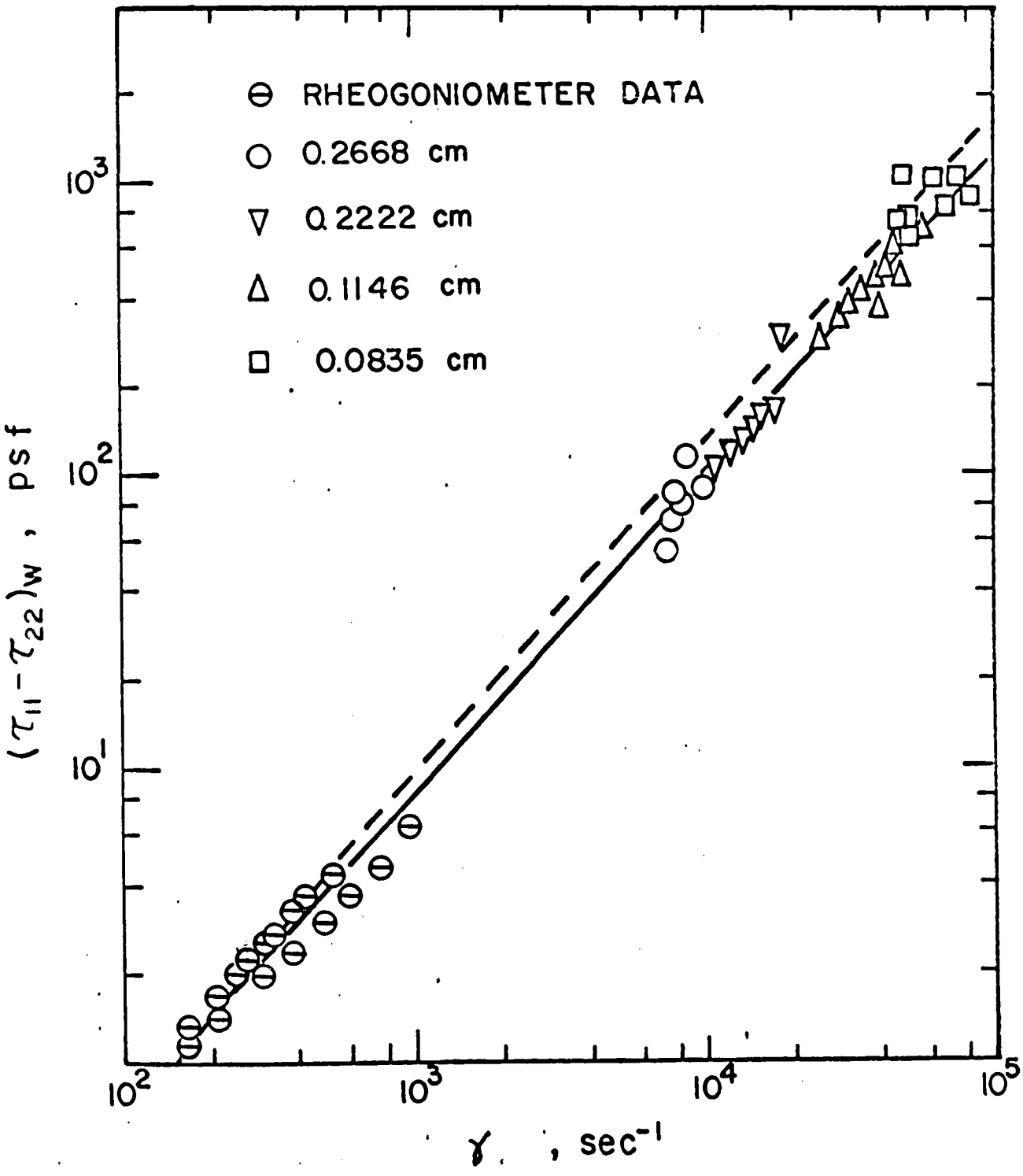

Fig. 25 Deviatoric Normal Stress Difference Versus Shear Rate from Shertzer's Thrust Measurements on 3% PIB Solution

points in the lower left-hand corner of Figs. 24 and 25, respectively, represent the rheogoniometer data, plotted as given by Shertzer. The points plotted in Fig. 24 represent values of $(\tau_{11} - \tau_{22})_w$ yielded by the present method using Eq.(175), which are generally lower than the values determined without consideration of the anomalous behaviour. It is seen that the interpolation line connecting the rheogoniometer and thrust data for the J-100 solution in Fig. 24 has less curvature (almost linear) than the one obtained by Shertzer. This suggests the possibility of prediction, to quite a good degree of approximation, of values of the normal stress difference in the high shear rate region by a simple extrapolation of the data obtained in the low shear rate region with a rheogoniometer, previously considered not possible. A similar extrapolation can also be achieved with the measurements for the PIB solution (Fig. 25). However, the differences between the previous values of $(\tau_{11} - \tau_{22})_w$ and those determined by the present analysis for the PIB solution are not as large as in the case for the J-100 solution, since lower effective slip velocities are found for the PIB solution.

The scattering of the data points in Figs. 24 and 25 are attributable to two major sources of error: (1) a certain lack of precision in the experimental measurements; and (2) uncertainties existing in the τ_w versus

$8(\langle u\rangle - u_w)/D$ correlation. Aberrations in the latter are magnified because of the form of Eq.(175), which involves taking a difference, which is small, between two large terms in the evaluation of the normal stress difference. A slight alteration in the slope determined from the log T_w versus log $8(\langle u\rangle - u_w)/D$ plot affects the final result significantly. Shertzer (59) also emphasized in his discussion of the thrust measurements, that a small error in the thrust F could magnify the error in $(\tau_{11} - \tau_{22})_w$ by several orders.

Figure 26 is a plot showing the normal stress difference plotted against $8\langle u\rangle/D$ and $8(\langle u\rangle - u_w)/D$ for 0.5% J-100 in water, which is an analogous plot to Figs. 21 and 22. Much the same as in these figures, the plots of $(\tau_{11} - \tau_{22})_w$ against $8\langle u\rangle/D$ also yield distinct curves, characteristic of the capillary diameter, depicting the anomalous surface effect. Additionally, the upper curve represents all of the data obtained with different capillaries plotted as $(\tau_{11} - \tau_{22})_w$ versus $8(\langle u\rangle - u_w)/D$. These points are now merged on a single smooth curve except for some scattering of data points in the low shear rate region. This is attributable to the experimental uncertainty in the thrust measurement using Tube-A as originally reported by Shertzer (59). This figure serves to illustrate the effect of the existence of anomalous surface behaviour on the normal stress measurement. A

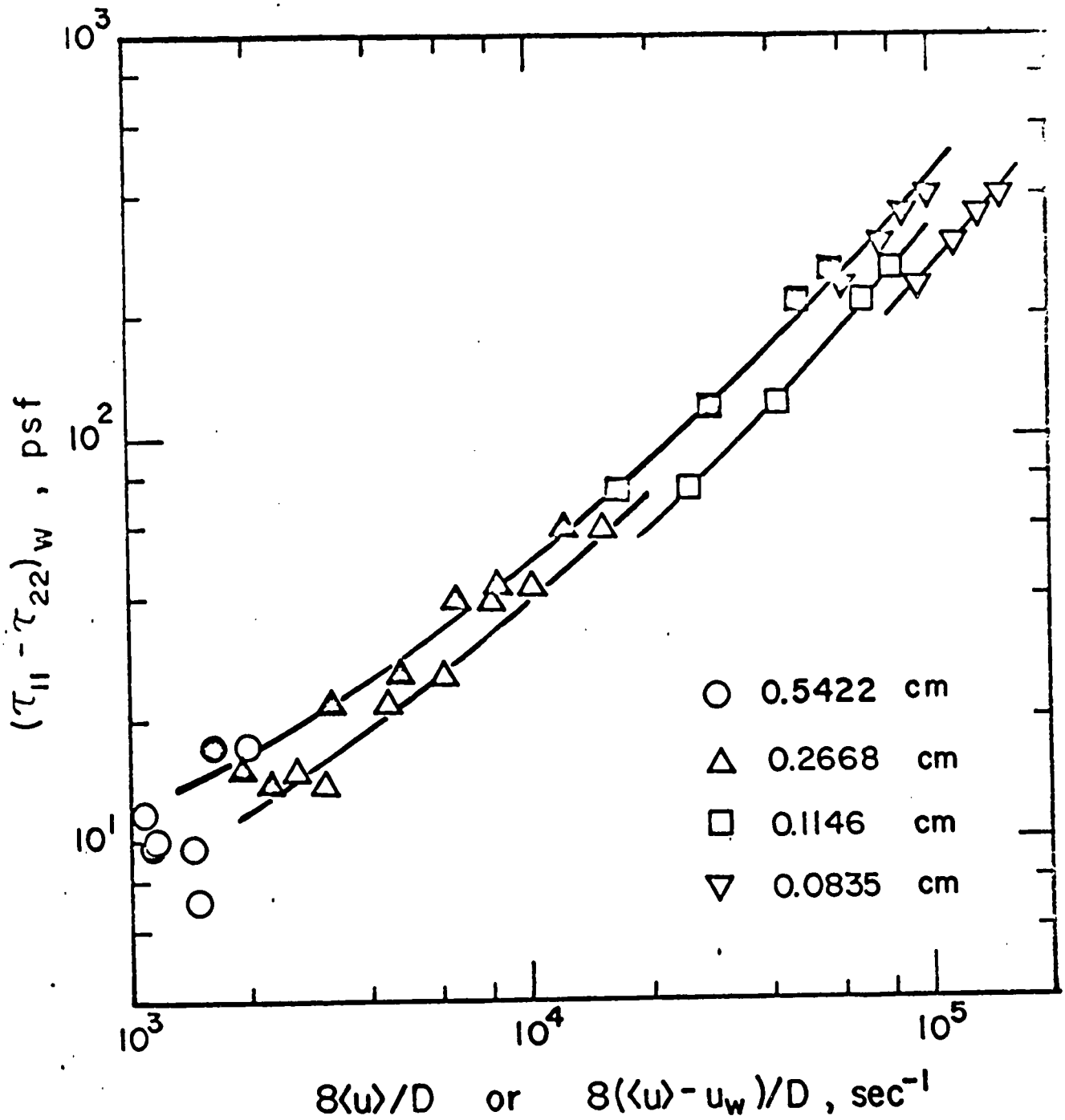

Fig. 26 Deviatoric Normal Stress Difference Versus $8\langle u\rangle/D$ and $8(\langle u\rangle - u_w)/D$ Curves for 0.5% J-100 Solution

similar plot obtained for the PIB solution is not shown.

Figure 27 shows values of $(\tau_{11} - \tau_{22})_w$ calculated for the same J-100 and PIB solutions from jet diameter measurements taken by Shertzer using a photographic technique, computed by taking into consideration the anomalous surface effect, plotted against shear rate as shown. The data are correlated successfully by a straight line on a logarithmic plot over the relatively narrow shear rate range. The new values of the normal stress difference are somewhat lower than those determined by Shertzer.

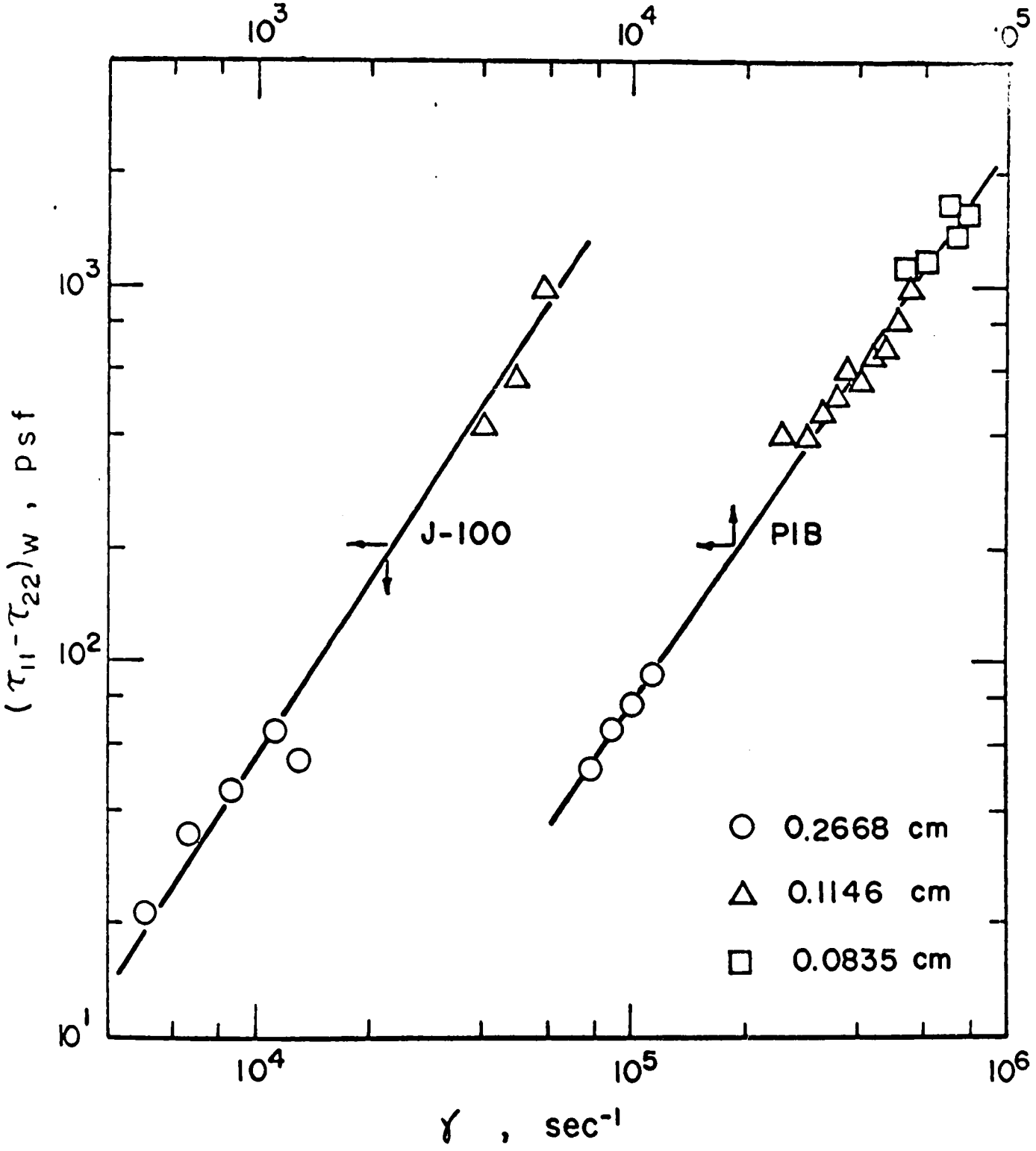

Fig. 27 Deviatoric Normal Stress Difference Versus Shear Rate for J-100 and PIB Solutions Determined from Jet Diameter Measurements

V - SUMMARY AND CONCLUSIONS

A simple and direct method for prediction of the average velocity and maximum velocity versus potential (pressure) gradient relationships in the isothermal, steady, uniform, laminar flow of any time-independent non-Newtonian fluid through ducts, either closed or open, of arbitrary cross section has been proposed. The method which utilizes two geometric parameters for characterization of the flow geometry eliminates extensive and laborous calculations necessitated by conventional techniques, when dealing with non-Newtonian fluids and other than the simplest cross-sectional flow geometries. The flow characteristics of the fluid under consideration is represented either analytically, in terms of $f(\tau)$ or η, or by experimental data obtained directly with the circular capillary tube viscometer.

The method can be applied equally readily to extremely complicated flow situations in regards to the fluid model and, in particular, flow geometry, which defy investigation by conventional methods. The geometric parameters may be evaluated in such situations from flow measurements obtained using simple fluids such as Newtonian (water) or Ostwald-de Waele type. Once the geometric parameters have been evaluated, the calculation of the pressure drop or flow rate for any other fluid of interest is readily performed.

Predictions based on the present analysis were found to be in good agreement with available analytical solutions and experimental data for various non-Newtonian fluids and different flow geometries.

The general average velocity - pressure drop relationship presented for the flow of any time-independent non-Newtonian fluid through packed beds or porous media, based on the Blake-Kozeny capillary model, appears to represent the relationship of the pertinent variables in good agreement with experiments. The general expression has successfully correlated the author's data, as well as the data of Sadowski for high molecular weight Natrosol-250H solutions by allowing for the existence of an anomalous layer on the solid surfaces.

In the reduction of the general expression to the various relationships applicable to specific situations, it was necessary in all cases to set the aspect factor equal to 3 to arrive at the expressions concordant with the experimental data. Nevertheless, the general expressions have been presented retaining the parameter ξ so as to allow for the possibility of values different from 3 in unusual situations such as might be encountered with beds of abnormal porosity, beds comprised of sharp-edged particles, etc.

Certain non-Newtonian fluids exhibit anomalous wall effects in laminar flow conditions. In many suspensions or dispersed liquids, the interaction between the wall of the

flow conduit and the dispersed particles may give rise to a positive effective velocity of slip at the wall and forming an anomalous layer which is less viscous than the fluid in the main stream. The other kind of anomalous behaviours exhibited by some polymer solutions is the negative wall effect. The alignment and orientation of the polymer molecules give rise to a more viscous anomalous layer and a negative effective velocity at the solid wall. In the present study of the flow of polymer solutions through packed beds, negative effective velocities were found for all cases suggesting the polymer adsorption and gel formation at the surface of the particles. This phenomenon was also observed experimentally by Sadowski.

An equation of motion has been developed for the flow of non-Newtonian fluids through compressible porous media. The equation has been shown to reduce to the non-linear partial differential equation derived by Tiller for the one-dimensional constant-pressure filtration of Newtonian slurries.

The agreement of the filtration theory for power law fluids with the experimental results was found to be satisfactory.

The average cake resistance γ and the slip velocity ratio u_{ws}/u_s were found to be functions of both CMC concentration and pressure drop across the filter cake. The coefficient χ, a function of the average cake resistance

and the slip velocity ratio, could be successfully correlated by a power function of the pressure drop.

In the present analysis, the friction factor and Reynolds number data were correlated by a single relationship given by $f = 16/Re$ in the laminar flow, independent of the flow geometry. The Ryan and Johnson stability parameter has been modified to predict the transition point from the laminar to turbulent flow of power law fluids exhibiting anomalous surface effects.

There is considerable evidence that drag reduction observed with viscoelastic non-Newtonian fluids can be attributed mainly to an increase in the laminar sub-layer thickness. This increased thickness may be a manifestation of eddy suppression, due to the mechanical resistance associated with preferred orientations and alignment of the polymer molecules in the high shear field. Stabilizing influences associated with normal stresses may also play a prominent role in suppression of eddies near the wall.

Finally, a generalization of the laminar flow behaviour of non-Newtonian jets has been presented which is applicable to arbitrary cross-sectional geometry and accounts for anomalous behaviour at the solid-fluid interface within the tube. The analysis which utilizes the geometric parameters to characterize the shape of the fluid jet is simple to apply for interpretation of data and prediction purposes. An improvement in agreement in the deviatoric normal stress

difference determined by the extrusion method with extrapolated rheogoniometer data is achieved by taking into consideration the anomalous behaviour of the fluid.

VI - NOMENCLATURE

A = cross-sectional area of the flow channel

A_i = coefficients defined by Eqs.(60) to (63)

A_j = cross-sectional area of the fluid jet

A_r = A/A_j, area ratio of the tube to the jet

A_r' = function defined by Eq.(167)

a, b = geometric parameters

b_1 = constant in Rabinowitsch fluid model

c = contour of the wetted periphery of the flow cross section

$c(y/R, Re)$ = function defined by Eq.(138)

C = mass of solid particles deposited per unit volume of filtrate

D = diameter of the circular pipe

D_p = particle diameter

E = aspect ratio, ratio of the minor to major sides of the rectangular duct

f = Fanning friction factor defined by Eq.(91); subscript c denotes critical value

$f(\tau_w)$ = τ_w/η, second invariant of the rate of deformation tensor; characteristics of the fluid

f = body force

g = acceleration due to gravity

$g(\delta_1, \tau, y)$ = correction term for the anomalous behaviour in laminar flow

h = elevation from the horizontal datum

$h(\tau,y)$ = velocity gradient ascribed to a purely viscous non-Newtonian fluid in turbulent flow

I = unit tensor

I' = integral defined by Eq.(160)

$I(n,He)$ = function defined by Eq.(137)

k = aspect ratio, ratio of inner to outer radii of concentric annuli; permeability factor to viscous flow defined by Eq.(48)

k_i = 2(a+b), impermeability factor

k_m = permeability factor to slip flow defined by Eq.(47)

K = fluid consistency index of a power law fluid

K^* = fluid consistency index defined by Eq.(95)

K' = value of K^* for the flow in circular pipes

$\bar{K}$ = stability parameter defined by Eq.(112); subscript c denotes the critical value

l = length of the equal side of the triangular duct; distance along the contour c

L = length of the capillary tube

m = surface resistance coefficient defined by Eq.(44)

m_o = mass of solids in the filter cake

m_x = mass of solids at any distance x in the filter cake

n = flow behaviour index of a power law fluid

n^* = flow behaviour index defined by Eq.(94)

n' = value of n^* for the flow in circular pipes

p = isotropic pressure

P' = $p + \rho gh$, potential function; fluid pressure for horizontal flow

P_s = solid compressive pressure

P_a = fluid upstream pressure at the surface layer of the filter cake

P_b = fluid downstream pressure at the exit of the filter medium

P^* = $\bar{\tau}_w/(1-k)\tau_{\frac{1}{2}}$, dimensionless pressure drop for the flow of Ellis fluids in concentric annuli; fluid interfacial pressure between the filter medium and the filter cake

$\Delta P'$ = overall pressure drop

$\Delta P'_c$ = pressure drop across the filter cake

$\Delta P'_m$ = pressure drop across the filter medium

Q = volumetric flow rate

Q^* = $Q\eta_o/\pi R^3\tau_{\frac{1}{2}}$, dimensionless flow rate for the flow of Ellis fluid in concentric annuli

q = empirical constant defined by Eq.(87)

$q(\tau,y)$ = correction term for the anomalous behaviour in turbulent flow

r = radial distance measured from the center of the pipe

R = radius of the pipe; outer radius of the concentric annulus

R_m = filter medium resistance

r_H = hydraulic radius

Re = Reynolds number defined by Eqs.(92) or (93); subscript c denotes the critical value

S = radius R for the circular pipe, or distance Y for the parallel plate section

S_o = specific surface per unit volume of solid particles

s = position variable measured from the axis of symmetry

s' = $\bar{u}_w/\langle u \rangle$, slip velocity ratio

s/r_o = ratio of the pitch, half distance between centers of two cylindrical rods, to the radius of the cylindrical rod in the square and triangular arrays of cylinders

T = tortuosity of the packed bed or porous medium; thrust of the fluid jet

T_w = function defined by Eq.(157)

$\bar{u}$ = velocity vector; subscript i, j denote components

u = local velocity

$\langle u \rangle$ = average velocity

u_{max} = maximum velocity

u_l = laminar velocity distribution

u_t = turbulent velocity distribution ascribed to purely viscous fluids

u_s = superficial velocity

u_w = effective velocity at the wall in laminar flow; over-bar denotes contour integrated average value

u_{ws} = superficial effective velocity at the pore wall

u_{wt} = effective velocity at the wall in turbulent flow

u_* = $\sqrt{\tau_w/\rho}$, friction velocity

u^+ = dimensionless velocity defined by Eq.(130)

u_4^+, u_5^+ = functions defined by Eqs.(140) and (141) respectively

V = volume of the filtrate

w = (subscript) refers to conditions at the wall

x = position variable; distance measured from the filter medium

x, z = dummy variables

y = inward normal distance measured from the solid boundary

y' = distance measured from the plane of symmetry of the parallel plate section

y^+ = dimensionless distance defined by Eq.(131)

y_0^+ = dimensionless sub-layer thickness defined by Eq.(136)

Y = half distance between two parallel plates

z = stability parameter defined by Eq.(111)

Greek Letter

α = half angle of the isosceles triangular duct

α_x = specific cake resistance defined by Eq.(66)

α, η_0
η_∞, τ_m = physical parameters of Meter's fluid model

$\alpha, \eta_0, \eta_\infty$ = physical parameters of Ellis fluid model

β = coefficient of plastic viscosity of Bingham plastic fluid; ratio of minor to major semi-axes of the elliptic duct

δ_1 = anomalous layer thickness in laminar flow

δ_2 = laminar sub-layer thickness ascribed to visco-elastic fluids

ϵ = porosity; laminar sub-layer thickness ascribed to purely viscous fluids

$\dot{\gamma}$ = rate of deformation tensor; $\dot{\gamma}_{ij}$ denotes the component

$\dot{\gamma}$ = second invariant of the rate of deformation tensor, shear rate; average generalized cake resistance defined by Eq.(76)

$\dot{\gamma}_x$ = generalized cake resistance defined by Eq.(75)

ζ = effective slip coefficient defined by Eq.(36); subscript e denotes the corrected coefficient defined by Eq.(37)

ξ = b/a, aspect factor

λ = r/R, radial position; subscript c denotes the critical value

η = non-Newtonian viscosity

η_{ap} = apparent viscosity defined by Eq.(51)

η_{eff} = effective viscosity for power law fluids defined by Eq.(55)

θ = time

ρ = density of the fluid

ρ_s = density of the solid particle

μ = viscosity of Newtonian fluids

μ_s = viscosity of the pure solvent

μ_o = constant in Rabinowitsch fluid model

π = total stress tensor; π_{ij} denotes the component, e.g., π_{11} denotes the component of the total normal stress in the direction of flow

τ = deviatoric stress tensor; τ_{ij} denotes the component

τ = second invariant of the deviatoric stress tensor, shear stress

$\langle \pi_{11} \rangle$ = average normal stress in the direction of fluid flow

τ_w = shear stress at the wall; over-bar denotes the contour integrated average value

τ_y = yield stress

ϕ = function defined by Eq.(134)

χ = function defined by Eq.(84)

χ_o = empirical constant defined by Eq.(87)

∇ = gradient (del operator)

$\nabla \cdot$ = divergence

∇^2 = Laplacian

VII - REFERENCES

1. Astarita, G., Ind. Eng. Chem. (Fund) 4 354 (1965)
2. Bird, R. B., Stewart, W. E., and Lightfoot, E. N., "Transport Phenomena", J. Wiley, N. Y., (1960)
3. Bogue, D. C., and Metzner, A. B., Ind. Eng. Chem. (Fund) 2 143 (1963)
4. Carman, P. C., "Flow of Gases Through Porous Media", Academic Press, N. Y., (1956)
5. Christopher, R. H., and Middleman, S., Ind. Eng. Chem. (Fund) 4 422 (1965)
6. Dodge, D. W., and Metzner, A. B., A. I. Ch. E. J., 5 189 (1959)
7. Elata, C., and Tirosh, J., Proc. VII Israel Amer. Conf. Avia. & Astro., Israel J. Tech., 5 1 (1965)
8. Ernst, W. D., A. I. Ch. E. J., 12 581 (1966)
9. Fredrickson, A. G., Bird, R. B., and Wilcox, W. R., Ind. Eng. Chem., 50 1599 (1958)
10. Gaskins, F. H., and Philippoff, W., Trans. Soc. Rheol., 3 181 (1959)
11. Gill, S. J., and Gavis, J., J. Polymer Sci., 20 287 (1956)
12. Ginn, R. F., and Metzner, A. B., Proc. 4th Int. Cong. on Rheol., 583 (1965)
13. Goren, Y., and Norbury, J. F., Trans. ASME 89D 814 (1967)
14. Hanks, R. W., A. I. Ch. E. J., 9 1 (1963)
15. Hanks, R. W., A. I. Ch. E. J., 9 45 (1963)
16. Hanks, R. W., and Ruo, H. C., Ind. Eng. Chem. (Fund) 5 558 (1966)

17. Harris, J., Nature 190 993(1961)

18. Harris, J., Proc. 4th Int. Cong. on Rheol., 417(1965)

19. Haynes, R. H., Trans. Soc. Rheol., V 85(1961)

20. Hershey, H., and Zakin, J. L., Ind. Eng. Chem. (Fund) 6 381(1967)

21. Hoyt, J. W., and Fabula, A. G., 5th Symp. Naval Hydrodynamics, Bergen, Norway, (1964)

22. Hoyt, J. W., "A Turbulent Flow Rheometer", Symp. on Rheol., ASME Appl. Mech. & Fluid Eng. Conf., Washington D.C., (1965)

23. Jastrzebski, Z. D., Ind. Eng. Chem. (Fund) 6 445(1967)

24. Kozicki, W., Chou, C. H., and Tiu, C., Chem. Eng. Sci., 21 665(1966)

25. Kozicki, W., and Tiu, C., Can. J. Chem. Eng., 45 127(1967)

26. Kozicki, W., Hsu, C. J., and Tiu, C., Chem. Eng. Sci., 22 487(1967)

27. Kozicki, W., Tiu, C., and Rao, A. R. K., Can. J. Chem. Eng., 46(1968)

28. Kozicki, W., and Tiu, C., Chem. Eng. Sci., 23(1968)

29. Krantz, W. B., and Wasan, D. T., "Fully Developed Turbulent Pipe Flow of Ostwald-de Waele Fluids", 59th National Meeting, A.I.Ch.E., Columbus, Ohio, (1966)

30. Longwell, P. A., "Mechanics of Fluid Flow", McGraw-Hill, N. Y., (1966)

31. Marshall, R. J., and Metzner, A. B., Ind. Eng. Chem. (Fund) 6 393(1967)

32. Maurer, G. W., and Le Tourneau, B. W., Trans. ASME 86D 627(1964)

33. McCabe, W. L., and Smith, J. C., "Unit Operation of Chemical Engineering", McGraw-Hill, N. Y., (1956)

34. McEachern, D. W., A. I. Ch. E. J., 12 328 (1966)

35. McKinley, R. M., Johns, H. O., Harris, W. W., and Greenkorn, R. A., A. I. Ch. E. J., 12 17 (1966)

36. Meter, D. M., and Bird, R. B., A. I. Ch. E. J., 10 878 (1964)

37. Metzner, A. B., and Reed, J. C., A. I. Ch. E. J., 1 434 (1955)

38. Metzner, A. B., and Park, G., J. Fluid Mech., 20 291 (1964); Park, G., M. Ch. E. Thesis, Univ. of Delaware (1963)

39. Metzner, A. B., Houghton, W. T., Sailor, R. A., and White, J. L., Trans. Soc. Rheol., 5 133 (1961)

40. Metzner, A. B., Houghton, W. T., Hurd, R. E., and Wolfe, C. C., Int. Symp. on Second Order Effects in Elasticity, Plasticity and Fluid Dynamics, Haifa, Israel, 650 (1962)

41. Middleman, S., Ind. Eng. Chem. (Fund) 3 119 (1964)

42. Mitsuishi, N., Kitayama, Y., and Aoyagi, Y., Chem. Eng. Japan, 31 570 (1967)

43. Mizushima, T., Mitsuishi, N., and Nakamura, R., Chem. Eng. Japan, 28 648 (1964)

44. Mooney, M., J. Rheol., 2 210 (1931)

45. Mooney, M., J. Rheol., 2 337 (1931)

46. Oldroyd, J. G., J. Colloid Sci., 4 333 (1949)

47. Pearson, J. R. A., and Petrie, C. J. S., Proc. 4th Int. Cong. on Rheol., 265 (1965)

48. Philippoff, W., and Gaskins, F. H., Trans. Soc. Rheol., 2 263 (1958)

49. Phung, T. Q., B. S. Ch. E. Thesis, Univ. of Ottawa, (1968); Tiu, C., Kozicki, W., and Phung, T. Q., paper to be published in Can. J. Chem. Eng.

50. Rabinowitsch, B., Z. Phys. Chem., A145 1 (1929).

51. Ryan, N. W., and Johnson, M. M., A. I. Ch. E. J. 5 433 (1959)

52. Sadowski, T. J., Ph. D. Thesis, Univ. of Wisconsin, (1963); Sadowski, T. J., and Bird, R. B., Trans. Soc. Rheol. 9 (1965)

53. Sakiadis, B. L., A. I. Ch. E. J., 8 317 (1962)

54. Savins, J. G., "Drag Reduction Characteristics of Solutions of Macromolecules in Turbulent Pipe Flow", A.I.Ch.E. Meeting, Houston, Texas, 1963; Soc. Petrol. Eng. J., 4 203 (1964)

55. Scheidegger, A. E., "The Physics of Flow Through Porous Media", Univ. of Toronto Press, (1957)

56. Shaver, R. G., and Merrill, E. W., A. I. Ch. E. J. 5 181 (1959)

57. Shertzer, C. R., and Metzner, A. B., Proc. 4th Int. Cong. on Rheol., 583 (1965)

58. Shertzer, C. R., and Metzner, A. B., Trans. Pl. Inst. London, 31 148 (1963)

59. Shertzer, C. R., M. S. Ch. E. Thesis, Univ. of Delaware (1964)

60. Skelland, A. H. P., "Non-Newtonian Flow and Heat Transfer", J. Wiley, N. Y., (1967)

61. Slattery, J. C., A. I. Ch. E. J., 13 1066 (1967)

62. Tiller, F. M., and Cooper, H. R., A. I. Ch. E. J., 6 595 (1960)

63. Tiu, C., M. S. Ch.E. Thesis, Univ. of Ottawa, (1965)

64. Toms, B. A., Proc. Int. Cong. Rheol. II, p.135, North Holland Publishing Co., Amsterdam (1949)

65. Wells, C. S., Am. Inst. Aero. Astro. J. 3 1800 (1965)

66. Whitaker, S., Chem. Eng. Sci., 21 291 (1966)

67. White, J. L., and Metzner, A. B., Trans. Soc. Rheol., 7 295 (1963)

Appendix A

Derivation of the Rabinowitsch-Mooney Equation

Derivation of the Rabinowitsch-Mooney Equation

1. Closed Conduit Flow

a. Flow in a Circular Pipe

The volumetric flow rate of a fluid in a circular pipe is obtained by integrating the velocity over the cross-sectional area as follows:

$$Q = \iint u dA = 2\pi \int_0^R ur dr \qquad (A-1)$$

The average velocity may then be obtained by dividing the volumetric flow rate by the area,

$$\langle u \rangle = \frac{2}{R^2} \int_0^R ur dr \qquad (A-2)$$

which may be integrated by parts to yield

$$\langle u \rangle = \frac{1}{R^2} \left\{ \left[ur^2 \right]_0^R + \int_0^R r^2 (-du/dr) dr \right\} \qquad (A-3)$$

The velocity gradient, $(-du/dr)$, may be expressed in terms of the shear stress by the fluid model equation:

$$-du/dr = f(\tau) = \tau/\eta \qquad (A-4)$$

Utilizing Eq.(A-4) and assuming that there is an effective slip at the wall, Eq.(A-3) becomes

$$\langle u \rangle = u_w + \frac{1}{R^2} \int_0^R r^2 f(\tau) dr \qquad (A-5)$$

The hydraulic radius of a circular pipe, defined as the cross-sectional area divided by the wetted perimeter, is

$$r_H = R/2 \qquad (A-6)$$

It can be shown easily from a momentum balance that the shear stress is a linear function of the radius,

$$\tau = \frac{r}{R} \tau_w = \frac{r}{2}\left(-\frac{dP'}{dx}\right) \qquad (A-7)$$

Substitution of Eqs.(A-6) and (A-7) into Eq.(A-5) gives

$$\frac{2(\langle u \rangle - u_w)}{r_H} = \frac{4}{\tau_w^3} \int_0^{\tau_w} \tau^2 f(\tau) d\tau \qquad (A-8)$$

Differentiating the above equation with respect to the wall shear stress τ_w using the Leibnitz formula, one obtains finally

$$f(\tau_w) = \left(-\frac{du}{dr}\right)_w = \frac{1}{4} \tau_w \frac{d\left[\frac{2(u - u_w)}{r_H}\right]}{d\tau_w} + \frac{3}{4}\left[\frac{2(\langle u \rangle - u_w)}{r_H}\right] \qquad (A-9)$$

b. <u>Flow Between Parallel Plates</u>

The analysis for flow between parallel plates is exactly analogous to that for flow in a circular pipe. The average velocity of a fluid between parallel plates is

$$\langle u \rangle = \frac{1}{Y} \int_0^Y u \, dy' \qquad (A-10)$$

which may be integrated by parts to yield

$$\langle u \rangle = \frac{1}{Y} \left\{ \left[uy' \right]_0^Y + \int_0^Y y' (-du/dy') \, dy' \right\} \qquad (A-11)$$

Replacing the velocity gradient inside the integral of Eq.(A-11) by $f(\tau)$, and assuming an effective velocity at the wall, one gets

$$\langle u \rangle = u_w + \frac{1}{Y} \int_0^Y y' \, f(\tau) \, dy' \qquad (A-12)$$

Similarly, it can be shown that the hydraulic radius for the parallel plate geometry is,

$$r_H = Y \qquad (A-13)$$

and the momentum flux is a linear function of the distance,

$$\tau = \frac{y'}{Y} \tau_w = y' \left(- \frac{dP'}{dx} \right) \qquad (A-14)$$

Substitution of Eqs.(A-13) and (A-14) into Eq.(A-12) gives

$$\frac{2(\langle u\rangle - u_w)}{r_H} = \frac{2}{\tau_w^2}\int_0^{\tau_w} \tau f(\tau)\, d\tau \qquad (A\text{-}15)$$

Differentiation of the above equation with respect to τ_w finally yields

$$f(\tau_w) = \left(-\frac{du}{dy'}\right)_w = \frac{1}{2}\tau_w \frac{d\left[\frac{2(\langle u\rangle - u_w)}{r_H}\right]}{d\tau_w} + \left[\frac{2(\langle u\rangle - u_w)}{r_H}\right] \qquad (A\text{-}16)$$

2. Open Channel Flow

The solutions for flow in open channels are the same as for the corresponding closed conduits obtained by reflecting the solid boundary in the free surface. Hence, Eqs.(A-9) and (A-16) are directly applicable to the flow down an inclined semi-circular open channel and inclined plane of infinite extent, respectively.

3. Generalized Flow Equation

Equations (A-9) and (A-16) satisfy the general equation

$$f(\bar{\tau}_w) = \left(-\frac{du}{ds}\right)_w = a\,\bar{\tau}_w \frac{\partial\left[\frac{2(\langle u\rangle - \bar{u}_w)}{r_H}\right]}{\partial\bar{\tau}_w} + b\left[\frac{2(\langle u\rangle - \bar{u}_w)}{r_H}\right] \qquad (A\text{-}17)$$

where "a" and "b" are defined as geometric parameters. The quantities $\bar{u}_w$ and $\bar{\tau}_w$ are the contour-integrated average values of u_w and τ_w, respectively. The geometric parameters for circular conduit or semi-circular open channel are $a = \frac{1}{4}$ and $b = 3/4$, and for parallel plates or the inclined plane of infinite width are $a = \frac{1}{2}$ and $b = 1$.

Equation (A-17) is a first order differential equation which may be integrated to yield

$$\frac{2(\langle u \rangle - \bar{u}_w)}{r_H} = \frac{1}{a} \bar{\tau}_w^{-\xi} \int_{\tau_y}^{\bar{\tau}_w} \tau^{\xi-1} f(\tau)\, d\tau \qquad \text{(A-18)}$$

where the aspect factor ξ is equal to b/a. For a fluid without a yield stress, the lower limit of integration in the above equation becomes zero.

Equation (A-18) is the general flow equation relating the flow rate to the shear rate or pressure drop applicable to any time-independent fluid and any arbitrary flow geometry.

Appendix B

Development of Velocity Relationships and the Averaging Operator

Development of Velocity Relationships and the Averaging Operator

In the following, the development of the relevant relationships is conveniently effected with reference to the circular and slit cross sections.

One begins with Eq.(11) describing the steady uniform flow of an arbitrary non-Newtonian fluid without a yield stress in a conduit of arbitrary cross-sectional geometry characterized by the geometric parameters:

$$\frac{2(\langle u\rangle - \bar{u}_w)}{r_H} = \frac{1}{a\,\bar{\tau}_w^{\xi}} \int_0^{\bar{\tau}_w} \tau^{\xi-1} f(\tau)\, d\tau \qquad (B\text{-}1)$$

When the substitution given by $f(\tau) = -du/ds$, where s denotes the position variable r for the circular tube, or y', measured from the plane of symmetry, in the case of the parallel plate geometry, is made to the above equation, one obtains:

$$\frac{2(\langle u\rangle - \bar{u}_w)}{r_H} = -\frac{1}{a\,\bar{\tau}_w^{\xi}} \int_0^{\bar{\tau}_w} \tau^{\xi-1}(d\tau/ds)\, du$$

$$= -\frac{\bar{\tau}_w^{1-\xi}}{a\xi} \int_0^{\bar{\tau}_w} \tau^{\xi-1}\, du \qquad (B\text{-}2)$$

The last equality in Eq.(B-2) is obtained with the aid of the relationship $d\tau/ds = \bar{\tau}_w/S$, where S equals R for the circular tube or Y for the parallel plate section.

Integration of Eq.(B-2) by parts gives

$$\frac{2(\langle u\rangle - \bar{u}_w)}{r_H} = -\frac{\bar{u}_w}{aS} + (\xi - 1)\frac{\bar{\tau}_w^{1-\xi}}{aS}\int_0^{\bar{\tau}_w} u\tau^{\xi-2}d\tau \qquad (B-3)$$

Setting $S = r_H/2a$ in Eq.(B-3) yields the desired relationship in terms of the geometric aspect factor ξ:

$$\langle u\rangle = (\xi - 1)\,\bar{\tau}_w^{\xi-1}\int_0^{\bar{\tau}_w} u\tau^{\xi-2}\,d\tau \qquad (B-4)$$

Equation (B-4) is the desired operator which averages a point function of the position, in this case the velocity, over the tube cross section.

Similarly, one can write the following relationship for the point velocity for each of the sections considered.

$$u - \bar{u}_w = \frac{S}{\bar{\tau}_w}\int_\tau^{\bar{\tau}_w} f(\tau)\,d\tau \qquad (B-5)$$

and setting $S = r_H/2a$ as above, obtain the following relationship for $(u - \bar{u}_w)$:

$$u - \bar{u}_w = \frac{r_H}{2a\bar{\tau}_w}\int_\tau^{\bar{\tau}_w} f(\tau)\,d\tau \qquad (B-6)$$

If τ is set equal to zero, $u = u_{max}$, and there is obtained

$$\frac{2(u_{max} - \bar{u}_w)}{r_H} = \frac{1}{a\,\bar{\tau}_w} \int_0^{\bar{\tau}_w} f(\tau)\, d\tau \qquad (B\text{-}7)$$

which agrees with Eq.(15) for a fluid without a yield stress.

It is readily verified that Eqs.(B-4) and (B-6) yield Eq.(B-1). Substitution of Eq.(B-6) into Eq.(B-4) gives, after some rearrangement:

$$\frac{2(\langle u \rangle - \bar{u}_w)}{r_H} = \frac{(\xi - 1)}{a\,\bar{\tau}_w^{\xi}} \int_0^{\bar{\tau}_w} \tau^{\xi-2}\, d\tau \int_\tau^{\bar{\tau}_w} f(\tau)\, d\tau \qquad (B\text{-}8)$$

The order of integration in Eq.(B-8) can be interchanged as follows:

$$\frac{2(\langle u \rangle - \bar{u}_w)}{r_H} = \frac{(\xi - 1)}{a\,\bar{\tau}_w^{\xi}} \int_0^{\bar{\tau}_w} f(\tau)\, d\tau \int_0^{\tau} \tau^{\xi-2}\, d\tau \qquad (B\text{-}9)$$

A single integration of Eq.(B-9) yields Eq.(B-1).

Appendix C

Various Fluid Models and Their Corresponding Velocity Expressions

Various Fluid Models and Their Corresponding Velocity Expressions

1. Newtonian

$$\eta = \mu$$

$$\frac{2\langle u \rangle}{r_H} = \frac{1}{a+b}\frac{\bar{\tau}_w}{\mu}$$

$$\frac{2\, u_{max}}{r_H} = \frac{\bar{\tau}_w}{2a\mu}$$

2. Ostwald-de Waele (Power Law)

$$\frac{1}{\eta} = \frac{1}{\tau}\left(\frac{\tau}{K}\right)^{1/n}$$

$$\frac{2(\langle u \rangle - \bar{u}_w)}{r_H} = \frac{n}{a+bn}\left(\frac{\bar{\tau}_w}{K}\right)^{1/n}$$

$$\frac{2(u_{max} - \bar{u}_w)}{r_H} = \frac{n}{a(1+n)}\left(\frac{\bar{\tau}_w}{K}\right)^{1/n}$$

3. Bingham Plastic

$$\frac{1}{\eta} = 0, \quad \text{if } |\tau| < \tau_y$$

$$\frac{1}{\eta} = \frac{1}{\beta}\left(1 - \left|\frac{\tau_y}{\tau}\right|\right), \quad \text{if } |\tau| > \tau_y$$

$$\frac{2(\langle u \rangle - \bar{u}_w)}{r_H} = \frac{\bar{\tau}_w}{\beta}\left[\frac{1}{a+b} - \frac{1}{b}\left(\frac{\tau_y}{\bar{\tau}_w}\right) + \frac{a}{b(a+b)}\left(\frac{\tau_y}{\bar{\tau}_w}\right)^{1 + b/a}\right]$$

$$\frac{2(u_{max} - \bar{u}_w)}{r_H} = \frac{\bar{\tau}_w}{2a\beta}\left[1 - 2\frac{\tau_y}{\bar{\tau}_w} + \left(\frac{\tau_y}{\bar{\tau}_w}\right)^2\right]$$

4. Ellis

$$\frac{1}{\eta} = \frac{1}{\eta_o}\left[1 + \left(\frac{\tau}{\tau_{\frac{1}{2}}}\right)^{\alpha-1}\right]$$

$$\frac{2(\langle u\rangle - \bar{u}_w)}{r_H} = \frac{\bar{\tau}_w}{\eta_o}\left[\frac{1}{a+b} + \frac{1}{a\alpha+b}\left(\frac{\bar{\tau}_w}{\tau_{\frac{1}{2}}}\right)^{\alpha-1}\right]$$

$$\frac{2(u_{max} - \bar{u}_w)}{r_H} = \frac{\bar{\tau}_w}{2a\eta_o}\left[1 + \frac{2}{\alpha+1}\left(\frac{\bar{\tau}_w}{\tau_{\frac{1}{2}}}\right)^{\alpha-1}\right]$$

5. Meter*

$$\eta = \eta_\infty + \frac{\eta_o - \eta_\infty}{1 + (\tau/\tau_m)^{\alpha-1}}$$

$$\frac{2(\langle u\rangle - \bar{u}_w)}{r_H} = \frac{\bar{\tau}_w}{\eta_o}\sum_{j=0}^{\infty}\left[\frac{1}{aj(\alpha-1)+a+b} + \frac{(\bar{\tau}_w/\tau_m)^{\alpha-1}}{a(j+1)(\alpha-1)+a+b}\right] x$$

$$\left[-\left(\frac{\eta_\infty}{\eta_o}\right)\left(\frac{\bar{\tau}_w}{\tau_m}\right)^{\alpha-1}\right]^j$$

$$\frac{2(u_{max} - \bar{u}_w)}{r_H} = \frac{\bar{\tau}_w}{a\eta_o}\sum_{j=0}^{\infty}\left[\frac{1}{j(\alpha-1)+2} + \frac{(\bar{\tau}_w/\tau_m)^{\alpha-1}}{j(\alpha-1)+\alpha+1}\right] x$$

$$\left[-\left(\frac{\eta_\infty}{\eta_o}\right)\left(\frac{\bar{\tau}_w}{\tau_m}\right)^{\alpha-1}\right]^j$$

6. Rabinowitsch

$$\frac{1}{\eta} = \frac{1}{\eta_o}(1 + b_1\tau^2)$$

$$\frac{2(\langle u\rangle - \bar{u}_w)}{r_H} = \frac{\bar{\tau}_w}{\mu_o}\left[\frac{1}{a+b} + b_1\frac{\bar{\tau}_w^2}{3a+b}\right]$$

$$\frac{2(u_{max} - \bar{u}_w)}{r_H} = \frac{\bar{\tau}_w}{2a\mu_o}\left[1 + \frac{b_1}{2}\bar{\tau}_w^2\right]$$

* The relationships presented are for η_∞ much smaller than η_o

Appendix

Geometric Parameters for Various Flow Geometries

Table D-1 Geometric Parameters for Circular and Slit Cross Sections

Geometry	a	b
Circular Pipe	0.2500	0.7500
Slit (Parallel Plates)	0.5000	1.0000

Table D-2 Geometric Parameters for Rectangular Ducts

E	a	b
0.00	0.5000	1.0000
0.25	0.3212	0.8182
0.50	0.2440	0.7276
0.75	0.2178	0.6866
1.00	0.2121	0.6766

Table D-3 Geometric Parameters for Concentric Annuli

k	a	b
0.00	0.2500	0.7500
0.01	0.3768	0.8751
0.03	0.4056	0.9085
0.05	0.4217	0.9263
0.07	0.4331	0.9383
0.10	0.4455	0.9510
0.20	0.4693	0.9737
0.30	0.4817	0.9847
0.40	0.4890	0.9911
0.50	0.4935	0.9946
0.60	0.4965	0.9972
0.70	0.4983	0.9987
0.80	0.4992	0.9994
0.90	0.4997	1.0000
1.00	0.5000	1.0000

Table D-4 Geometric Parameters for Elliptical Ducts

β	a	b
0.00	0.3084	0.9253
0.10	0.3018	0.9053
0.20	0.2907	0.8720
0.30	0.2796	0.8389
0.40	0.2702	0.8107
0.50	0.2629	0.7886
0.60	0.2575	0.7725
0.70	0.2538	0.7614
0.80	0.2515	0.7546
0.90	0.2504	0.7510
1.00	0.2500	0.7500

Table D-5 Geometric Parameters for Isosceles Triangular Ducts

2α	a	b
10°	0.1547	0.6278
20°	0.1693	0.6332
40°	0.1840	0.6422
60°	0.1875	0.6462
80°	0.1849	0.6438
90°	0.1830	0.6395

Table D-6 Geometric Parameters for Star-Shaped and Regular Polygonal Conduits

1. Star-Shaped Conduits

No. of Point	a	b
3	0.0792	0.3272
4	0.0871	0.3258
5	0.0910	0.3237
6	0.0933	0.3217
8	0.0958	0.3185

2. Regular Polygonal Conduits

No. of Side	a	b
4	0.2121	0.6771
5	0.2245	0.6966
6	0.2316	0.7092
8	0.2391	0.7241

Table D-7 Geometric Parameters for Infinite Arrays of Circular Cylinders

1. Square Array

S/r_o	a	b
1.00	-	-
1.05	0.1310	0.5521
1.10	0.1810	0.7368
1.20	0.2471	1.0196
1.50	0.4474	1.4107
2.00	0.7891	1.7288
4.00	2.0174	3.3397

2. Triangular Array

S/r_o	a	b
1.00	0.0789	0.3271
1.05	0.1818	0.7851
1.10	0.2658	1.0074
1.20	0.3895	1.1699
1.50	0.6080	1.3319
2.00	0.8642	1.5973
4.00	1.9829	3.0046

Table D-8 Geometric Parameters for Finite Arrays of Circular Cylinders

Square Array		Triangular Array	
S/r_o	a + b	S/r_o	a + b
1.07	1.2006	1.11	1.4163
1.23	1.8919	1.27	2.0788
1.47	2.5519	1.51	2.5631
2.00	3.6650	2.06	3.4797

Appendix E

Impermeability Factors for Particles of Various Shapes in Beds of Different Porosities

Table 3-1 Values of a+b for Different Particle Shapes and Porosities

Particle Shape	ϵ	a + b
Sphere	0.38	2.40
Cylinder	0.35	2.08
$\frac{1}{8}$" x $\frac{1}{8}$"	0.40	2.19
Hexagonal prisms	0.35	2.31
3/16" x 3/16"	0.48	1.85
Cubes	0.19	2.70
	0.35	2.20
	0.48	2.04
Square plates	0.35	1.72
$\frac{1}{8}$" x $\frac{1}{8}$" x 1/16"	0.48	2.23
Square plates	0.45	2.52
$\frac{1}{8}$" x $\frac{1}{8}$" x 1/32"	0.48	2.81
Triangular prisms	0.361	1.61
	0.518	2.43

Appendix F

Development of the Final Relationship for A_r'

Development of the Final Relationship for A_r'

In this section, it is shown that Eq.(182) follows directly from Eq.(181). Introduction of a change in dummy variables in the numerator of Eq.(181), and interchanging the order of integration of the resulting triple integral enables one to write the following:

$$\int_0^{\bar{\tau}_w} \tau^{\xi-2}\, d\tau \left[\int_\tau^{\bar{\tau}_w} f(\tau)d\tau\right]^2 = \int_0^{\bar{\tau}_w} \tau^{\xi-2}\, d\tau \int_\tau^{\bar{\tau}_w} f(x)dx \int_\tau^{\bar{\tau}_w} f(z)dz$$

$$= 2\int_0^{\bar{\tau}_w} f(x)dx \int_x^{\bar{\tau}_w} f(z)dz \int_0^x \tau^{\xi-2}\, d\tau$$

$$= \frac{2}{\xi-1}\int_0^{\bar{\tau}_w} x^{\xi-1} f(x)dx \int_x^{\bar{\tau}_w} f(z)dz \qquad \text{(D-1)}$$

A second interchange in the order of integration of Eq.(D-1), and replacing the dummy variables x and z by τ yields

$$\int_0^{\bar{\tau}_w} \tau^{\xi-2}\, d\tau \left[\int_\tau^{\bar{\tau}_w} f(\tau)d\tau\right]^2 = \frac{2}{\xi-1}\int_0^{\bar{\tau}_w} f(\tau)d\tau \int_0^\tau \tau^{\xi-1} f(\tau)d\tau \qquad \text{(D-2)}$$

The above result when combined with Eq.(181), yields the desired expression given by Eq.(182).

Appendix C

Experimental Data and Results for the Flow of CMC and Carbopol Solutions Through Packed Beds and Capillary Tubes

Table G-1 Diameter Specifications

Capillary Tube	Tube Diameter D, cm	Hydraulic Radius r_H, cm
1	0.2456	0.06140
3	0.1865	0.04663
4	0.1681	0.04205
5	0.1478	0.03620
6	0.1150	0.02875

Packed Bed	Particle Diameter D_p, cm	Hydraulic Radius r_H, cm
A	0.3175	0.03242
B	0.3967	0.04152

Table G-2 Data for the Flow of 2% CMC Solution Through Packed Beds of Spheres

Porosity of the beds = 0.38

Bed	$\bar{\tau}_w$.gm$_f$/cm^2	$2\langle u\rangle/r_H$.sec^{-1}	$-\bar{u}_w$.cm/sec	$2(\langle u\rangle-\bar{u}_w)/r_H$.sec^{-1}
A	0.2724	214.9	1.77	324.1
	0.2254	176.7	1.46	266.8
	0.1620	124.5	1.05	189.3
	0.1315	101.2	0.85	153.6
	0.3170	249.9	2.06	377.0
	0.3358	265.9	2.19	401.0
B	0.2121	179.2	1.38	247.3
	0.1225	105.5	0.80	145.0
	0.1509	127.9	0.98	176.3
	0.2241	189.7	1.45	261.3

Table G-3 Data for the Flow of 2% CMC Solution Through Capillary Tubes

Tube	$\bar{\tau}_w$, gm_f/cm^2	$2\langle u\rangle/r_H$, sec^{-1}	$-\bar{u}_w$, cm/sec	$2(\langle u\rangle-\bar{u}_w)/r_H$, sec^{-1}
4	0.1482	340.2	1.76	415.7
	0.1269	285.1	1.51	349.9
	0.1080	238.0	1.29	293.3
	0.0851	186.4	1.02	230.2
	0.0662	144.1	0.79	178.0
	0.0553	119.8	0.66	148.1
5	0.0973	219.5	1.15	281.7
	0.0875	196.1	1.04	252.4
	0.0771	171.9	0.92	221.7
	0.0688	157.6	0.82	202.0
	0.0593	132.6	0.70	170.5

Table G-4 Data for the Flow of 2.85% CMC Solution Through Packed Beds of Spheres

Porosity of the beds = 0.38

Bed	$\bar{\tau}_w$, gm_f/cm^2	$2\langle u\rangle/r_H$, sec^{-1}	$-\bar{u}_w$, cm/sec	$2(\langle u\rangle-\bar{u}_w)/r_H$, sec^{-1}
A	0.2700	149.6	1.93	268.6
	0.3346	187.8	2.40	335.8
	0.0728	35.2	0.51	66.7
	0.1972	107.0	1.41	194.0
	0.0881	44.1	0.63	83.0
	0.3851	227.5	2.75	397.1
	0.4426	272.7	3.15	467.0
	0.0650	29.3	0.46	57.7
	0.1282	61.1	0.92	117.8
	0.1608	78.8	1.15	149.7
	0.2184	111.0	1.56	207.2
	0.1691	84.2	1.20	158.2
	0.2538	134.0	1.81	245.6
B	0.1016	60.2	0.73	96.2
	0.2492	155.6	1.78	243.5
	0.1569	91.4	1.12	146.7
	0.0523	29.5	0.37	47.8
	0.2644	165.0	1.89	258.3
	0.2121	132.4	1.51	206.9
	0.1150	68.0	0.81	108.0

Table G-5 Data for the Flow of 2.85% CMC Solution Through Capillary Tubes

Tube	$\bar{\tau}_w$.gm$_f$/cm^2	$2\langle u\rangle/r_H$.sec^{-1}	$-\bar{u}_w$.cm/sec	$2(\langle u\rangle-\bar{u}_w)/r_H$.sec^{-1}
1	0.0716	102.6	1.32	145.6
	0.1155	178.7	2.13	248.1
	0.1411	232.6	2.60	317.3
	0.1826	322.1	3.37	431.7
	0.2127	378.9	3.92	506.6
	0.1555	263.4	2.87	356.7
	0.1254	207.1	2.31	282.4
	0.0874	135.7	1.61	188.2
3	0.0527	61.0	0.97	102.6
	0.0853	112.3	1.57	179.7
	0.1085	147.8	2.00	233.6
	0.1422	208.2	2.62	320.6
	0.1830	283.1	3.37	427.9
	0.2395	402.7	4.41	592.1
4	0.0605	71.6	1.12	124.7
	0.0710	88.4	1.31	150.8
	0.1027	136.7	1.89	226.9
5	0.0815	99.4	1.50	180.9
	0.1136	148.4	2.09	261.8
	0.1359	202.7	2.51	338.3
	0.0697	70.7	1.28	140.2

Table G-6 Data for the Flow of 0.3% Carbopol Solution Through Packed Beds of Spheres

Porosity of the beds= 0.38

Bed	τ_w.gm$_f$/cm^2	$2\langle u\rangle/r_H$.sec^{-1}	$-\bar{u}_w$.cm/sec	$2(\langle u\rangle-\bar{u}_w)/r_H$.sec^{-1}
A	0.1151	143.30	1.61	242.7
	0.0857	81.25	1.20	155.2
	0.1608	250.00	2.25	388.8
	0.2118	383.8	2.97	566.7
	0.1256	187.0	1.76	295.4
	0.1855	303.6	2.60	463.8
	0.0963	115.4	1.35	198.5
	0.0540	41.86	0.76	88.46
	0.0798	81.69	1.12	150.7
B	0.1703	285.9	2.38	403.6
	0.1031	138.6	1.44	209.8
	0.0508	46.46	0.71	81.6
	0.0732	81.16	1.03	131.8
	0.0941	117.3	1.32	182.4
	0.1315	188.8	1.84	279.7

Table G-7 Data for the Flow of 0.3% Carbopol Solution Through Capillary Tubes

Tube	$\bar{\tau}_w$.gm$_f$/cm^2	$2\langle u\rangle/r_H$.sec^{-1}	$-\bar{u}_w$.cm/sec	$2(\langle u\rangle-\bar{u}_w)/r_H$.sec^{-1}
3	0.0505	110.6	1.13	158.9
	0.0625	167.8	1.39	227.6
	0.0767	241.6	1.71	315.0
	0.0924	350.4	2.06	438.8
	0.1089	480.9	2.43	585.1
4	0.0461	112.6	1.03	161.5
	0.0559	156.6	1.25	215.9
	0.0680	210.7	1.52	282.9
	0.0825	272.8	1.84	360.4
	0.0960	350.5	2.14	452.4
	0.1150	485.4	2.56	607.4
5	0.0403	86.48	0.90	135.1
	0.0525	135.6	1.17	198.9
	0.0638	196.4	1.42	273.4
	0.0715	219.5	1.59	305.8
	0.0840	275.3	1.87	376.7
	0.1003	373.6	2.24	494.7

Table G-8 Data for the Flow of 0.35% Carbopol Solution Through Packed Beds of Spheres

Porosity of beds= 0.38

Bed	$\bar{\tau}_w$, gm$_f$/cm^2	$2\langle u\rangle/r_H$, sec^{-1}	$-\bar{u}_w$, cm/sec	$2(\langle u\rangle-\bar{u}_w)/r_H$, sec^{-1}
A	0.02465	41.57	0.62	79.8
	0.04109	77.02	1.03	140.2
	0.05870	126.51	1.46	216.6
	0.07866	202.72	1.95	323.0
	0.08805	220.17	2.20	355.9
	0.13850	398.58	3.45	611.4
	0.17960	572.03	4.48	848.4
B	0.02689	51.63	0.67	84.7
	0.05080	123.8	1.27	186.5
	0.07022	185.6	1.75	272.0
	0.08068	225.3	2.01	324.5
	0.09711	282.1	2.42	401.6

Table C-9 Data for the Flow of 0.35% Carbopol Solution Through Capillary Tubes

Tube	$\bar{\tau}_w$, gm$_f$/cm^2	$2\langle u\rangle/r_t$, sec^{-1}	$-\bar{s}_w$, cm/sec	$2(\langle u\rangle-\bar{s}_w)/r_t$, sec^{-1}
4	0.04750	291.3	2.25	398.3
	0.06135	403.5	2.91	542.0
5	0.04059	212.3	1.93	319.3
	0.05069	288.4	2.40	421.1
	0.06347	406.7	3.00	572.7
	0.07892	569.5	3.64	771.0
	0.09497	771.4	4.50	1019.6
6	0.03199	143.3	1.52	249.1
	0.03870	196.9	1.84	324.9
	0.04772	266.6	2.36	430.6
	0.05721	352.3	2.72	541.3
	0.06554	437.4	3.11	653.4